Ultra-Wideband Positioning using Reflections from Known Indoor Features

Jan Kietlinski-Zaleski

Ultra-Wideband Positioning using Reflections from Known Indoor Features

Jan Kietlinski-Zaleski
Nagoya University, JAPAN
2011

Contents

List of Figures

List of Tables

Chapter 1

Introduction

1.1 Background

Positioning is becoming an integral part of our daily lives. Paper maps are disappearing from car glove compartments, as people use car navigation to reach their destination. Virtually all smartphones sold today are equipped with a GPS receiver. However, GPS cannot be effectively used indoors. GPS signal does not penetrate walls well, and it has low accuracy, when compared with the small scale of indoor environments. A new research field, Indoor Positioning, was created to address the problem of positioning in indoor environments.

1.1.1 Indoor Positioning

Indoor Positioning focuses on small-scale, high accuracy systems, with the service area being a building or a collection of buildings. The main applications targeted by indoor positioning are: in-building goods tracking, person tracking, and access control. The accuracy required by those applications varies from centimeters to under 3[m]. According to [1], the required accuracy for goods tracking and worker/person tracking is 1[m], while access control requires 3[m] accuracy. On the other hand, according to [2] goods tracking requires 3[m] accuracy, while guard/firefighter/miner tracking requires 30[cm] accuracy.

A successful indoor positioning system has to provide the required level of accuracy for a low cost. In order to achieve low cost, the number of reference nodes that needs to be installed in the service area has to be small. In an indoor environment, that requires the positioning signals to be able to penetrate walls and other obstacles. In practice, only technologies based on RF(Radio Frequency) meet this requirement, although other technologies are also reviewed in Chapter 2.

Although a sizable part of RF signal's power can penetrate walls and obstacles, some of it is reflected back. Reflections from many obstacles present in an indoor environment cause multipath fading, which severely degrades the positioning accuracy of narrowband RF systems. However, the influence of multipath fading can be mitigated by increasing the bandwidth. In addition, increasing bandwidth also increases the accuracy of time-based ranging methods. In summary, a RF system, using very wide bandwidth, should be a good candidate for use in indoor positioning.

1.1.2 UWB Technology

In recent years, Ultra-Wideband(UWB) radio technology has been gaining popularity. Technological advances in receivers and integrated circuits have made extremely high bandwidth systems financially viable. At the same time, starting with the Federal Communications Commission(FCC) decision in 2002[3], unlicensed usage of low transmitted power UWB devices in certain bands became authorized in many important markets, including USA, Europe[4] and Japan[5]. Although IEEE standardization of high rate UWB (IEEE 802.15.3a) failed, WiMedia Alliance[6]-supported Wireless USB standard, based on the OFDM UWB variety, already has a presence on the market. The successful standardization of the low-rate UWB, based on the Direct Sequence UWB variety, which focuses on low power and cost, resulted in the IEEE 802.15.4a standard[7]. IEEE 802.15.4a is meant for use in wireless personal area networks(WPAN) and wireless sensor networks(WSN), and includes positioning. Another standard, IEEE 802.15.4f[8], targeting low-cost Real Time Location Services(RRTLS) applications, is currently being worked upon.

The main feature of the UWB technology is its very large bandwidth. Very large bandwidth is advantageous for communications and positioning[9]. High speed data communications and high accuracy ranging are possible. Low cost, low power implementations are also achievable. Additionally, as already mentioned, wideband signals are more resistant to fading. Finally, because of the low spectral energy density of the UWB signal, interference with narrowband systems using the same frequencies is minimal, which makes using UWB in already occupied frequency bands possible.

Because of its advantages, UWB is an ideal candidate for indoor positioning. UWB is capable of high accuracy ranging and it is resistant to multipath. In addition, as with other RF technologies, UWB signals can penetrate obstacles, allowing using a lower number of reference nodes.

1.1.3 Applications of UWB Indoor Positioning

There are currently two main usage scenarios for UWB Indoor Positioning. The first is a Wireless Sensor Network(WSN) with ranging capabilities. In most WSNs, sensor node positions are important. As well as low power communications solution, UWB delivers good sensor node positioning accuracy. IEEE 802.15.4a standard was devised for use in this scenario. The second scenario is network-based positioning. In this case, a network of set-position reference receiver nodes tracks a large number of mobile target transmitter nodes (tags). This is the scenrio targeted by the IEEE 802.15.4f standard.

Both usage scenarios require cheap, energy efficient UWB nodes. Both WSN nodes and network-based positioning transmitter tags need to be able to operate on one battery for a long time. Additionally, both the WSN nodes and the tags will be deployed in large numbers, making low price a priority. However, receivers in the network-based positioning scenario can be more expensive, since only a limited number of them will be deployed.

In this dissertation I focus on the network-based positioning scenario. This is currently the most practically applicable scenario, as evidenced by the already commercially available platforms from Ubisense[10], Time Domain [11] and Zebra Solutions[12].

1.2 Motivations

1.2.1 Increasing Accuracy

The main motivation for the research presented in this dissertation was to increase the accuracy of UWB positioning. By increasing the accuracy, new applications become available, and the performance of already existing applications improves. For example, with positioning accuracy on the level of 1-2m, it is possible to localize a patient in a hospital, but if 30cm accuracy is available, it is also possible to determine if the patient has just fallen over on the floor.

Ubisense already claims a 30cm 3D accuracy of its Ubisense Platform, which should be enough for most positioning applications. However, those are producer claims, which suggests that the results were obtained in a best-case scenario. Accuracy in less than optimum scenarios, especially for cases when only one, two or three receivers are in the tag's range, or when a direct path to the receiver is blocked (Non-Line of Sigtht, NLOS, case) will be much lower.

This dissertation concentrates on improving the accuracy in situations where only a few receivers are in the Line-of-Sight(LOS) range of the transmitter. In these often occurring but undesirable cases, the average positioning error is high. Consequently, this is an area of great potential improvement. Reducing error in

these worst-case scenarios improves the overall accuracy of UWB more than modest error reduction possible for the relatively accurate best case scenarios. Thus, the research proposed in this dissertation contributes to increasing the accuracy and viability of UWB as a serious contender for indoor positioning.

1.2.2 Multi-Path Components

In order to increase the accuracy of few receivers positioning cases, I use the Multi-Path Components(MPCs) detected in the received signals. The very high bandwidth of the UWB signal translates into very good time resolution. Consequently, the received UWB signal contains distinguishable MPCs, alongside the direct path component. MPCs are signals caused mainly by reflections and diffractions from objects in the environment. Some of the detected MPCs are caused by reflections from indoor features, such as ceiling, walls and floor. If the positions of those features are known, the MPCs become an additional, currently practically untapped, source of information about the position of the target node.

Three challenges to the use of MPCs for positioning exist. The first, greatest, challenge is the multiple MPCs problem. There are many MPCs in the received waveform. Among them, finding the MPC caused by the reflection from a given indoor feature is not straightforward. The second problem is the reduced accuracy of the solution. Since MPCs are caused by reflections, the power of each MPC is generally lower than that of the direct path component. Additionally, the position of the features is never known with perfect accuracy. Because of those two reasons, information contained in MPCs has lower accuracy than the information from direct-path ranges. This limits the usefulness of MPCs if many receivers, and many direct-path ranges, are available. However, as mentioned above, they may provide a valuable support in situations where few receivers are available, causing an increase in accuracy. Finally, to detect MPCs, advanced, currently very expensive, receiver architectures have to be used. However, due to ongoing improvements in the technology, such receivers will become, in time, affordable.

1.3 Contributions

The dissertation makes three contributions. First, two new positioning methods are presented. Then, the methods are verified using measurement data, and the results analyzed. Finally, the most important contribution is proving the validity of the Reflection-Aided approach.

1.3.1 Positioning Methods

I present two new positioning methods for positioning using received MPCs and the knowledge of major indoor features in the environment. The first one is the TOA Reflection-Aided Maximum Likelihood(RAML) method, for two receiver time-of-arrival(TOA) ranging. The second one is the TDOA Reflection-Aided Maximum Likelihood(RAML) method, for two receiver time-difference-of-arrival(TDOA) ranging. The methods proposed in this dissertation solve the multiple MPCs problem by using a Maximum Likelihood approach, without explicitly knowing the correct matches. This is a novel approach to the problem.

1.3.2 Validation of the Proposed Methods

In order to verify the real world usefulness of the idea in general, and the methods in particular, measurements were performed. The data obtained in the measurement campaign was used to verify the usefulness of the proposed methods. The results show that, under certain conditions, both the RAML and DRAML methods outperform the conventional methods using the same number of receivers. The two most important requirements were found to be the availability of at least three reasonably flat reflectors/walls and a relatively uncluttered environment. Also, especially in the case of the RAML method, the position of the reflectors in respect to the receivers strongly influences the results.

1.3.3 Reflection-Aided Positioning Approach

The main contribution of this dissertation is proving the validity of the reflection-aided positioning approach in general. The proposed methods will most probably not be used in the form presented. A practical method would rather use Reflection-Aided Positioning in conjunction with tracking and Angle of Arrival(AOA), which greatly improve the accuracy over RAML and DRAML methods. However, the measurement campaign proves that even a pure Reflection-Aided method improved results over the conventional method.

1.4 Organization of the Dissertation

Chapter 2 presents a general description of the field of Indoor Positioning. The chapter introduces the background of time-based UWB positioning and presents other currently available positioning options.

Chapter 3 presents an overview of UWB indoor positioning. The chapter begins with a general introduction to UWB indoor positioning. Next, the currently active fields of research are discussed, placing my research in the greater

picture.

In the following **Chapter 4**, both the conventional and the proposed positioning methods are presented in detail. First, conventional Assumed Height and Direct Solution methods for both TOA and TDOA ranging are introduced. Next, the proposed TOA Reflection-Aided Maximum Likelihood(RAML) and TDOA Reflection-Aided Maximum Likelihood(DRAML) methods are presented in detail.

Chapter 5 presents the measurements conducted in order to verify the proposed methods. First, the measurement setup used for measurements is shown, then the three environments in which the measurements were conducted are presented. Also, the algorithm used for extracting TOA measurements from the received waveform is discussed.

Chapter 6 presents the results of the conventional and the proposed methods when used with data collected during the measurements. Four studies are presented: general TOA results, results for different receiver positions, results for different environments, and general TDOA results. Both TOA RAML and TDOA DRAML are shown to achieve better accuracy than the conventional methods using the same number of receivers, for some scenarios. The main obstacles to reflection-aided positioning are identified: the availability of flat reflectors and the number of reflections in the environment.

Finally, **Chapter 7** presents a summary of the results of the dissertation, discusses the contribution of the dissertation and the future directions of development of the reflection-aided methods.

Chapter 2

Indoor Positioning Overview

This chapter presents an overview of the Indoor Positioning field, without focusing on the UWB technology. The chapter starts with a general definition of positioning and a discussion about the reasons for a separate Indoor Positioning field. Next, possible applications of indoor positioning are presented. Subsequently, non-RF technologies that can be used for positioning are described, followed by RF technologies that can be used. The sections afterwards concentrate on RF positioning. A more strict definition of the positioning problem is first presented. Then, theoretical limits on positioning accuracy are introduced. Next, possible positioning techniques are shown. Finally, a summary of the chapter is presented.

2.1 Definition of Positioning

Positioning is defined as "a process used to determine the location of one position relative to other defined reference positions". Actually, "locating" is a semantically more precise term, but because of the inclusion of the word "positioning" in the name of the currently predominant Global Positioning System(GPS), the two terms became synonyms.

The first large-scale positioning systems, GEE[13] and LORAN[14], were deployed during the Second World War for airplane navigation. Since that time, general positioning came to be dominated by Global Navigation Satellite Systems(GNSS), GPS[15] in particular. With cheap receivers and accuracy in the tens of meters, GPS applications now range from plane, missile, ship, car, personal navigation, to surveying, geotagging and even as a high precision time

source.

Another important class of currently available large scale positioning systems are those using cellular network Base Stations, which is a solution with no added cost. Much interest in such systems was generated by a Federal Communications Commission(FCC, the USA communications regulator) order requiring wireless service providers to deliver an accurate position of callers calling emergency numbers, such as police or ambulance[16].

2.2 Indoor Positioning

The field of Indoor Positioning is concerned with positioning of objects located inside of buildings. With good accuracy of GPS and other general-purpose positioning systems mentioned above, it can be argued that those systems can also be used indoors. That would mean that there is no need for a separate research field specialized in indoor positioning.

However, indoor positioning presents additional challenges that standard systems were not engineered to cope with. Two challenges are particularly important. The first is the much greater number of reflections in the indoor environment. Those reflections cause strong fading, which is especially damaging for positioning methods based on signal strength. Additionally, one of the reflections can be mis-detected as the direct signal, causing the so called Non-Line of Sight(NLOS) error. The second challenge is the attenuation of building's walls and ceilings. Buildings strongly attenuate the signals coming from outside, which often makes such signals undetectable. GPS signals are especially affected, since they are very weak.

The other problem is that indoor positioning has higher accuracy requirements than the general-purpose positioning systems can provide. For most applications, accuracy of at least 3m is needed, as discussed in the next section. GPS cannot consistently provide this level of accuracy, even in ideal conditions . For example, [17] reports errors of up to 10m using Differential GPS(DGPS) in the ideal conditions of open water.

2.3 Applications of Indoor Positioning

Applications of positioning have widely varying accuracy requirements. Two accuracy requirements lists are presented in [1] and [2]. For example, for finding the closest restaurant, accuracy of 30 meters is acceptable (after [1]), and consequently it is possible to use general purpose systems. In this section I describe applications that require accuracy unavailable for general purpose systems. The

two main application areas of indoor positioning are person tracking and item tracking.

2.3.1 Person Tracking Applications

In a person tracking scenario, the position of a person is known at all times. In order to do that, the person has to carry a positioning target node, for example an ID card or a bracelet with a built-in transmitter.

Probably the most common application of person tracking will be personnel tracking, that can be used by companies. Personnel here may mean for example factory workers, miners, doctors and nurses, office workers, and other. Personnel tracking has multiple advantages:

1. The crucial personnel (ie. doctors) can be quickly found at all times.
2. Automatic, proximity-based access control systems can be implemented. In such a system, doors could open automatically if an employee with the right clearance approaches, obsoleting magnetic cards.
3. In the event of an emergency, for example a fire, all personnel can be easily and quickly found and accounted for. This can be of particular importance in the case of mines.
4. Lights and air conditioning can be automatically controlled to save energy.
5. The time spent in work can be accurately calculated.
6. Employees can be caught taking excessively long coffee breaks.

Person tracking can also be applied in prisons. By incorporating a target node in, for example, prisoner bracelets, the position of each prisoner can be ascertained at all times. In particular, an automatic alarm can be quickly raised if a prisoner leaves an area he is assigned to. This would be similar to the current large scope parolee tracking systems.

Another application is in museums and other institutions attracting visitors. If the target node is integrated into audio guides, it is possible to provide automatic commentary when the visitor approaches an exhibit [18]. Additionally, using visitor trajectory data, administrators can judge the popularity of exhibits and possible improvements in the layout of the exhibits.

A similar application is also possible for supermarkets. By integrating the positioning target into a shopping cart, it is possible to measure customer flow, to better optimize the placement of products and the layout of the supermarket.

Another, positioning application is the so called “first responder” positioning. This term is used to describe the emergency service personnel, for example firefighters or policemen, who arrive first at a place of an incident, for example fire or a crime. By tracking everybody’s position constantly, it is, for example,

possible to guide firefighters in the building even in minimal visibility conditions, and, in the case of police, it is possible to avoid friendly fire. In this case, there is no infrastructure to rely on, making it a hard positioning case.

The applications mentioned above require an accuracy of 1m, after [1]. An example of a person tracking application with an even higher accuracy requirement would be patient tracking in a hospital, if the height of the patient would also be of interest. Height is useful to detect patients who fall.

2.3.2 Item Tracking Applications

In the item tracking scenario, the position of an item is known at all times. The positioning target would be a tag attached to the item or it could be built into the device itself. I present here two possible applications.

The first possible application is inventory tracking, in a warehouse, factory or a store[19]. By using tracking, it is possible to check what is present in the warehouse at any time, and accurately find any piece of inventory. Also, it can be quickly detected if a given product is running out and has to be restocked. The accuracy requirement depends on the type of inventory. A container cargo depot would require accuracy of about 10m; a standard warehouse would require an accuracy of 1m, including height; a library would require an accuracy as high as 20cm.

The second application is theft prevention, such as in advanced anti-theft tags attached to the item. Unlike the standard RFID-based solutions common in stores, gates are not required, and the theft can be detected even if the thief bypassed the gates in some way. Additionally, even if the theft was successful, by using the item trajectory together with security cameras, it is easy to identify the thief on a video.

2.3.3 Other Applications

As always, it is hard to predict all the possible uses of a new technology. Here I mention some more applications discussed in the literature. One application could be robot navigation[20]. Indoor robot navigation would require accuracy of 8cm (after [1]). Another application could be indoor environment surveying. Surveying requires an even higher accuracy, in the order of 1cm. It is also practically certain that indoor positioning will also be used for different kinds of toys.

The applications presented in this chapter are not an exhaustive list. Also, in a practical system, many of the applications will be used at the same time. For example, in a hospital, the positions of doctors, patients and expensive

equipment would be monitored all at the same time, using the same positioning system.

2.4 Technologies for Indoor Positioning

Although RF-based technologies are most commonly used for positioning, there are several other technologies to choose from. This section presents an overview of the other possible technologies, their advantages and disadvantages, while the following section presents different versions of RF positioning.

2.4.1 Optical

Optical signals, infrared or visible light, can be used for ranging and positioning. The advantages of systems employing these technologies are a very good ranging accuracy, low cost and low energy consumption. Laser range finders, now in common use, serve as an example of the good ranging accuracy. However, optical signals cannot penetrate through walls and other obstacles. For this reason, optical positioning systems require many more sensors than RF in order to cover an indoor environment. Additionally, optical systems are susceptible to interference from sunlight and artificial lighting.

2.4.2 Ultra-sound

Systems based on ultra-sound can be relatively inexpensive, while precise at the same time. Because of the low speed of sound, good ranging accuracy is possible[21]. The system can be also inexpensive, because the low speed of sound signifies that the signal does not have to be sampled very often, limiting the required sampling rate and processor speed. Unfortunately, although low frequency, audible sound waves penetrate obstacles quite well, ultrasound signals do not, forcing the use of more nodes, as compared with RF. Transmitters are also energy inefficient.

2.4.3 Inertial Navigation

Using accelerometers it is possible to measure a node's acceleration, from which it is possible to calculate its speed and position. The advantages of this approach are its energy efficiency and low cost. This is due to the fact that tiny, energy efficient and cheap MEMS(Micro-Electro-Mechanical System) accelerometers have become available recently. Unfortunately, small acceleration errors can quickly cause a huge position error, making inertial navigation ill-suited for longer autonomous operation. For this reason, this technique is used usually in

conjunction with other techniques. Currently, virtually all new GPS-equipped smartphones and navigation units have a MEMS accelerometer built-in. The field of such hybrid positioning systems is very active because of this recent popularization of the MEMS accelerometers[22, 23].

2.5 Indoor Positioning RF Systems

The technologies most commonly used for positioning are RF-based. The main advantage of RF over other technologies is the ability to penetrate obstacles, and, consequently, a longer range. Due to obstacle penetration, the same service area can be covered using a smaller number of nodes. For this reason, all of the current general purpose positioning systems use RF. Its properties, and consequently its suitability for indoor positioning, are strongly dependent on its bandwidth.

2.5.1 Narrowband

Narrow-band systems have a low time resolution, and are unsuitable for precise time-based ranging. However, AOA and TDOA systems based on a signal's phase difference are possible. Two example TDOA systems are OMEGA[24] or LORAN(phase used for precise timing). Received signal strength(RSS)-based systems are also possible. Unfortunately, both phase difference and RSS approaches are very susceptible to reflection-caused multipath fading, which is strong in indoor environments.

2.5.2 Wideband

Wideband systems have an average time resolution, and are suitable for time-based ranging. However, time-based ranging positioning accuracy can be generally not satisfactory for indoor positioning. Received Signal Strength(RSS)-based methods are possible, and less affected by multipath fading than in the narrowband case, due to higher bandwidth. Also, since wideband systems usually use higher frequencies, RSS variations caused by fast fading change quicker with position. For that reason, RSS can be used for medium accuracy positioning, if paired with averaging techniques or pattern-matching.

The real advantage of wideband RSS is that devices capable of RSS measurement are cheap and ubiquitous in today's world. For example, cellphones and WiFi receivers are RSS capable. This has lead the development of systems relying on those ubiquitous devices, such as WiFi-using system by Skyhook[25].

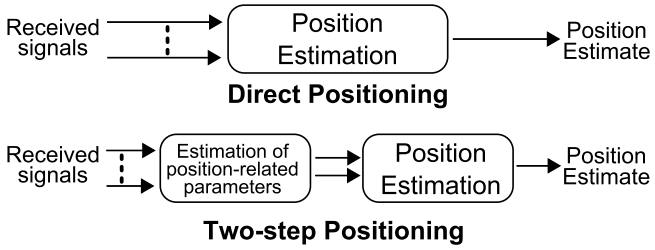

Figure 2.1: Comparison of direct and two-step positioning.

2.5.3 UWB

UWB is characterized by a very wide bandwidth and very high time resolution. When time-based ranging is used, accuracies on the level of centimeters can be achieved, much smaller than for RSS-based systems. The high bandwidth also makes the UWB signal resistant to multipath. RSS ranging is also possible, although it does not fully makes use of UWB bandwidth. Additional advantage of UWB is that the transmitters can be energy efficient and cheap. The disadvantages of the UWB technology are the comparatively complicated receivers and short range.

2.6 General Definition of the Positioning Problem

Strictly speaking, a positioning problem should be defined in terms of received waveforms. This approach is called direct positioning[26]. However, in practice, in most cases a two-step approach is used, where certain parameters are first extracted from the signal, and then the position is estimated based on those parameters. Both approaches are presented in Fig. 2.1.

The two-step approach is generally suboptimal, but it has a much lower complexity than the direct positioning approach. Additionally, for sufficiently high Signal-to-Noise Ratios(SNRs) and / or signal bandwidths, its performance is close to the accuracy achieved using direct positioning[27]. Therefore, most practical systems use the two-step approach, differing in the number and type of parameters used. The most common parameters extracted in the first step are: received signal strength(RSS); time of arrival(TOA); angle of arrival(AOA). Other possible parameters include parameters connected with the impulse response of the channel, such as mean excess delay, RMS delay spread, or maximum excess delay, and parameters connected with multipath propagation, TOAs and RSSes of MPCs. My methods are also two step methods, and they use the MPC TOAs as parameters.

2.7 Theoretical Limits of Positioning Accuracy

Two theoretical error bounds are commonly used for evaluating the positioning accuracy; Cramer-Rao Lower Bound(CRLB) and Ziv-Zakai Lower Bound(ZZLB)[28]. CRLB is easier to calculate, but the bound is tight, that is to say, it is close to achievable accuracy, only for high SNR values. On the other hand, calculating ZZLB is more complicated, but the bound is tight also for low SNR region.

Cramer-Rao Lower Bound sets a lower limit on the Mean Square Error(MSE) of an unbiased position estimator. The bound is derived from the Fisher's inequality equation for general variance of any estimator:

$$\mathrm{Var}[\hat{a}] \leq \left(1 + \frac{\delta b}{\delta a}\right)^2 \Bigg/ E\left[-\frac{\delta^2 \ln P}{\delta a^2}\right] \tag{2.1}$$

where a is the estimated parameter, in the context of positioning usually range or position, while $\hat{a}$ is the estimator. $\mathrm{Var}[\cdot]$ is the variance operator, b is the estimator's bias (assumed to be 0 in CRLB), $E(\cdot)$ is the expected value operator and P stands for the population of $P(\mathbf{x}|\mathbf{a})$, measurements conditioned on the parameter a. A general discussion of CRLB is presented in [29], while a more in-depth discussion can be found in [30].

CRLB is useful because Maximum Likelihood (ML) estimators can achieve CRLB asymptotically under certain conditions. However, that is true only for high SNRs. The disadvantage of CRLB is the underlying assumption that the transmitted signal was correctly detected, with some error. In the case of low SNR, that is not always the case. In that case, noise can be mis-detected as the transmitted signal. For that reason, the CRLB is not a tight bound for low SNR region. To solve this problem, the Ziv-Zakai Lower Bound(ZZLB) was introduced. ZZLB can be derived from the following general identity for the MSE of an estimator:

$$\mathbb{E}\{\epsilon^2\} = \frac{1}{2}\int_0^\infty z\mathbb{P}\left\{|\epsilon| \leq \frac{z}{2}\right\} \mathrm{d}z \tag{2.2}$$

where ϵ is the estimation error $(\hat{a} - a)$, z is the integration parameter and $\mathbb{P}$ denotes probability. For an in-depth discussion, please see [31]. Often ZZLB cannot be obtained in a closed form, but it provides a tighter bound on MSE of the positioning estimator than CRLB.

Other papers discussing CRLB and ZZLB in different positioning situations with single-path and multipath channels, LOS and NLOS, include: [29, 32, 33, 34, 35, 36].

2.8 Positioning Techniques

This section presents common positioning techniques used for RF positioning. All techniques use the two-step approach mentioned in 2.6, but differ in the choice of parameters.

The first five techniques presented, RSS, AOA, TOA, TDOA and Fingerprinting, are often described as "range based". This is because the used parameters correspond to the range or angle between each receiver and transmitter. CRLB of range measurements with each technique is given when possible.

The last two techniques, Closest Neighbor and Average of Neighbors, are examples of low complexity techniques that need very little hardware and processing, but require dense networks to achieve good accuracy. Such methods are especially useful in the case of wireless sensor networks(WSN).

2.8.1 Received Signal Strength - RSS

In RSS ranging, Received Signal Strength parameter is used. The transmitted signal strength and the relation between the distance and power loss is assumed to be known. If that is the case, by measuring the RSS, it is possible to calculate the distance between the reference and target nodes.

Unfortunately, one of the features of the indoor environment is strong multipath(fast) fading and shadowing(slow fading). Multipath fading describes quick changes in the signal level caused by interference between direct and reflected signals. It can cause variations in the signal strength as great as 30-40 dB over distances in the order of a half wavelength. In the case of a moving target or reference nodes, signal strength averaging may help to remove the influence of this kind of fading. Shadowing, on the other hand, describes slower variations of local mean power caused by additional signal energy from reflections or losses due to transmission through obstacles. It is impossible to remove the influence of shadowing through averaging, which limits the accuracy achievable by RSS.

The average RSS falls exponentially with distance:

$$\bar{P}(d) = P_0 - 10n \log_{10}(d/d_0) \tag{2.3}$$

where n is the path loss exponent, $\bar{P}(d)$ is the average received power at a distance of d in dB, and P_0 is the received power at a reference distance d_0. The shadowing effects (and remaining multipath fading effects) can be modeled as log-normal random variable, a Gaussian random variable with mean $\bar{P}(d)$ and variance σ^2_{sh}; i.e.

$$10 \log_{10} P(d) \sim \mathcal{N}(\bar{P}(d), \sigma^2_{\text{sh}}) \tag{2.4}$$

Assuming this model, the CRLB of range estimation can be expressed as(after [37, 30, 29]):

$$\sqrt{\mathrm{Var}\{\hat{d}\}} \geq \frac{\ln 10}{10}\frac{\sigma_{\mathrm{sh}}^2}{n}d \tag{2.5}$$

where $\mathrm{Var}\{\hat{d}\}$ stands for variation and $\hat{d}$ is an unbiased estimate of d.

Equation (2.5) shows that accuracy of RSS positioning decreases with stronger variance of shadowing σ_{sh}^2. Additionally, higher loss exponent n increases the accuracy, as the received power becomes more susceptible to distance. Finally, the bound implies that the accuracy of RSS ranging deteriorates with distance. It should be noted that the bound does not depend on the signal bandwidth, although higher bandwidth does reduce multipath fading.

In practice, in order to achieve a reasonable positioning accuracy with RSS, averaging has to be used to reduce the influence of fading. This is possible if one of the nodes is mobile or if the environment changes. Additionally, because the accuracy depends on distance, RSS can only be used for short range positioning. The big advantage of RSS is the low cost and ubiquity of devices capable of RSS. As mentioned before, every cellphone and WiFi receiver is capable of RSS.

2.8.2 Angle of Arrival - AOA

In AOA ranging, the angle of arrival parameter is used. In order to obtain AOA, antenna arrays are most commonly employed. Times of arrival at each array element are recorded, and the incoming angle is calculated from the differences between the TOAs at each element. An illustration of the process is shown in Fig. 2.2

In the case of an uniform linear array(ULA), the CRLB can be expressed as:

$$\sqrt{\mathrm{Var}\{\hat{\psi}\}} \geq \frac{\sqrt{3}C}{\sqrt{2}\pi\sqrt{SNR}\beta\sqrt{N_{\mathrm{a}}(N_{\mathrm{a}}^2-1)}l\cos\psi} \tag{2.6}$$

where $\hat{\psi}$ is the estimated angle of arrival, C is the speed of light, SNR is the signal-to-noise ratio (assumed to be equal for all elements), β is the effective bandwidth, N_{a} is the number of elements in the array and l is the inter-element spacing. SNR is calculated as: $\mathrm{SNR} = \alpha^2 E/N_0$, where α is the channel's attenuation, E is the transmitted energy and N_0 is the noise power spectral density. Effective bandwidth β can be calculated as:

$$\beta = \left(\frac{1}{E}\int_{-\infty}^{\infty} f^2|S(f)|^2\mathrm{d}f\right)^{1/2} \tag{2.7}$$

where $S(f)$ is the transmitted signal's frequency spectrum.

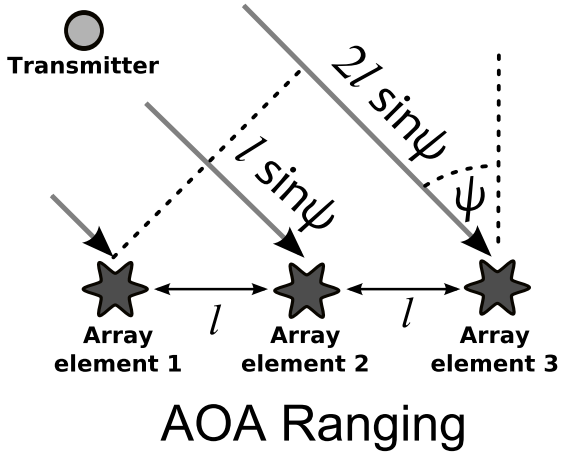

Figure 2.2: Illustration of Angle of Arrival ranging. The angle is calculated using differences in TOA at each array element.

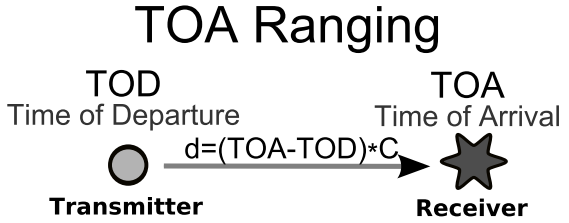

Figure 2.3: Illustration of Time of Arrival ranging. Both Time of Departure(TOD) and Time of Arrival(TOA) is needed.

It can be observed from (2.6) that increasing SNR, bandwidth, number of elements or spacing of elements improves the accuracy of angle estimation. This makes high bandwidth systems, like UWB, well suited for using AOA. Additionally, it should be noted that the accuracy of AOA is best for transmitters in front of the array, but becomes very low for transmitters to the side of the array. Finally, although AOA angular accuracy does not fall quickly with distance, If expressed in the terms of meters, the accuracy falls with the distance.

2.8.3 Time of Arrival - TOA

In TOA, the time of arrival parameter is used, while the time of departure(TOD) is assumed to be known. The range between two nodes is calculated using the flight time of the signal sent from one node to another. In order to perform TOA ranging, either the clocks at both nodes have to be synchronized or a ranging protocol, such as two-way ranging, included, among others in the 802.15.4a standard, must be used. An illustration is shown in Fig. 2.3.

To estimate TOA, the standard technique is to use a matched filter. A

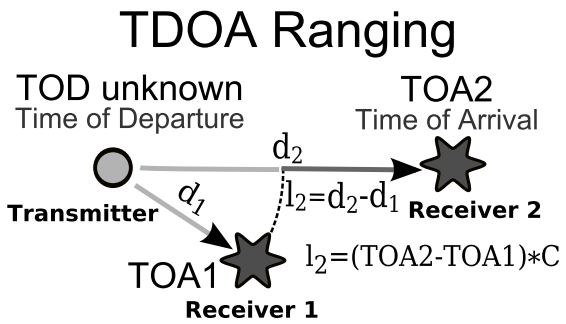

Figure 2.4: Illustration of Time Difference of Arrival ranging. At least two Time of Arrivals(TOAs) are needed.

matched filter is the optimal detector in single-path AWGN channels. It has to be noted that in reality channels are much more complicated, but for general analysis of TOA ranging, such a simplified channel is sufficient.

CRLB for TOA estimation with a matched filter can be expressed as(after [37, 29, 31]):

$$\sqrt{\mathrm{Var}\{\hat{\tau}\}} \geq \frac{1}{2\sqrt{2}\pi\sqrt{SNR}\beta} \tag{2.8}$$

where $\hat{\tau}$ is the time-of-flight estimate. Unlike in the case of RSS, the accuracy of TOA measurements can be increased by increasing SNR and the effective bandwidth β. This allows for very accurate distance estimation, even within a centimeter, when a very high bandwidth UWB signal is used. Additionally, unlike in the RSS and AOA cases, the accuracy of distance estimation does not depend on the distance, making TOA the technique of choice for longer ranges.

2.8.4 Time Difference of Arrival - TDOA

In some cases, TOD is not known. In that case, TOA ranging is not possible. However, if different reference nodes are synchronized, TDOA measurements can still be obtained. In the case of a TDOA measurement, the difference of ranges from the target node to two reference nodes is estimated. This places the target node on a hyperbola, with two reference nodes being the foci of the hyperbola. An example of TDOA ranging is presented in Fig. 2.4.

The range difference can be estimated by performing TOA estimation at both reference nodes and subtracting the results:

$$\hat{l}_{\mathrm{TDOA}} = (\hat{t}_1 - \hat{t}_2)C \tag{2.9}$$

where $\hat{l}_{\mathrm{TDOA}}$ is the estimated range difference, $\hat{t}_1$ and $\hat{t}_1$ are the estimated times

of arrival at both reference nodes. Since TDOA measurements are based on two TOA measurements, accuracy of TDOA also improves with SNR and bandwidth. Unfortunately, the accuracy of TDOA is always worse than that of TOA because, even if both TOA measurements are LOS, an additional parameter, time of departure(TOD) has to be estimated.

2.8.5 Fingerprinting

In some cases, the propagation environment is so hard that the standard ranging methods cannot be used, or the number of receivers is low, or only RSS measurements are possible, but accuracy higher than that of RSS ranging is desired. In such cases, fingerprinting methods can be used.

In fingerprinting, a set of measured parameters is compared with a database of pre-measured location "fingerprints". Next, either the closest matching location or some combination of close matching positions is used as the position estimate. The choice of the fingerprint parameters depends on the capabilities of the receivers.

The advantages of fingerprinting method are its low requirements, in terms of capabilities and the number of receivers. Fingerprinting can be more accurate than RSS. Additionally, fingerprinting works even in strongly NLOS environments, where other ranged solutions fail.

Unfortunately, the great disadvantage of fingerprinting is the need for many measurements in the system initiation phase. Additionally, with time the environment can change, changing the parameters used for fingerprinting and forcing re-measurement.

Currently the most popular fingerprinting systems are based on 802.11 networks, using RSS for fingerprinting[38]. Channel Impulse Response(CIR) is also often used for calculating fingerprints. [39] presents a CIR-based fingerprinting system for use inside mines, an extremely NLOS environment. An in-depth discussion of fingerprinting is also presented in [40].

2.8.6 Closest Neighbor

In some cases, range-based solutions cannot be used. Possible reasons can be, for example, power constraints or lack of any ranging functionality in the used protocol. In such cases, simplified methods have to be used.

The simplest method is the closest neighbor solution. The position of the closest reference node is reported as the position of the target node. This technique can be used in any communications system, but, apart from very dense systems, positioning accuracy is very low. In the case of a cellular network, this technique corresponds to finding the Cell ID currently used by the subscriber.

2.8.7 Average of Neighbors

A more advanced technique than Closest Neighbor is Average of Neighbors. This technique can be used if the target node is in range of a few reference nodes, which it can detect. The target node's position is reported as the average of the seen target nodes. This approach can be extended to cooperative positioning. The accuracy can be much improved when compared with Closest Neighbor technique, although a dense network is required. This method is particularly suited for WSNs.

2.9 Summary

This chapter presented an overview of the field of Indoor Positioning. After defining the term and discussing the reason for a separate field, possible technologies for Indoor Positioning were introduced. From the proposed technologies, only RF-based technologies had signals that were able to penetrate obstacles. From the RF-based technologies, UWB had the best ranging accuracy and multipath fading resistance.

Next, the general definition of positioning in the RF case was presented, as well as theoretical limits for positioning. Finally, different positioning techniques were evaluated. From among the presented methods, Closest Neighbor and Average of Neighbors can provide a rough position; RSS with averaging can provide accuracy in the range of 1-3m, while TOA,TDOA and AOA can provide accuracies below one meter, in optimal case even 1cm. Fingerprinting, with right parameters and/or large number of receivers, can achieve accuracy below 1 meter, but that requires many calibration measurements, which have to be repeated frequently.

Chapter 3

UWB Indoor Positioning Overview

This chapter presents an overview of UWB positioning. First, the definition of UWB and legal limits on its usage are discussed. Next, UWB systems currently in use are presented. Finally, an overview of the research topics in UWB Positioning is presented. A good general introduction to UWB positioning is presented in [9]. A good general treatment is given in [37, 29].

3.1 Definition of UWB

A UWB signal is characterized by its very large bandwidth compared to the conventional narrowband systems. According to the definition used by the FCC[3], the signal has to have either an absolute bandwidth of over 500MHz, or fractional bandwidth greater than 0.2. The bandwidth here is defined as -10dB bandwidth, between -10dB emission points.

The definition does not set the modulation used inside the band, but in practice two main UWB types emerged. Multi Band(MB) OFDM is an extension of standard OFDM techniques, used, for example in Wi-Fi networks. It is particularly well suited to high data throughputs. WiMedia Alliance Wireless USB standard uses this modulation[6].

The other possible modulation is called "impulse radio"(IR) or "direct sequence" (DS) UWB. In this case, ultra short pulses are used for transmitting information. This approach has lower cost and lower energy consumption, making it preferable for WSN type solutions. Because this dissertation focuses on positioning using cheap, energy effective devices, only IR-UWB will be discussed further.

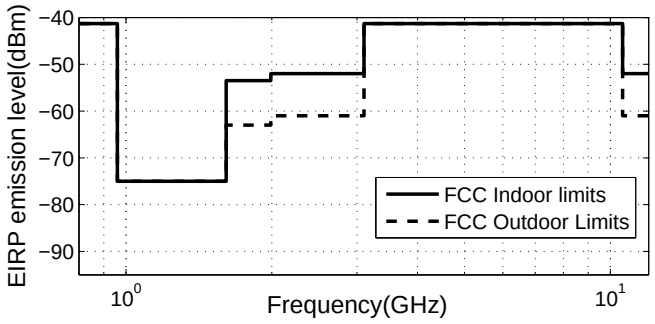

Figure 3.1: FCC(USA) emission limits for indoor and outdoor UWB systems.

3.2 UWB Regulations

The first country to codify the unlicensed use of UWB was the USA in 2002[3]. Japan followed in 2006, and the EU in 2007. The regulations imposed emission limits and other regulations on unlicensed UWB use in order to limit the interference to narrowband systems that use the same band. The original idea was to have international, synchronized UWB regulations. However, in practice different regions have different bands and slightly different regulations for UWB use.

The most lax regulations were introduced by FCC in USA[3]. The regulations set the main UWB band to from 3.1 GHz to 10.6 GHz. The radiated power in this band is limited to -41.3dBm/MHz, both indoors and outdoors. Fig. 3.1 presents the emission limits for indoor use.

European regulations are in comparison much stricter[4]. Two narrower bands, 3.4 to 4.8GHz and 6.0 to 8.5GHz, with the -41.3dBm/MHz emission limit, were designated for indoor/portable UWB systems use. Fixed outdoor systems are not covered. The lower 3.4 to 4.8GHz band can only be used with proper interference mitigation techniques. Fig. 3.2 presents the emission limits for indoor use.

Finally, the Japanese Ministry of Internal Affairs and Communications(MIC) also designated two bands, 3.4 to 4.8GHz and 7.25GHz to 10.25GHz for UWB use[5]. Emissions limits for those bands are again -41.3dBm/MHz. Only indoor systems are allowed. Interference mitigation techniques are required in the lower band. Maximum data rate is 50Mbps. Mobile, not AC mains-connected devices can only send signals after receiving a signal from a mains-connected device. Fig. 3.3 presents the emission limits for indoor use.

Singapore and Korea also have UWB regulations at the present time, and regulations in other countries will follow.

For cost reduction reasons, most mass market UWB systems will have to

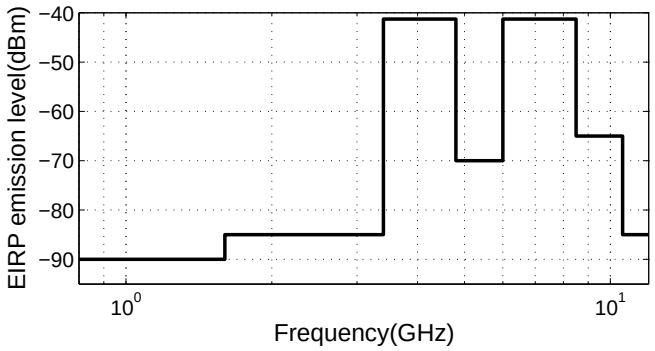

Figure 3.2: ECC(European Union) emission limits for indoor UWB systems.

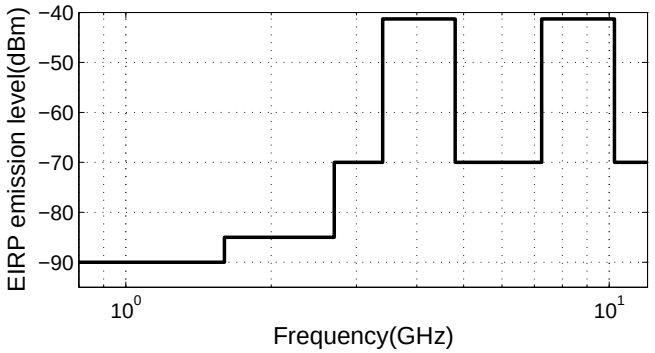

Figure 3.3: MIC(Japan) emission limits for indoor UWB systems.

comply with regulations of all major world markets. Comparing the emission limits in the USA, the EU and Japan, it can be seen that there are two bands common to all regions, 3.4 to 4.8GHz band and 7.25 to 8.5GHz band. Most of the systems will therefore use one of those two bands. Since the lower band requires interference mitigation techniques, as mentioned above, the upper band is used by most of the commercial systems. The 3.4 to 4.8GHz band was used in my measurements.

Comparing to the FCC 7.1GHz-long block of spectrum, these two bands seem small, but each band has still over 1GHz bandwidth. Also, even if the device is only designed to comply with FCC regulations, it might be wise to avoid the use of the frequencies belonging to the 5GHz ISM band. The 5GHz ISM band will in foreseeable future become as saturated with WiFi and other systems as the 2.4GHz ISM band currently is, causing strong interference to UWB systems using those frequencies.

3.3 Characteristics of UWB

The characteristics of UWB are formed by two factors; its high bandwidth and the strict power limits imposed on it. Strict limits on the radiated power seriously limit the range of UWB systems. The longest achievable range is in the order of a few hundred meters, but practical achievable indoor ranges are below a hundred meters. This limits the usefulness of UWB systems to indoors or short range outdoors applications.

The advantages of high bandwidth/good time resolution are:

- Good ranging accuracy
- Direct path resistant to multipath
- Possibility of high-speed data communications
- Low cost - baseband processing possible
- Low energy consumption - burst operation possible

The disadvantage of the high bandwidth is the amount of captured noise and interference. This disadvantage can be mitigated using one of two methods. The first method uses the fact that, if IR-UWB is used, the energy of the signal is concentrated in short pulses, usually less than 1ns in length, which, in low-rate applications, can be sparsely placed. At the same time, the noise energy is spread over time. By applying a narrow time window to the received signal, it is possible to capture most of the signal's energy while limiting the amount of captured noise. This method can be used for ranging with the proposed 802.15.4f [8] OOK-UWB PHY, or 802.15.4a UWB PHY

Another method is to encode each bit using not one, but multiple lower power pulse chips, offsetting the higher captured noise with processing gain. This approach has an advantage in the presence of interference, but, because it requires more processing and more advanced transmitter and receiver architectures, it is more expensive and power-hungry. Note that even if the first method is used, code-spreading or repetition would still be employed on top of it, but with smaller spread. The largest source of interference in the FCC UWB band are the Wi-Fi and other systems working in the 5GHz ISM band.

An additional consequence of the high bandwidth is the resolvable MPCs in the received waveform. The additional, reflection-caused delay of MPCs is usually longer than the transmitted pulse width (if IR-UWB is used). For that reason, the direct and multipath components overlap much less than in the case of less wideband systems. This makes many of the MPCs resolvable, and improves the accuracy of the direct path component detection.

Fig. 4.1 presents an example received waveform for the case of one pulse being sent. MPCs detected using CLEAN algorithm (see 5.1.5) are marked with

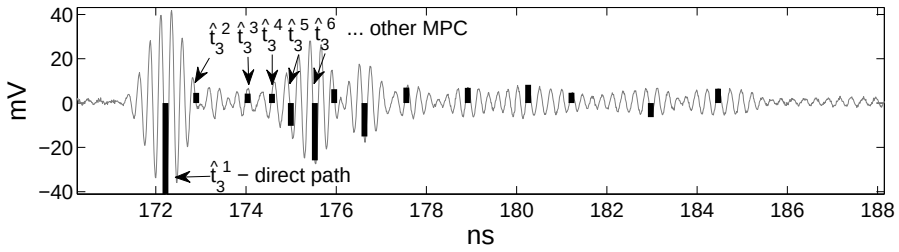

Figure 3.4: Example received waveform recorded in the lecture room environment, receiver R_3 (see Fig. 5.5). Black bars mark the detected MPCs. $\hat{t}_3^j$ are estimated TOAs of those MPCs. CLEAN algorithm (see Section 5.1.5) was used for detection.

black bars. MPCs resolvability does not principally depend on the modulation type, but on the bandwidth. MPCs are also resolvable if OFDM UWB is used, although the explanation is harder in that case.

MPC resolvability can be exploited in many ways. In the simplest approach, if the transmitted UWB pulses are sparse in time, by setting a longer integration window in the receiver, power of all the MPCs can be used, instead of just the direct path component power. This increases the energy of the signal, and limits the multipath fading effect. However, by increasing the length of an integration window more noise is also captured. The integration window's length has to be chosen so that to capture the strongest MPCs, but at the same time as little noise as possible.

Another approach is to use the channel impulse response shape as a fingerprint in fingerprinting positioning methods[40]. Coarser impulse response statistics, like mean excess delay, RMS delay spread, or maximum excess delay, can also be used for this goal. As with other fingerprinting approaches, extensive pre-measurements are needed.

Next, the impulse response statistics can be used for NLOS situation detection [41]. The impulse response shape was proven to be noticeably for LOS and NLOS cases.

Finally, MPC estimates might be used separately, as an additional source of positioning information, the approach I use.

3.4 Current UWB Positioning Systems

A few UWB-based positioning systems are already commercially available. Basing on the company literature, this section describes the two most popular commercial systems, Ubisense and Dart UWB platforms. Both systems are proprietary. The descriptions include the claimed accuracies of each system. Those

Figure 3.5: Ubisense 7000 series sensor and tag (not to scale). Taken from Ubisense website [10].

have to be taken with a grain of salt, since these accuracies were most probably achieved in best-case scenarios.

3.4.1 Ubisense

The most successful company in the field of UWB positioning is, to date, Ubisense[10]. Ubisense delivers a precise, real-time location system consisting of sensor receivers and small wearable/attachable tags. Fig. 3.5 presents the Ubisense sensor receiver and tag. The system is claimed to achieve 30cm 3D accuracy even in complex indoor environments, have a maximum sensor-tag range of 50m and be able to track the tags position a few times a second. The system is all purpose, with the main applications being in industry, transit and military training.

As to the technology, IR-UWB pulses in 6-8GHz band are used, making the system compliant with both EU and USA regulations. Each sensor uses a two by two antenna array, making 3D AOA possible. TDOA, using signals received at different sensors, is also concurrently used. UWB is used only for positioning. Communication with tags is done using conventional 2.4GHz links. Sensors communicate among themselves using standard Ethernet links, cable or Wi-Fi. The tags are reported to work for over 4 years on one battery, if 3 second update interval is used.

3.4.2 Dart UWB

Another commercial UWB positioning system is the Dart (formerly Sapphire) UWB system by Zebra Enterprise Solutions (formerly Multispectral Solutions)[12]. The system design is the same as Ubisense's, wall-mounted sensor receivers and movable tags. This system claims under 30cm accuracy, 50m indoor range, and 3500 tags per hub maximum. The system is clearly aimed at harsh industrial environments/outdoor settings.

The systems uses 6.35 to 6.75 GHz band, making it compliant with both EU and USA regulations. The used positioning technique was not specified in the literature, which suggests TDOA, a standard solution in the UWB case. UWB is used only for positioning, communication with the tags is not possible. The sensors are connected using wired Ethernet connections. The tags are reported to work for over 7 years on one battery, if 1 second update interval is used.

3.5 UWB Standards Supporting Positioning

Although standardization of high-rate UWB in the IEEE 802.15.3a task group was unsuccessful, IEEE 802.15.4a task group successfully standardized UWB PHY for low-rate WPAN, with ranging capabilities. Additionally, IEEE 802.15.4f task group[8] is currently in process of standardizing a simpler, very low-cost OOK-UWB PHY for active RFID and Real Time Location Services(RTLS).

3.5.1 IEEE 802.15.4a

The IEEE 802.15.4a UWB alternative PHY is designed for low-rate, low-power WPAN applications, such as Wireless Sensor Networks(WSN). It includes ranging capabilities, using the set preamble of 802.15.4a UWB PHY packets and a dedicated two-way ranging protocol. Ranging accuracy of below 1[m] was envisaged.

To date, two companies have created products based on this standard: IMEC[42] and Decawave[43]. IMEC has presented the first working 802.15.4a system, but the commercial-grade system is still unavailable.

In comparison, samples of the Decawave UWB ScenSor chip were already shipped to select customers. Manufacturer claims 10[cm] accuracy and 10 year life on a standard watch battery. The advantages of integrated solutions based on international standards, such as Decawave's, are low per-unit cost and versatility. The same chip can be used for either a sensor or a tag and no additional channel is needed for data. Furthermore in the future, chips from other makers should be able to work together with Decawave devices.

3.5.2 IEEE 802.15.4f

Another alternative PHY for IEEE 802.15.4 is currently being standardized by the 4f task group. This OOK-UWB PHY is aimed for very low-cost active RFID tags for RTLS. Ranging is the core functionality in these applications. Comparing to IEEE 802.15.4a, the proposed PHY uses simpler modulation scheme, lower pulse and data rate, and has generally lower requirements. My research is envisaging using this type of system for localization.

3.6 UWB Research topics

This section presents an overview of the current research topics in UWB, finishing with a subsection on using the Channel Impulse Response for positioning, the subject closest to my research.

3.6.1 UWB Channel Characterization

One of the first topics of UWB research was characterization of the indoor UWB channel[44]. Narrowband propagation models cannot be straightforwardly used for UWB propagation, because those models assume a narrowband channel. Many bigger measurement campaigns for channel characterization were motivated by the work on the IEEE 802.15.3a and IEEE 802.15.4a standards.

During work on 802.15.4a, nine environments, in which positioning systems might operate, were chosen for comparisons: residential, office, outdoor and industrial, in LOS and NLOS conditions, in addition open outdoor environment NLOS [45]. UWB channel measurement campaigns were performed in those environments [46, 47].

From these results, the model for UWB propagation channel was selected. Saleh-Valenzuela model[48] was used to model the channel impulse response. Saleh-Valenzuela models MPCs as arriving in clusters. After choosing the model, model parameters for different environments were calculated using the measurement data. Research for IEEE 802.15.4a used those models to compare different communication or positioning schemes. Presently those models are still used for method comparisons.

3.6.2 Theoretical UWB Positioning Bounds

Using a propagation model, it is possible to calculate a theoretical limit for positioning accuracy. As discussed in 2.7, Cramer-Rao(CRLB) and the Ziv-Zakai(ZZLB) lower bounds are commonly used. Some papers on the subject are [31, 33, 49, 50, 34, 27, 51].

Early papers concentrated on CRLB and simpler propagation models, while the current papers generally calculate the tighter ZZLB in different NLOS scenarios.

3.6.3 UWB Receivers

Because of the unique problems of UWB receivers, there is much research on them. The first problem is that, because of the high bandwidth signal, reception of the UWB signal is problematic. The second problem is the resolvable multi-

path nature of the channel, a challenge but also an opportunity. Three receiver types are usually considered.

Early papers concentrated on RAKE-type receivers[52, 53]. RAKE receivers have many taps, or "fingers". Each finger is synchronized to one delayed copy of the received signal, MPC. The energy from each finger is then combined for optimal detection. RAKE receivers are able to efficiently utilize the energy of later arriving MPCs. However, it became clear that the number of RAKE fingers needed to capture a big part of the UWB signal is very high, making the receivers complex, power-hungry and expensive. Additionally, the high data rate UWB become dominated by MB-OFDM-based systems (Wimedia Alliance's Wireless USB), and not IR-UWB. In low-rate, low-cost applications, low cost and low power of the receiver are the primary concerns.

The focus has since then moved to reduced complexity receivers, such as threshold[33], Transmitted Reference [54, 55] and Energy receivers[56]. Those receivers are more appropriate for low-cost applications predicted by 802.15.4a. The energy receiver is a subject of special attention because of the low complexity and possibility of non-coherent use.

The third receiver type is a direct sampling receiver. It is at presently possible to directly sample a UWB signal, but it is very difficult, with multiple high speed Analog-Digital Converters(ADC), wide data buses and huge power consumption. This type of receiver is the most versatile, it potentially offers the best possible quality of reception. However, at present it is confined to laboratories.

It is important to note that, although currently the reduced complexity receivers are the mainstream of used receivers, with advances in miniaturization, more sophisticated receiver architectures, RAKE and direct sampling, will become cost-effective.

3.6.4 NLOS Problem

One of the greatest problems for UWB indoor positioning is when a link to a reference node is in NLOS condition. The majority of the time-based positioning methods assume that it is possible to detect the direct path component, whose delay corresponds to the distance between the reference and target nodes. However, in a NLOS condition, this path is blocked by an obstacle. If the direct path is not detected, the receiver will miss-interpret a later MPC as the direct path, causing the so called NLOS error. The NLOS error is always positive and, because of UWB's good ranging accuracy, usually dominates the total error.

The NLOS problem was analyzed theoretically in [27]. An important result of this study was that, unless there is information available about the NLOS error (probability density function, mean error, etc.), ranges containing NLOS

error should be ignored.

Many methods for the mitigation of the NLOS error were proposed. The simplest method, for greater than necessary number of reference nodes, relies on performing least squares-based positioning using subsets of the reference nodes. The subset has to contain at least 3 receivers in the case of 2D TOA ranging, 4 for 3D TOA, or 5 for 3D TDOA. Each subset is then assessed basing on the residual of the LS solution. Subsets containing reference nodes with links in NLOS condition should have much higher residual. [57] proposes to choose the best set basing on the lowest residual. [58] proposes a weighted solution, the estimated position is a weighted average of positions calculated for each set, weight being an inverse of the residual.

Other approach is to first detect links in the NLOS condition, and then either ignore those links, or use them in a different way. [41] presents a comprehensive list of NLOS condition detection methods. The methods mentioned include: calculating variance of a series of range measurements, using the channel impulse response statistics(also proposed in [59]) and changes in SNR. In [60] this approach is used for 3 receiver TOA positioning. If all three measurements are detected as LOS, all three are used. If one of is detected as NLOS, it is ignored, and the position is calculated assuming instead that the hight didn't change since the last three receiver measurement.

This is one of the cases when the methods proposed in this dissertation can be used. If, after rejecting NLOS links, the number of available receivers is only 2(for TOA) or 3(for TDOA), the proposed methods can be used to improve positioning accuracy.

If the range error probability density function(PDF) for the environment is known, a simple solution is to use a Maximum Likelihood solution for the position of the target node, instead of LS. However, to know the PDF, premeasurements are required. To partially remove this restriction, PDF can be modeled by assuming a simplified NLOS scattering model[61].

Finally, if tracking is used, movement from a LOS to NLOS region produces a quick change in position. This can be detected and used to filter out NLOS measurements.

3.6.5 Tracking

In practical systems, there will be multiple observations of a target node's position over a period of time. Using all observations, more accurate position estimation can be performed. If the target is stationary, many simple techniques, such as position averaging, can be used to improve the position estimate. However, in many practical cases, the target node will be moving. The problem of

estimating an object's position at consecutive time instants is called tracking. The problem is usually expressed in mathematical terms as a Markov process.

The simplest way of position tracking is the Kalman filter[62]. Kalman filter can be used for tracking the position, or the position and speed. The advantage of the Kalman filter is the low computational complexity. The disadvantages are the underlying assumptions of a linear system and a Gaussian error distribution. Unfortunately, positioning is not a linear problem, and the error distribution is, in many cases, poorly approximated by Gaussian. This is especially the case if NLOS error is taken into consideration.

To address those problems of the Kalman filter, more advanced approaches were proposed. Extended Kalman filters and unscented Kalman filters were designed to function properly also for non-linear problems. Finally, a method called Particle Filter, also known as sequential Monte Carlo(SMC), was proposed. Particle filters approximate the posterior probability of a state with a number of samples. Any probability distribution can be represented, not only Gaussian. [63] presents a good example of using a particle filter for tracking. NLOS errors were among the parameters tracked.

It also interesting to note that the method described in [63] makes use of inertial positioning. Inertial positioning can be easily incorporated into tracking.

3.6.6 Using Channel Impulse Response/MPCs

One of the features of UWB is its good time resolution of the UWB signal, and, consequently, resolvable MPCs in the received waveforms, forming a Channel Impulse response(CIR). This feature can be used to improve positioning in many ways.

On way is to use the shape of the CIR to detect the NLOS condition as mentioned in section 3.6.4[41]. CIR shape is, on average, significantly different between LOS and NLOS cases, and can be used for distinguishing the two cases.

Another approach is proposed in [64]. A few strong MPCs are being continually tracked using an Extended Kalman Filter. In the event of the disappearance of a direct path, the MPCs are used as a backup for ranging positioning information until the direct path reappears.

The paper closest to my own research is [65]. The authors perform 2D positioning using a single receiver and the knowledge of the walls in the environment. The idea of using MPC ranges and reflector-mirrored receivers/anchors is very close to my approach, but by performing only a 2D simulation with walls as the only reflectors, the achieved results are not representative of a real environment.

Chapter 4

Proposed Reflection-Aided Positioning Methods

The aim of this chapter is to describe in detail the proposed reflection-based positioning methods. The proposed methods assume a detectable direct path, in other words a LOS situation. The first section presents an overview of the problem, the reason for using reflections, and the problems inherent in it. The second section describes the system model. It contains the definitions of the terms and system elements used in the method descriptions. Conventional positioning methods, that the proposed methods will be compared with, are presented in the third section. The next three sections present the three proposed methods, 2 Receiver TOA RAML, 2 Receiver TOA RALS and 3 Receiver TDOA DRAML. Finally, the last section contains a summary of the chapter.

4.1 Problem Overview

This section presents the problem of positioning with few receivers, reasons for using reflections, and problems caused by this approach.

Conventional 3D Positioning methods require at least 3 receivers for TOA, or 4 receivers for TDOA positioning. Those numbers already assume a basic a-priori knowledge, since solving positioning equations with 3/4 receivers will usually result in two possible transmitter positions, one of which has to be chosen. As an example of such required a-priori knowledge, GPS system assumes that the user is not in outer space, but close to Earth, and most indoor ceiling-mounted positioning systems will assume that the user is below, not above, the ceiling.

In some situations, the minimum required number of LOS receivers for 3D

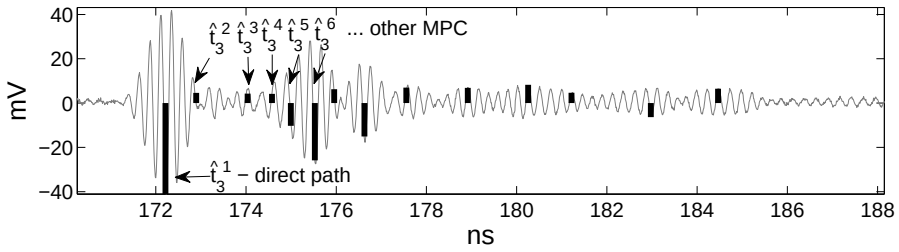

Figure 4.1: Example received waveform recorded in the lecture room environment, receiver R_3 (see Fig. 5.5). Black bars mark the detected MPCs. $\hat{t}_3^j$ are estimated TOAs of those MPCs. CLEAN algorithm (see Section 5.1.5) was used for detection.

positioning is not available. The UWB transmitters have a short range, and shadowing caused by obstacles can block the direct path. Additionally, for financial reasons, the receiver density will often be as low as possible. If the number of receivers is one too few, the conventional approach is to reduce the problem to 2D by assuming height [60]. The advantage of this approach is its simplicity. However, in this approach, the height of the transmitter cannot be determined, which might be a problem for some applications. Additionally, even if only 2D position is considered, wrongly assumed height can introduce a significant positioning error.

To be able to perform 3D positioning, but with fewer than the conventional minimal number of receivers, more information is needed. My proposed solution is to use the later arriving MPCs in the received waveform, together with the knowledge of big flat reflective surfaces in the environment. Time resolution of the UWB signal is high enough to distinguish not only the direct-path component, but also later arriving MPCs. MPCs are largely caused by reflections and diffractions from indoor features, furniture or people. Indoor features usually include big, flat reflective surfaces, ceilings and walls, subsequently called reflectors. MPCs caused by reflections from the reflectors can be used for positioning. Fig. 4.1 presents an example received waveform. MPCs detected using CLEAN algorithm (see 5.1.5) are marked with black bars.

If, considering one reflector-receiver pair, it was known which MPC detected in the received waveform matched the reflection from the reflector, using this MPC for positioning would be relatively easy. In an example shown in Fig. 4.2, 5 MPCs with time of arrival (TOA) estimates $[\hat{t}_n^1, \cdots, \hat{t}_n^5]^T$ are detected in the waveform received by the receiver R_n, where n is the receiver number. First TOA, $\hat{t}_n^1$, in LOS conditions, corresponds to the direct path, making it useful for positioning. If it is known that $\hat{t}_n^4$ corresponds to reflection from the reflector FR_m, where m is the reflector's number, $\hat{t}_n^4$ can also be useful. $\hat{t}_n^4$ can be used as

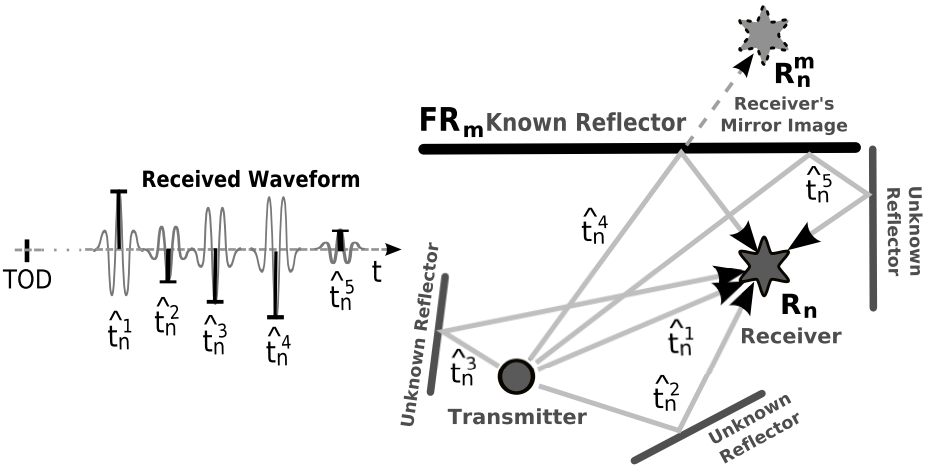

Figure 4.2: Reflections example – 5 MPC TOAs $[\hat{t}_n^1, \cdots, \hat{t}_n^5]^T$ are detected at receiver R_n. In LOS conditions, the first TOA matches the direct path. Problem - Which TOA matches the FR_m-reflected path?

Table 4.1: Methods used for TOA and TDOA positioning.

No. of receivers	**4**	**3**	**2**
TDOA 4 unknowns	Direct Solution (DS)	**DRAML**, Assumed Height(AH)	Future research
TOA 3 unknowns	Least Squares, ML, etc.	Direct Solution (DS)	**RAML**, **RALS**, Assumed Height(AH)

an additional TOA measurement at R_n^m, the mirror image of the real receiver through reflector. However, in reality, it is not known which MPC matches the reflection. In the example, it could be any of the detected MPCs, including MPCs caused by the three unknown reflectors, and also direct-path $\hat{t}_n^1$.

In my research, I developed two positioning methods for TOA and TDOA positioning that use later arriving MPCs, while solving the problem discussed in the previous paragraph. The relationship between the conventional methods and the methods that will be described in this chapter is illustrated in Table 4.1. Methods proposed by me are distinguished with bold font.

The marked methods in the table have already been presented in a series of papers. In [66], I presented a Reflection-Based Least Squares method(RALS) for 2 receiver TOA positioning. In [67], I presented a more accurate Reflection-Aided Maximum Likelihood(RAML) method for 2 receiver TOA positioning. This method is described in Section 4.4. In [68], I presented the TDOA Reflection-Aided Maximum Likelihood(DRAML) method for 3 receiver TDOA positioning.

This method is described in Section 4.6.

4.2 System Model

This section defines the terms used in the method description. Those include the system components: transmitter, receivers, reflectors; as well as the terms used to describe MPCs in the received waveforms.

Consider a system with a mobile UWB transmitter and a set of N stationary, synchronized receivers $\mathcal{R} = \{\mathrm{R}_1, \ldots, \mathrm{R}_N\}$. Let $\mathbf{b} = [x_b,\ y_b,\ z_b]^T$ be a vector representing the unknown 3D position of the transmitter and let $\mathbf{r}_n = [x_n,\ y_n,\ z_n]^T, n \in \{1, \ldots, N\}$ vector represent the known position of R_n. The superscript "T" stands for transpose. The transmitter transmits a pulse waveform. Waveform received by $\mathrm{R}_n \in \mathcal{R}$ is often represented in the literature as:

$$r_n(t) = \sum_{k=1}^{K_n} \alpha_n^k s(t - \tau_n^k) + e_n(t) \tag{4.1}$$

where K_n is the number of MPCs, α_n^k and τ_n^k are the fading coefficient and the delay of the k_{th} MPC, respectively, $e_n(t)$ is a zero-mean additive white Gaussian noise (AWGN) and $s(t)$ is the transmitted pulse waveform. Subscript n is the receiver number to which the parameter applies, $n \in \{1, \cdots, N\}$.

The position of the transmitter $\mathbf{b}$ is considered to be inside a Service Area SA, defined by a vector $[x_{\min},\ y_{\min},\ z_{\min},\ x_{\max},\ y_{\max},\ z_{\max}]^T$:

$$\mathbf{b} \in \mathrm{SA} \Leftrightarrow \begin{array}{l} x_{\min} \le x_b \le x_{\max} \\ y_{\min} \le y_b \le y_{\max} \\ z_{\min} \le z_b \le z_{\max} \end{array} \tag{4.2}$$

The transmitter position probability distribution in the SA is considered to be unknown.

Let $\mathcal{FR} = \{\mathrm{FR}_1, \cdots, \mathrm{FR}_M\}$ be a set of known M big, flat reflective surfaces, for example ceilings and walls. Each reflector FR_m is defined by roughness $\sigma^2_{\mathrm{FR}_m}$ and a 3D surface equation:

$$\begin{array}{l} A_m x + B_m y + C_m z + D_m = 0 \\ \sqrt{A_m^2 + B_m^2 + C_m^2} = 1 \end{array} \tag{4.3}$$

where $[A_m,\ B_m,\ C_m,\ D_m]^T$ is a vector of the normalized surface coefficients of FR_m and $[x,\ y,\ z]^T$ is a vector of coordinates in 3D space. $[A_m,\ B_m,\ C_m]^T$ is the normal vector of FR_m, which is one of the advantages of this surface's

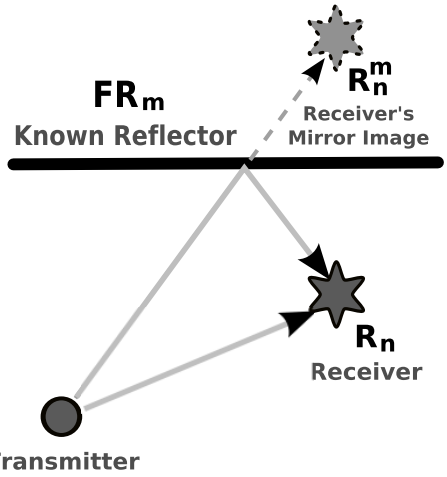

Figure 4.3: Relationship between the receiver R_n, reflector FR_m and reflected receiver R_n^m.

representation.

Roughness $\sigma^2_{FR_m}$ is the MPC range variance caused by the reflection from FR_m. $\sigma^2_{FR_m}$ models the error in the reflector position and the influence of the irregularities of the reflector. Reflector position error is caused by imperfect surveying/estimation of the position. Reflector irregularities are the differences between the modeled flat reflector and the real reflector. Some examples are: wall outcroppings/niches, lights, blackboards, etc. . A Gaussian, non-angle dependent error function is the simplest way to statistically model the mentioned two error sources.

A FR_m-reflected path between the transmitter and R_n can be represented by a direct path between the transmitter and R_n's mirror image through FR_m. Let R_n^m designate the mirror image of R_n through FR_m. In addition, let $\mathbf{r}_n^m = [x_n^m,\ y_n^m,\ z_n^m]^T$ designate the position vector of R_n^m. $\mathbf{r}_n^m$ can be calculated as:

$$\mathbf{r}_n^m = \mathbf{r}_n - 2\Big(\mathbf{r}_n \cdot \begin{bmatrix} A_m \\ B_m \\ C_m \end{bmatrix} + D_m\Big) \begin{bmatrix} A_m \\ B_m \\ C_m \end{bmatrix} \tag{4.4}$$

where "$\cdot$" is the scalar product. Fig. 4.3 shows the relationship between R_n,FR_m and R_n^m.

In the ranging step, each receiver R_n can detect not only the first, but all distinct MPCs in the received waveform. For each R_n, let $\mathbf{t}_n$ be a vector of detected MPC Time of Arrival(TOA) estimates $\mathbf{t}_n = [\hat{t}_n^1, \ldots, \hat{t}_n^{J_n}]^T$, where J_n is the number of detected MPCs. Each TOA is an estimate of the sum of MPC's delay τ_n^j and a Time of Departure(TOD), $\hat{t}_n^j = \hat{\tau}_n^j + t_D$. $\hat{t}_n^j$ is assumed to have a

Gaussian error distribution, $\hat{t}_n^j \sim N(t_n^j, (\sigma_n^j/C)^2)$. This assumption implies that the direct path was detected, LOS situation.

In the case of TOA ranging, TOD is known and, assuming free space propagation, a vector of MPC range estimates $\mathbf{d}_n = [\hat{d}_n^1, \cdots, \hat{d}_n^{J_n}]^T$ can be calculated as:

$$\hat{d}_n^j = (\hat{t}_n^j - t_{\mathrm{D}})\mathrm{C}, \quad j = 1, \ldots, J_n \tag{4.5}$$

$$\hat{d}_n^j = d_n^j + e_n^j \sim N(0, {\sigma_n^j}^2) \tag{4.6}$$

where C is the speed of light and t_{D} is the TOD.

In the case of TDOA ranging, TOD is not known. Without the knowledge of TOD, the direct calculation of ranges is impossible. Range differences, using the first MPC detected at R_1 ($\hat{t}_1^1$) as reference, are calculated instead. In order for the range differences to be always positive, the receivers are reordered so that $\hat{t}_1^1$ is the lowest TOA. R_1 is swapped with the receiver corresponding to the lowest $\hat{t}_n^1$, R_n. Assuming free space propagation, a vector of MPC range difference estimates $\mathbf{l}_n = [\hat{l}_n^1, \cdots, \hat{l}_n^{J_n}]^T$ is calculated as:

$$\hat{l}_n^j = (\hat{t}_n^j - \hat{t}_1^1)C, \quad j = 1, \ldots, J_n \tag{4.7}$$

$$\hat{l}_n^j = l_n^j + e_n^j \sim N(0, {\sigma_n^j}^2 + {\sigma_1^1}^2) \tag{4.8}$$

A total of N vectors is calculated, one for each receiver. This includes R_1, for which $\hat{l}_1^1 = 0$.

4.3 Conventional Positioning Methods

This section describes the conventional positioning methods, starting with TOA methods and continuing with TDOA methods.

4.3.1 Conventional TOA Positioning

In a general case, if N receivers are available, the transmitter's position vector, $\mathbf{b} = [x_b,\ y_b,\ z_b]^T$, can be estimated by solving a set of quadratic equations:

$$\begin{cases} (x_b - x_1)^2 + (y_b - y_1)^2 + (z_b - z_1)^2 = {\hat{d}_1^1}^2 \\ \qquad\qquad\qquad \vdots \\ (x_b - x_N)^2 + (y_b - y_N)^2 + (z_b - z_N)^2 = {\hat{d}_N^1}^2 \end{cases} \tag{4.9}$$

where $\mathbf{r}_n = [x_n,\ y_n,\ z_n]^T$ is the position vector of receiver R_n and $\hat{d}_n^1$ is the estimate of the direct-path distance to R_n.

For $N > 3$, this set of equations is overdetermined. Many positioning methods have been proposed for use in this case. The simplest method is to calculate the least squares solution, which corresponds to the maximum likelihood solution in the case of equal, Gaussian ranging errors. If more information about the ranging error probability distribution is known, more elaborate maximum likelihood methods can be used.

In the case of $N = 3$, the conventional method is to solve the equation set directly. This case, the TOA Direct Solution(TOA-DS), will be discussed in detail in this section.

In the case of $N = 2$, the conventional method is to assume height and solve the equation set in 2D. This case, the TOA Assumed Height(TOA-AH), will also be discussed in detail in this section, after DS.

3 Receiver TOA Direct Solution(TOA-DS)

If $N = 3$, three receivers are available, the equation set (4.9) becomes:

$$\begin{cases} (x_b-x_1)^2+(y_b-y_1)^2+(z_b-z_1)^2 = \hat{d_1^1}^2 \\ (x_b-x_2)^2+(y_b-y_2)^2+(z_b-z_2)^2 = \hat{d_2^1}^2 \\ (x_b-x_3)^2+(y_b-y_3)^2+(z_b-z_3)^2 = \hat{d_3^1}^2 \end{cases} \tag{4.10}$$

This equation set is normally directly solvable, yielding two solutions. One of them has to be chosen, which can be a problem. In many cases, one of the solutions will fall outside of the Service Area(SA) of the system, and can be discarded. This is usually the case for indoor positioning systems. If the positioning system is ceiling-mounted, one solution will always be above the ceiling. Another common way of dealing with the problem of two solutions is to choose the solution closer to the previous transmitter's position, if that is available. Fig. 4.4 presents an example of TOA-DS positioning.

2 Receiver TOA Assumed Height(TOA-AH)

Equation set (4.9) does not have point solutions for $N = 2$. The conventional approach in this case, proposed for example in [60], is to reduce the problem to 2D by assuming the value of the height coordinate. With that assumption, the equation set becomes:

$$\begin{cases} (x_b-x_1)^2+(y_b-y_1)^2+(z_b-z_1)^2 = \hat{d_1^1}^2 \\ (x_b-x_2)^2+(y_b-y_2)^2+(z_b-z_2)^2 = \hat{d_2^1}^2 \\ y_b = h_b \end{cases} \tag{4.11}$$

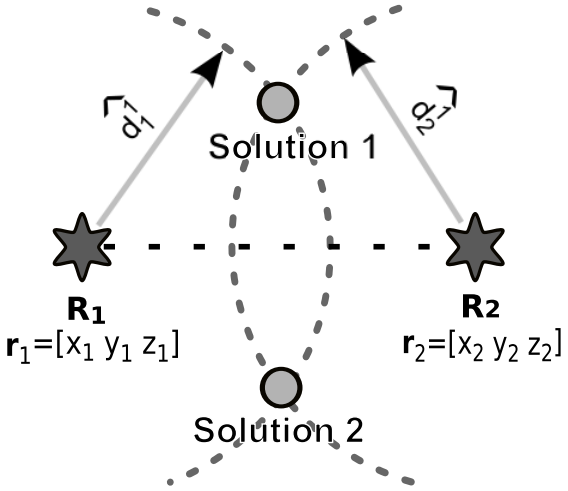

Figure 4.4: Example of TOA-DS Positioning. 2 receiver 2D example shown for ease of presentation. Two solutions can be observed.

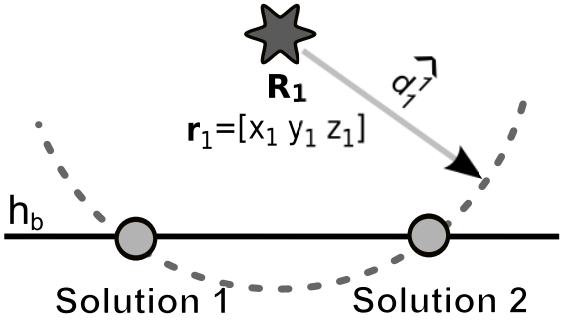

Figure 4.5: Example of TOA-AH Positioning. 1 receiver 2D example shown for ease of presentation. Two solutions can be observed.

where h_b is the receiver's assumed height. h_b should be set to the mean expected height of the transmitter. If no information on height is available, then the mean height of the Service Area(SA) can be used.

This method performs well if the transmitter's height is nearly constant. One example is a transmitter attached to a shopping cart. However, if the height changes, as it does in the case, for example, when the transmitter is attached to a warehouse box, the result can have a large error, also when only 2D position is considered.

Additionally, the equation set has, like in the 3 receiver DS case, two solutions. Unfortunately, compared with the DS case, both of those solutions fall inside SA bounds in many more usage scenarios.

Fig. 4.5 presents an example of TOA-AH positioning.

4.3.2 Conventional TDOA Positioning

In a general TDOA positioning case, if N receivers are available, the transmitter's position vector, $\mathbf{b} = [x_b,\ y_b,\ z_b]^T$, can be estimated by solving a set of equations:

$$\begin{cases} \hat{l}_2^1 = \sqrt{(x_b - x_2)^2 + (y_b - y_2)^2 + (z_b - z_2)^2} \\ \qquad -\sqrt{(x_b - x_1)^2 + (y_b - y_1)^2 + (z_b - z_1)^2} \\ \qquad\qquad \vdots \\ \hat{l}_N^1 = \sqrt{(x_b - x_N)^2 + (y_b - y_N)^2 + (z_b - z_N)^2} \\ \qquad -\sqrt{(x_b - x_1)^2 + (y_b - y_1)^2 + (z_b - z_1)^2} \end{cases} \tag{4.12}$$

where $\mathbf{r}_n = [x_n,\ y_n,\ z_n]^T$ is the position vector of receiver R_n and $\hat{l_n^1}$ is the estimate of the range difference between the range to R_n and to R_1. Each equation of (4.12) expresses a hyperboloid. This hyperboloid is a locus of points with difference of ranges to R_1 and R_n equal to $\hat{l}_n^1$.

For $N > 4$, this set of equations is overdetermined and, as in the TOA case, many different positioning methods are possible. This includes least squares, maximum likelihood, discarding unreliable measurements, and others.

In the case of $N = 4$, the conventional method is to solve the equation set directly. This case, the TDOA Direct Solution(TDOA-DS), will be discussed in detail in this section.

In the case of $N = 3$, the conventional method is to assume height and solve the equation set in 2D. This case, the TDOA Assumed Height(TDOA-AH), will also be discussed in detail in this section, after DS.

4 Receiver TDOA Direct Solution(TDOA-DS)

If $N = 4$, three range differences are available, the equation set (4.12) becomes:

$$\begin{cases} \hat{l}_2^1 = \sqrt{(x_b - x_2)^2 + (y_b - y_2)^2 + (z_b - z_2)^2} \\ \qquad -\sqrt{(x_b - x_1)^2 + (y_b - y_1)^2 + (z_b - z_1)^2} \\ \hat{l}_3^1 = \sqrt{(x_b - x_3)^2 + (y_b - y_3)^2 + (z_b - z_3)^2} \\ \qquad -\sqrt{(x_b - x_1)^2 + (y_b - y_1)^2 + (z_b - z_1)^2} \\ \hat{l}_4^1 = \sqrt{(x_b - x_4)^2 + (y_b - y_4)^2 + (z_b - z_4)^2} \\ \qquad -\sqrt{(x_b - x_1)^2 + (y_b - y_1)^2 + (z_b - z_1)^2} \end{cases} \tag{4.13}$$

This equation set is normally directly solvable, yielding one or two solutions. As in TOA-DS, in most cases, one of the solutions will fall outside of the SA of the system, and can be discarded. This is usually the case for indoor positioning systems. Fig. 4.6 presents an example of TDOA-DS positioning.

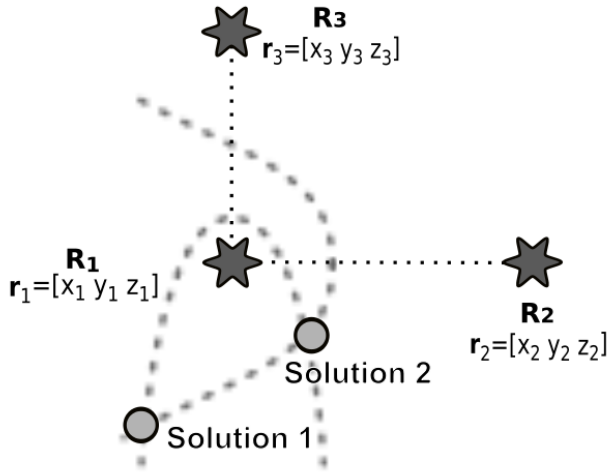

Figure 4.6: Example of TDOA-DS Positioning. 3 receiver 2D example shown for ease of presentation. Either one or two solutions can be observed.

3 Receiver TDOA Assumed Height(TDOA-AH)

The equation set (4.12) does not have point solutions for $N = 3$. As in the TOA-AH case, the conventional solution here is to reduce the problem to 2D by assuming the height coordinate. With that assumption, the equation set becomes:

$$\begin{cases} \hat{l}_2^1 = \sqrt{(x_b - x_2)^2 + (y_b - y_2)^2 + (z_b - z_2)^2} \\ \qquad -\sqrt{(x_b - x_1)^2 + (y_b - y_1)^2 + (z_b - z_1)^2} \\ \hat{l}_3^1 = \sqrt{(x_b - x_3)^2 + (y_b - y_3)^2 + (z_b - z_3)^2} \\ \qquad -\sqrt{(x_b - x_1)^2 + (y_b - y_1)^2 + (z_b - z_1)^2} \\ \quad y_b = h_b \end{cases} \tag{4.14}$$

where h_b is the assumed receiver's height.

As in the TOA-AH case, this method performs well if the transmitter's height is nearly constant, but if the height varies, the result can have a large error, regardless of whether 3D or 2D position is considered.

In another similarity with the TOA-AH case, this equation set has, in some cases, two solutions. However, if receivers are at similar heights, there will be only one solution. For that reason, the two-solution problem occurs very rarely in the case of TDOA-AH. Fig. 4.7 presents an example of TDOA-DS positioning.

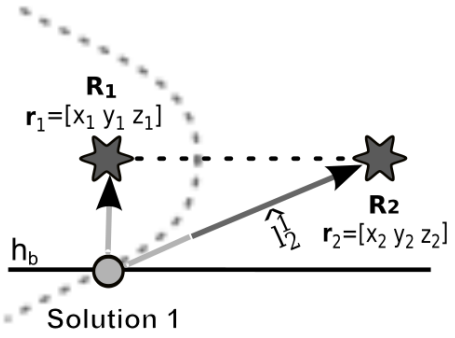

Figure 4.7: Common example of TDOA-AH Positioning. 2 receiver 2D example shown for ease of presentation. Although in some cases two solutions are possible, in most practical cases only one is observed.

4.4 TOA Reflection-Aided Maximum Likelihood (RAML) 2 Receiver Positioning Method

This section presents the Reflection-Aided Maximum Likelihood method for 2 receiver 3D positioning. The method is divided into two steps. The first step consists of using the positions of two receivers, $\mathbf{r}_1$ and $\mathbf{r}_2$, in addition to the detected direct ranges, $\hat{d}_1^1$ and $\hat{d}_2^1$, for finding the Result Circle(RC). The transmitter's position is assumed to be near RC. The second step consists of finding the best transmitter position estimate on the RC. This is achieved by calculating a likelihood function for the points on the RC, using the knowledge of all detected MPCs ($\mathbf{d}_1$, $\mathbf{d}_2$), $\mathcal{FR}$ and SA. The point on the RC with the maximum likelihood is chosen as the estimated transmitter position.

For the method to succeed, the following two assumptions must hold. First, for each R_n, the MPC corresponding to the direct path is detected in the received waveform. In other words, LOS conditions. Second, most MPCs caused by reflection from $\mathrm{FR}_m \in \mathcal{FR}$ are also detected. Under these assumptions, the first MPC range, $\hat{d}_n^1$, corresponds to the direct path between transmitter and R_n. $\mathbf{d_n}$ also contains a subset corresponding to reflections from $\mathrm{FR}_m \in \mathcal{FR}$. This subset is not known in advance.

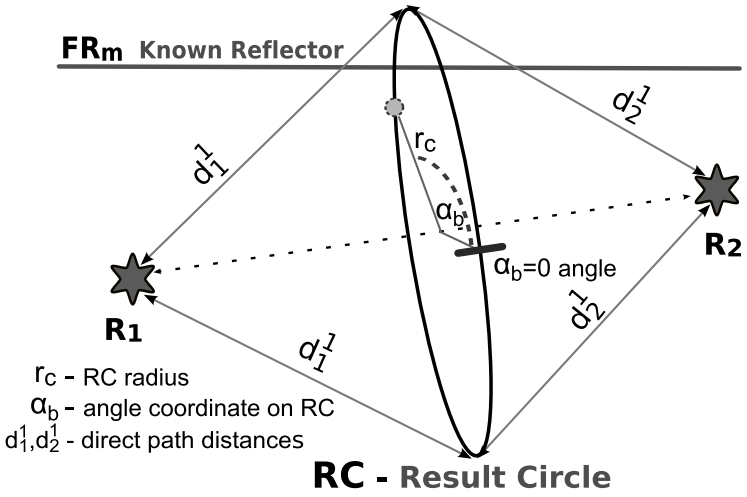

Figure 4.8: Result Circle - locus of points at a range of $\hat{d}_1^1$ from R_1 and $\hat{d}_2^1$ from R_2. Point's position on RC is described by $\alpha_b r_c$.

4.4.1 Result Circle (RC)

If direct range estimates to only two receivers are available, equation set (4.9) becomes:

$$\begin{cases} (x_b-x_1)^2+(y_b-y_1)^2+(z_b-z_1)^2 = \hat{d}_1^{1\,2} \\ (x_b-x_2)^2+(y_b-y_2)^2+(z_b-z_2)^2 = \hat{d}_2^{1\,2} \end{cases} \tag{4.15}$$

Each equation represents a 3D sphere. Consequently, the solution of (4.15) is an intersection of the two spheres, in a non-degenerate case, a 3D circle. Let the circle be designated as the Result Circle (RC). An example RC is shown in Fig. 4.8. A reference zero angle is marked. The transmitter is near the RC, if errors of direct-path range estimates, $\hat{d}_1^1$ and $\hat{d}_2^1$, are small. In particular, the Non-Line of Sight(NLOS) error, error which appears if direct-path MPC was not detected, needs to be zero or very small. Since the transmitter should be near the RC, the transmitter position estimate will be chosen from points on the RC, $\hat{\mathbf{b}} \in$ RC. The transmitter is also considered to be inside the SA, therefore $\hat{\mathbf{b}} \in \text{SA} \cap \text{RC}$.

The RC can be described with radius r_c and transformation $Q(\cdot)$, where $Q(\cdot)$ is a translation plus rotation that moves a flat($z_b' = 0$) 2D circle of radius r_c centered at $[0,\ 0,\ 0]^T$ from XY plane to RC's position. A point on the RC can be described as a function of, equivalently, either angle α_b or arc (radius times angle) $r_c\alpha_b$, from a chosen $\alpha_b = 0$ reference. Arc is used because it is also used in the method's implementation. Since the point is a transmitter position estimate candidate vector, it will be denoted as $\hat{\mathbf{b}}(r_c\alpha_b) = [x_b,\ y_b,\ z_b]^T$. $\hat{\mathbf{b}}(r_c\alpha_b)$

for a given $r_c\alpha_b$ can be calculated as:

$$\begin{cases} x'_b = r_c \cos\alpha_b \\ y'_b = r_c \sin\alpha_b \\ z'_b = 0 \end{cases} , \hat{\mathbf{b}}(r_c\alpha_b) = Q\Big(\begin{bmatrix} x'_b \\ y'_b \\ z'_b \end{bmatrix} \Big) \tag{4.16}$$

where $\hat{\mathbf{b}}' = [x'_b,\ y'_b,\ z'_b]^T$ is the point's position on the RC in the prime base, before $Q(\cdot)$ transformation, while $\hat{\mathbf{b}}(r_c\alpha_b)$ is point's position after RC is moved to its actual location. Only $r_c\alpha_b : \hat{\mathbf{b}}(r_c\alpha_b) \in SA$, are considered.

4.4.2 Position on RC Calculation Algorithm

The second step of the proposed method consists of finding the best transmitter position estimate on the RC, $\hat{\mathbf{b}}(r_c\alpha_b)$. To accomplish this, a maximum likelihood estimator using later detected MPCs contained in vectors $\mathbf{d_1}$ and $\mathbf{d_2}$, in addition to knowledge of $\mathcal{FR}$, is used.

Instead of considering $\mathcal{R}$, $\mathcal{FR}$, $\mathbf{d_1}$ and $\mathbf{d_2}$ together, the problem can be divided, with each $(\mathrm{R}_n, \mathrm{FR}_m) \in \mathcal{R} \times \mathcal{FR}$ pair being considered separately. "$\times$" here is the Cartesian product. The result for each pair is a partial likelihood function defined for $\hat{\mathbf{b}} \in \mathrm{SA} \cap \mathrm{RC}$, $L_n^m(\mathbf{d_n}; r_c\alpha_b)$. Functions for each pair can then be combined for a final result. A $(\mathrm{R}_n, \mathrm{FR}_m)$ pair represents a FR_m-reflected path from transmitter to R_n. As mentioned in Section 4.2, this path can be also represented with a direct path from transmitter to R_n^m, R_n's reflection through FR_m.

Partial Likelihood Function Derivation

As the first approach, let $\hat{d}_n^j$ be a known a priori MPC range matching the FR_m-reflected path to R_n. This assumption is for explanation purposes only, since it is not true for the proposed method. Let $d_{(n,m)}$ be the real FR_m-reflected path length to R_n, of which $\hat{d}_n^j$ is an estimate. If $\hat{d}_n^j$ error is assumed to be Gaussian, $\hat{d}_n^j \sim N(d_{(n,m)}, {\sigma_n^j}^2 + {\sigma_{\mathrm{FR}_m}}^2)$, the likelihood function is:

$$L_n^m(\hat{d}_n^j; d_{(n,m)}) = N_{\mathrm{rm}} \exp\Big(\frac{-1}{2} \frac{(d_{(n,m)} - \hat{d}_n^j)^2}{{\sigma_n^j}^2 + {\sigma_{\mathrm{FR}_m}}^2} \Big) \tag{4.17}$$

where N_{rm} is a normalization constant, and exp is the exponential function. $L_n^m(\hat{d}_n^j; d_{(n,m)})$ should be considered as a function of $d_{(n,m)}$. $L_n^m(\hat{d}_n^j; d_{(n,m)})$ is a Gaussian function centered at $\hat{d}_n^j$. This result is understandable since this simple case corresponds to having one direct-path range estimate to R_n^m.

In practice, there is no a priori knowledge about FR_m-MPC matches. Any detected MPC range may match $d_{(n,m)}$. Additionally, the matching MPC range

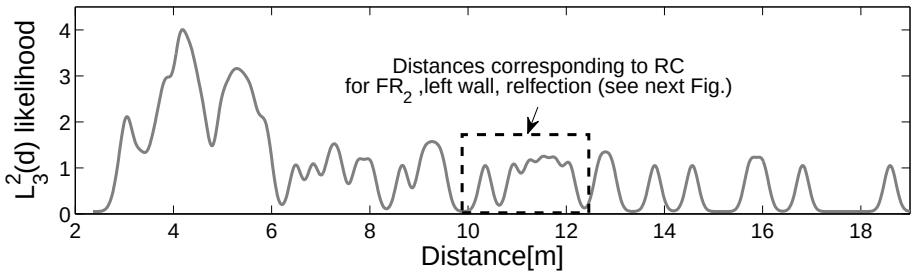

Figure 4.9: Example $L_n^m(\mathbf{d}_n; d)$ partial likelihood function plotted as a function of range from R_n^m. Measurement data for lecture room environment, $\mathrm{B_{REF}}$, and R_3 are used (see Fig. 5.5). N_{rm} is set to 1(see Eq. (4.18)).

is not always detected and present in $\mathbf{d}_n$. Considering those two problems, a more realistic $d_{(n,m)}$ likelihood function can be constructed as:

$$L_n^m(\mathbf{d_n}; d_{(n,m)}) = N_{\mathrm{rm}} \left(P_{\mathrm{ndet}} + \sum_{j=1}^{J_n} P_j \exp\left(\frac{-1}{2} \frac{(d_{(n,m)} - \hat{d}_n^j)^2}{{\sigma_n^j}^2 + {\sigma_{\mathrm{FR}_m}}^2} \right) \right)$$
$$P_1 = P_{\mathrm{fst}} \ , \ P_j \overset{j \in [2 \cdots J_n]}{=} 1 \tag{4.18}$$

where P_{ndet} represents the chance that the matching MPC range was not detected, J_n is the number of detected MPCs, $\hat{d}_n^j$ is the j_{th} MPC range estimate. Instead of one Gaussian function in (4.17), (4.18) is a sum of Gaussian functions, each representing the likelihood of $d_{(n,m)}$ being near to one $\hat{d}_n^j$. The contribution of the first MPC range, direct-path range, P_1 is set lower to P_{fst} to offset the tendency of the algorithm to assign high likelihood directly near the reflector FR_m. An example $L_n^m(\mathbf{d}_n; d_{(n,m)})$ plotted against $d_{(n,m)}$ is presented in Fig. 4.9. As noted in the figure, only a small interval of $d_{(n,m)}$ values corresponds to points on the RC.

The two previous paragraphs discussed the likelihood functions of the reflected path legth $d_{(n,m)}$. However, the function of real interest is $L_n^m(\mathbf{d}_n; r_c\alpha_b)$, which is the likelihood function defined for $\hat{\mathbf{b}}(r_c\alpha_b)$, points on the RC. Equation (4.18) can be changed to a function of $r_c\alpha_b$ by replacing $d_{(n,m)}$ with the range between the reflected receiver R_n^m and the point on the RC, $|\mathbf{r}_n^m - \hat{\mathbf{b}}(r_c\alpha_b)|$:

$$L_n^m(\mathbf{d_n}; r_c\alpha_b) = N_{\mathrm{rm}} \left(P_{\mathrm{ndet}} + \sum_{j=1}^{J_n} P_j \exp\left(\frac{-1}{2} \frac{(|\mathbf{r}_n^m - \hat{\mathbf{b}}(r_c\alpha_b)| - \hat{d}_n^j)^2}{{\sigma_n^j}^2 + {\sigma_{\mathrm{FR}_m}}^2} \right) \right) \tag{4.19}$$

Fig. 4.10 illustrates the connection between $L_n^m(\mathbf{d}_n; d_{(n,m)})$ and $L_n^m(\mathbf{d}_n; r_c\alpha_b)$. Fig. 4.11 presents an example of $L_n^m(\mathbf{d}_n; r_c\alpha_b)$. In this case, RC$\cap$SA, the domain of $L_n^m(\mathbf{d}_n; r_c\alpha_b)$, is an arc from the ceiling to the floor. The rest of RC lies outside

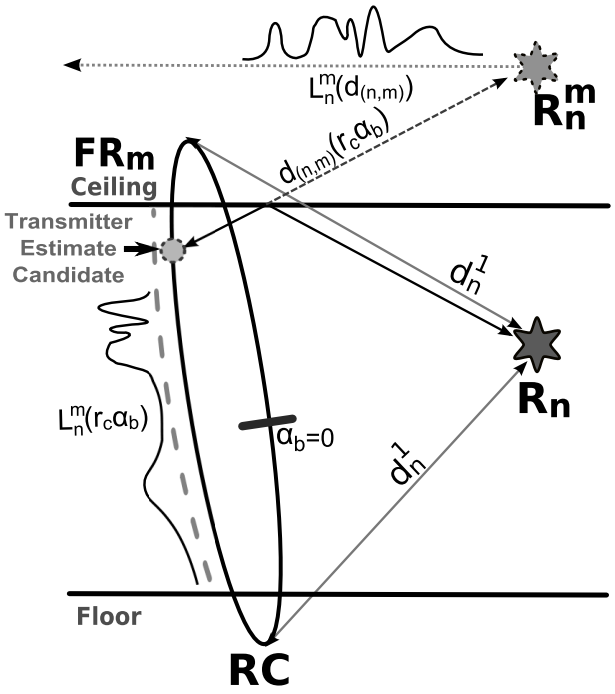

Figure 4.10: Two partial likelihood functions, $L_n^m(\mathbf{d_n}; d_{(n,m)})$ and $L_n^m(\mathbf{d_n}; r_c\alpha_b)$, for one $\mathrm{R_n}$-$\mathrm{FR_m}$ pair. $L_n^m(\mathbf{d}_n; d_{(n,m)})$ is a function of range from $\mathrm{R_n^m}$. $L_n^m(\mathbf{d_n}; r_c\alpha_b)$ is a function of position on RC.

of the SA, either over the ceiling, below the floor or outside the wall.

Combining Likelihood Functions

After calculating the partial likelihood functions for each $(\mathrm{R}_n, \mathrm{FR}_m) \in \mathcal{R} \times \mathcal{FR}$ pair, the total likelihood function $L(r_c\alpha_b)$ can be calculated. As can be seen in Fig. 4.11, the partial results for one $(\mathrm{R}_n, \mathrm{FR}_m)$ pair do not usually provide a good position estimate. However, if the probability of not detecting a matching MPC is low, the $L_n^m(\mathbf{d}_n; r_c\alpha_b)$ likelihood value for most $(\mathrm{R}_n, \mathrm{FR}_m)$ pairs will be high for $r_c\alpha_b$ corresponding to the best transmitter position estimate $\hat{\mathbf{b}}(r_c\alpha_b)$. Consequently, total likelihood for $\hat{\mathbf{b}}(r_c\alpha_b)$ should also be high. If $L_n^m(\mathbf{d}_n; r_c\alpha_b)$ are mutually independent, the total likelihood function can be calculated as:

$$L(r_c\alpha_b) = \prod_{n\in[1,N], m\in[1,M]} L_n^m(r_c\alpha_b). \tag{4.20}$$

Assuming the independence of $L_n^m(\mathbf{d}_n; r_c\alpha_b)$ is not strictly correct, but the introduced error is small. An example of the total likelihood function $L(r_c\alpha_b)$, for the same transmitter as before, is presented in Fig. 4.12.

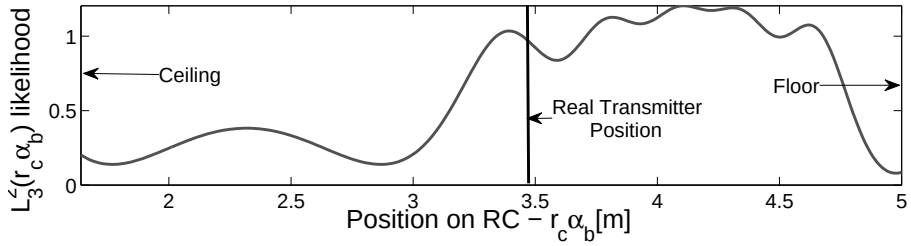

Figure 4.11: $L_n^m(\mathbf{d}_n;r_c\alpha_b)$ partial likelihood function plotted as a function of position on the RC. Only positions on an arc inside SA are considered. The measurement data for the lecture room environment, $\mathrm{B_{REF}}$, $\mathrm{R_3}$ and left wall reflection are used (see Fig. 5.5).

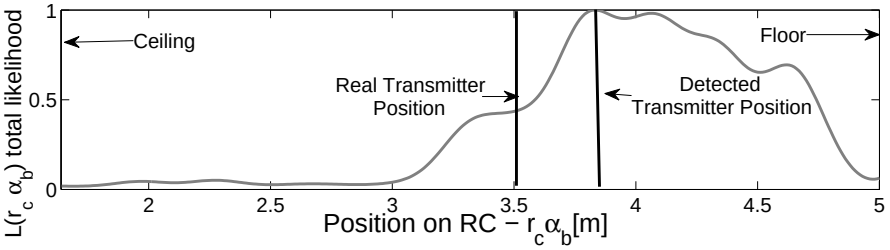

Figure 4.12: $L(\mathbf{d}_n;r_c\alpha_b)$ total likelihood function plotted as a function of position on the RC. The measurement data for the lecture room environment and $\mathrm{R_3}$ are used (see Fig. 5.5).

Finally, the $r_c\alpha_b$ estimate can be found by maximizing the likelihood:

$$r_c\hat{\alpha}_b = \arg\max_{r_c\alpha_b}\left(\sum_{n\in[1,N],m\in[1,M]} \ln L_n^m(r_c\alpha_b)\right) \tag{4.21}$$

The result transmitter position estimate is $\hat{\mathbf{b}}(r_c\hat{\alpha}_b)$.

4.5 TOA Reflection-Aided Least Squares (RALS) 2 Receiver Positioning Method

This section presents the Reflection-Aided Least Squares method for 2 receiver 3D positioning. Although this was the first method I developed and presented, it achieves worse results than RAML, and for that reason it is discussed second.

The method is divided into two steps. The first step consists of using the positions of two receivers, $\mathbf{r}_1$ and $\mathbf{r}_2$, in addition to the detected direct ranges, $\hat{d}_1^1$ and $\hat{d}_2^1$, for finding the Result Circle(RC), the same as in RAML. The transmitter's position is assumed to be near RC. The second step consists of finding the best transmitter position estimate on the RC. This is achieved by using a

least-squares algorithm for the points on the RC, using the knowledge of all detected MPCs ($\mathbf{d}_1$, $\mathbf{d}_2$), $\mathcal{FR}$ and SA.

For the method to succeed, the following two assumptions must hold. First, for each R_n, the MPC corresponding to the direct path is detected in the received waveform. In other words, LOS conditions. Second, most MPCs caused by reflection from $\mathrm{FR}_m \in \mathcal{FR}$ are also detected. Under these assumptions, the first MPC range, $\hat{d}_n^1$, corresponds to the direct path between transmitter and R_n. $\mathbf{d_n}$ also contains a subset corresponding to reflections from $\mathrm{FR}_m \in \mathcal{FR}$. This subset is not known in advance.

4.5.1 Result Circle (RC)

The RC is calculated in the same way as in RAML. Please refer to the calculation description there, Section 4.4.1. Receiver's position, $\hat{\mathbf{b}}(r_c\alpha_b)$, is assumed to be on the RC.

4.5.2 Position on RC Calculation Algorithm

The second step of the proposed method consists of finding the best transmitter position estimate on the RC, $\hat{\mathbf{b}}(r_c\alpha_b)$. To accomplish this, a least squares estimator using later detected MPCs contained in vectors $\mathbf{d_1}$ and $\mathbf{d_2}$, in addition to knowledge of $\mathcal{FR}$, is used.

Instead of considering $\mathcal{R}$, $\mathcal{FR}$, $\mathbf{d_1}$ and $\mathbf{d_2}$ together, the problem can be divided, with each $(\mathrm{R}_n, \mathrm{FR}_m) \in \mathcal{R} \times \mathcal{FR}$ pair being considered separately.

Results for each pair can then be combined for a final result. A $(\mathrm{R}_n, \mathrm{FR}_m)$ pair represents a FR_m-reflected path from transmitter to R_n. As mentioned in Section 4.2, this path can be also represented with a direct path from transmitter to R_n^m, R_n's reflection through FR_m.

4.5.3 Transmitter Position Candidate(TPC) Calculation

First, for each $(\mathrm{R}_n, \mathrm{FR}_m) \in \mathcal{R} \times \mathcal{FR}$ pair, all possible Transmitter Position Candidates(TPCs) are found, together with the standard deviance for each TPC. A TPC is a possible transmitter position on the RC, assuming that one of the detected MPCs was caused by reflection from FR_m. For each MPC distance $\hat{d}_n^j$, $j \in (1, \cdots, J_n)$, corresponding TPCs can be found by solving:

$$\mathbf{r}_n^m - \hat{\mathbf{b}}(r_c\alpha_b) = \hat{d}_n^j \tag{4.22}$$

In other words, the solutions of this equation are points on RC $\hat{\mathbf{b}}(r_c\alpha_b)$ that are at a distance of $\hat{d}_n^j$ from the position of the reflected transmitter R_n^m, $\mathbf{r}_n^m$. This equation will have 0,1 or 2 solutions. Each solution is a Transmitter Position

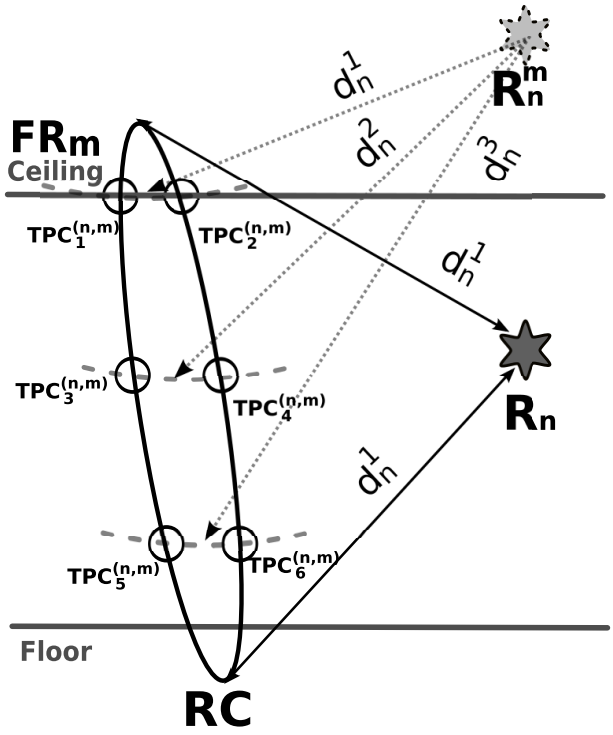

Figure 4.13: Illustration to calculating TPCs and creation of $\mathbf{TPC}^{(n,m)}$ vector.

Candidate, TPC_p. By solving eq. 4.22 for all $\hat{d}_n^j$, $j \in (1, \cdots, J_n)$, a vector of all possible TPCs is compiled, $\mathbf{TPC}^{(n,m)}$. TPCs outside of SA are removed from the vector. Let $P^{(n,m)}$ be the the number of detected MPCs and $\mathrm{TPC}_p^{(n,m)}$ be a single TPC, $p \in (1, \cdots, P^{(n,m)})$. Fig. 4.13 presents an example of TPC calculation. Each TPC is described by it's arc position on the RC, $r_c\alpha_p^{(n,m)}$.

In order to account for the error of ranging measurements, the variance of the arc $r_c\alpha_p^{(n,m)}$ for each TPC is calculated:

$$\begin{aligned} &{\sigma_p^{(n,m)}}^2 = \left(\frac{\delta r_c \alpha_p^{(n,m)}}{\mathrm{d}\hat{d}_n^j}\right)^2 ({\sigma_n^j}^2 + {\sigma_{\mathrm{FR}_m}}^2) = \frac{{\sigma_n^j}^2 + {\sigma_{\mathrm{FR}_m}}^2}{\cos\beta^2} \\ &\beta = \angle(|\mathrm{R}_n^m, \mathrm{TPC}_p^{(n,m)}|, \perp|\mathrm{RC}, \mathrm{TPC}_p^{(n,m)}|) \end{aligned} \tag{4.23}$$

where β is the angle between the line from R_n^m to $\mathrm{TPC}_p^{(n,m)}$, $|\mathrm{R}_n^m, \mathrm{TPC}_p^{(n,m)}|$ and tangent line to RC at point $\mathrm{TPC}_p^{(n,m)}$, $\perp|\mathrm{RC}, \mathrm{TPC}_p^{(n,m)}|$.

4.5.4 Combining TPCs

After finding $\mathbf{TPC}^{(n,m)}$ for each $(\mathrm{R}_n, \mathrm{FR}_m) \in \mathcal{R} \times \mathcal{FR}$ pair, the next step is to estimate the transmitter's position using Least Squares approach. We are looking for arc $r_c\alpha_b$ that would minimize the variance-weighted sum over all

$(\mathrm{R}_n, \mathrm{FR}_m) \in \mathcal{R} \times \mathcal{FR}$ of squared errors to the closest calculated TPC, or, in other words, we want to minimize the following expression:

$$r_c\hat{\alpha}_b = \arg\min_{r_c\alpha_b} \left(\sum_{n\in[1,N], m\in[1,M]} \min_{p\in[1,P]} \frac{(r_c\alpha_b - r_c\alpha_p^{(n,m)})^2}{{\sigma_p^{(n,m)}}^2} \right) \tag{4.24}$$

$\hat{\mathbf{b}}(r_c\hat{\alpha}_b)$is the result of the method.

4.6 TDOA Reflection-Aided Maximum Likelihood (DRAML) 3 Receiver Positioning Method

This section presents the TDOA Reflection-Aided Maximum Likelihood method for 3 receiver 3D positioning. The method is divided into two steps. In the first step, a Result Curve(RC) is calculated using the receiver positions: $\mathbf{r}_1$, $\mathbf{r}_2$ and $\mathbf{r}_3$, in addition to two direct-path range difference estimates, $\hat{l}_2^1$ and $\hat{l}_3^1$. The transmitter's position is assumed to be close to the RC. The second step consists of finding the best transmitter position estimate on the RC. This is achieved by calculating a likelihood function for points on the RC, using the knowledge of all detected MPCs: $\mathbf{l}_1$,$\mathbf{l}_2$ and $\mathbf{l}_3$, $\mathcal{FR}$ and SA. The point on RC with the maximum likelihood is chosen as the estimated transmitter position.

For the method to succeed, the following two assumptions must hold: First, for each R_n, the MPC corresponding to the direct path is detected in the received waveform. Secondly, most of the MPCs caused by a reflection from $\mathrm{FR}_m \in \mathcal{FR}$ are also detected. Under those assumptions, the first MPC range difference, $\hat{l}_n^1$, corresponds to the direct path between transmitter and R_n. $\mathbf{l}_n$ also contains a subset corresponding to reflections from $\mathrm{FR}_m \in \mathcal{FR}$. This subset is not known a priori.

4.6.1 Result Curve(RC)

If only three TOAs, or two range differences, are available, the equation set (4.12) becomes:

$$\begin{cases} \hat{l}_2^1 = \sqrt{(x_b - x_2)^2 + (y_b - y_2)^2 + (z_b - z_2)^2} \\ \qquad -\sqrt{(x_b - x_1)^2 + (y_b - y_1)^2 + (z_b - z_1)^2} \\ \hat{l}_3^1 = \sqrt{(x_b - x_3)^2 + (y_b - y_3)^2 + (z_b - z_3)^2} \\ \qquad -\sqrt{(x_b - x_1)^2 + (y_b - y_1)^2 + (z_b - z_1)^2} \end{cases} \tag{4.25}$$

Each equation corresponds to a hyperboloid. The solution of (4.25) is the intersection of the two hyperboloids. This solution is, in a non-degenerate case, a

second degree curve, mostly a hyperbola, but occasionally an ellipse or parabola. It is denoted as RC. Assuming that the errors of the direct-path TOA estimates are small, the transmitter is near the RC. Consequently, the transmitter position estimate will be chosen from points on the RC, $\hat{\mathbf{b}} \in \text{RC}$. The transmitter is also considered to be inside the SA, therefore $\hat{\mathbf{b}} \in \text{SA} \cap \text{RC}$.

The RC is defined with a transformation $Q(\cdot)$ and a $[g,\ h,\ d,\ e,\ f]^T$ parameter vector, following [69]. Description of a hyperbola or ellipse in arbitrary 3D coordinates system is complex. For this reason, the RC is described in a convenient coordinate system, in which position vectors of receivers R_1, R_2 and R_3 are: $\mathbf{r}'_1 = [0,\ 0,\ 0]^T$; $\mathbf{r}'_2 = [b,\ 0,\ 0]^T$; $\mathbf{r}'_3 = [c_x,\ c_y,\ 0]^T$, respectively. The transformation $Q(\cdot)$, rotation + translation, is used to convert the positions in the real coordinate system, later referred to as "real base", to positions in the convenient coordinate system, later referred to as "prime base". The parameter vector $[g,\ h,\ d,\ e,\ f]^T$ describes the RC in the prime base:

$$\begin{cases} y'_b = g x'_b + h \\ z'_b = \pm\sqrt{d {x'_b}^2 + e x'_b + f} \end{cases}, \hat{\mathbf{b}} = Q^{-1}\Big(\begin{bmatrix} x'_b \\ y'_b \\ z'_b \end{bmatrix} \Big) \tag{4.26}$$

where $\hat{\mathbf{b}}' = [x'_b,\ y'_b,\ z'_b]^T$ is a vector representing the point's position on RC in the prime base, before $Q^{-1}(\cdot)$ transformation, while $\hat{\mathbf{b}} = [x_b,\ y_b,\ z_b]^T$ is a vector representing the point's position in the real base. $\hat{\mathbf{b}}$ is used to describe a point because each point on RC is a transmitter position estimate candidate. Fig. 4.14 shows an example RC in the prime base.

To describe a point's position on the RC, z'_b is used, $\hat{\mathbf{b}}(z'_b)$. In eq. 4.26, position is presented as a function of x'_b, for ease of representation. However, for each x'_b, there are two corresponding points on RC: $[x'_b, y'_b, z'_b]^T$ and $[x'_b, y'_b, -z'_b]^T$. In comparison, for each z'_b, there is only one corresponding point, as long as RC is a hyperbola. In the rare case that RC is an ellipse, the point closer to R_1 is chosen.

4.6.2 Position on RC Calculation Algorithm

The second step of the proposed method consists of finding the best transmitter position estimate on the RC, $\hat{\mathbf{b}}(z'_b)$. To accomplish this, a maximum likelihood estimator using the later detected MPCs: $\mathbf{l}_1$, $\mathbf{l}_2$ and $\mathbf{l}_3$, in addition to the knowledge of $\mathcal{FR}$, is used.

The algorithm is broadly similar to the algorithm used in the RAML method. Both rely on the maximum likelihood approach, assuming a Gaussian error distribution of the MPC TOA estimates. However, the DRAML method relies on TDOA ranging. Consequently, range differences are used in the algorithm,

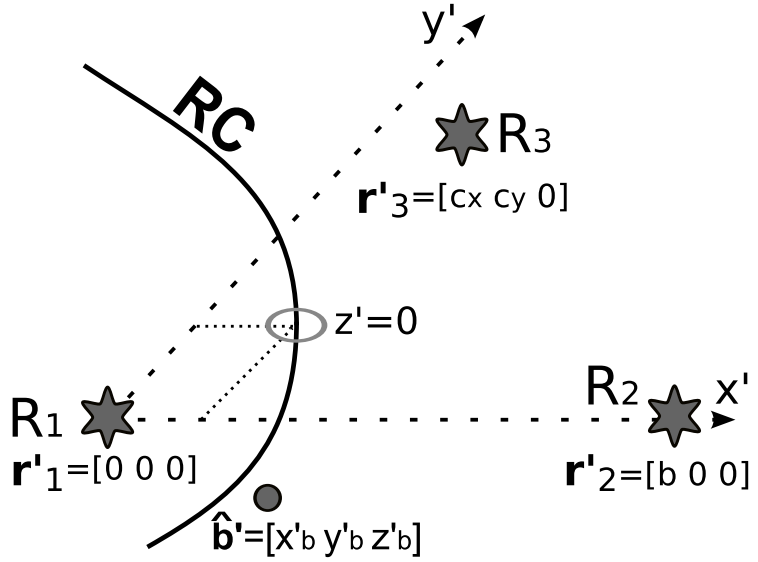

Figure 4.14: Result Curve (RC), second degree curve, presented in prime base. Real transmitter position ($\mathbf{b}'$) should be close to RC.

as opposed to ranges in RAML. Additionally, a more elaborate P_j weighing function is used.

Instead of considering $\mathcal{R}$, $\mathcal{FR}$ and $\mathbf{l}_n$ for each receiver together, the problem can be divided, with each $(\mathrm{R}_n, \mathrm{FR}_m) \in \mathcal{R} \times \mathcal{FR}$ pair being considered separately. "$\times$" here is the Cartesian product. The result for each pair is a partial likelihood function defined for $\hat{\mathbf{b}} \in \mathrm{SA} \cap \mathrm{RC}$, $L_n^m(\mathbf{l}_n; z_b')$. The functions for each pair can then be combined for a final result. A $(\mathrm{R}_n, \mathrm{FR}_m)$ pair represents a FR_m-reflected path from the transmitter to R_n. As mentioned in the Section 4.2, this path can also be represented by a direct path from the transmitter to R_n^m, R_n's reflection through FR_m.

Partial Likelihood Function Derivation

As the first approach, let $\hat{l}_n^j$ be a known a priori range difference estimate matching the FR_m-reflected path to R_n. This assumption is for explanation purposes only, as it is generally not true. Let the error of $\hat{l}_n^j$ be Gaussian, with $\sigma_{(n,m)}^{j\,2} = \sigma_n^{j\,2} + \sigma_1^{j\,2} + \sigma_{\mathrm{FR}_m}^2$. $\sigma_{(n,m)}^j$ models both the measurement error of $\hat{l}_n^j$ and the uncertainity of the reflected path length it corresponds to. A likelihood function for the points on the RC, $L(\hat{l}_n^j; z_b')$, can then be constructed as:

$$L_n^m(\hat{l}_n^j; z_b') = N_{\mathrm{rm}} * \exp\left(\frac{-1}{2}\left(\frac{|\hat{\mathbf{b}}(z_b') - \mathbf{r}_n^m| - (\hat{l}_n^j + |\hat{\mathbf{b}}(z_b') - \mathbf{r}_1|)}{\sigma_{(n,m)}^j}\right)^2\right) \tag{4.27}$$

where N_{rm} is a normalization constant, exp is the exponential function, $|\hat{\mathbf{b}}(z'_b) - \mathbf{r}_n^m|$ is the distance between the considered point and R_n^m, later denoted as $d_n^m(z'_b)$, and $|\hat{\mathbf{b}}(z'_b) - \mathbf{r}_1|$ is the distance to R_1, later denoted as $d_1(z'_b)$. $L(\hat{l}_n^j; z'_b)$ should be considered as a function of z'_b. In this simple case, for each $\hat{\mathbf{b}}(z'_b)$, the distance from $\hat{\mathbf{b}}$ to $\mathbf{r}_1$ and to $\mathbf{r}_n^m$ is calculated and their difference is compared with the estimated range difference, $\hat{l}_n^j$. The likelihood is assigned based on the error between $\hat{l}_n^j$ and the range difference for considered $\hat{\mathbf{b}}(z'_b)$, assuming Gaussian error model.

In practice, there is no a priori knowledge about the FR_m-MPC matches. Any detected MPC range may match R_n^m, the FR_m-reflected path. Additionally, the matching MPC is not always detected. Considering those two problems, a more realistic likelihood function can be constructed as:

$$L_n^m(\mathbf{l}_n; z'_b) = N_{\mathrm{rm}} P_{\mathrm{ndet}} + N_{\mathrm{rm}} \sum_{j=1}^{J_n} P_j \exp\Big(\frac{-1}{2}\big(\frac{d_n^m(z'_b) - (\hat{l}_n^j + d_1(z'_b)}{\sigma_{(n,m)}^j}\big)^2\Big) \tag{4.28}$$

where P_{ndet} represents the likelihood that the matching MPC range was not detected and J_n is the number of detected MPCs. This is the function used in the proposed method. Instead of one Gaussian function in (4.27), (4.28) is a sum of Gaussian functions, each representing the likelihood of the R_1-R_n^m range difference being near to one estimated range difference $\hat{l}_n^j$.

P_j is a weighing function. It is used to lower the contribution of the first MPCs, including direct-path MPC. This is done because the algorithm has a tendency to assign high likelihood directly near the reflector FR_m, corresponding to the early MPCs. This is caused by a big number of MPCs detected just after the first MPC. The following formula is used for P_j calculation:

$$P_j = \min\Big(\exp\big(-P_{\mathrm{fst}}(1 - \frac{\hat{l}_n^j - \hat{l}_n^1}{d_{\max}})\big), 1\Big) \tag{4.29}$$

where P_{fst}, the first MPC penalty, and $d_{\max}$, the maximum penalty length, are method parameters. An example of $L_n^m(\mathbf{l}_n; z'_b)$ plotted against z'_t is presented on Fig. 4.15. The domain is a hyperbola piece limited by the SA.

Combining Likelihood Functions

After calculating the partial likelihood functions for each $(\mathrm{R}_n, \mathrm{FR}_m) \in \mathcal{R} \times \mathcal{FR}$ pair, the total likelihood function $L(z'_b)$ is calculated. As can be seen in Fig. 4.15, a partial result for one $(\mathrm{R}_n, \mathrm{FR}_m)$ pair does not provide a good position estimate. However, assuming that the probability of detecting a matching MPC, as one of many, is high, $L_n^m(\mathbf{l}_{n,1}; z'_b)$ likelihood for most $(\mathrm{R}_n, \mathrm{FR}_m)$ pairs will be high for z'_b corresponding to the best transmitter position estimate $\hat{\mathbf{b}}(z'_b)$. Consequently,

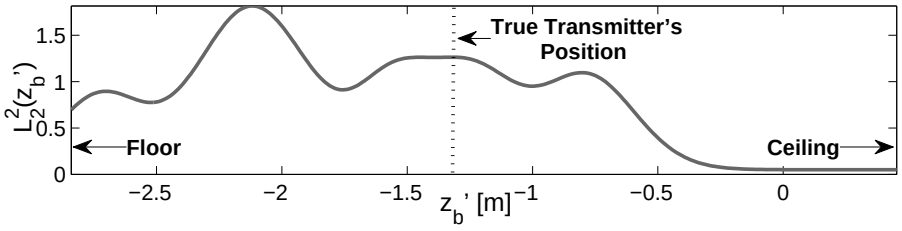

Figure 4.15: Example $L_n^m(\mathbf{l}_n; z_b')$ partial likelihood function plotted vs. z_b', the position on the RC. The measurement data for the lecture room environment, $\mathrm{B_{REF}}$, $\mathrm{R_3}$ and the floor reflection are used (see Fig. 5.5). N_{rm} is set to 1.

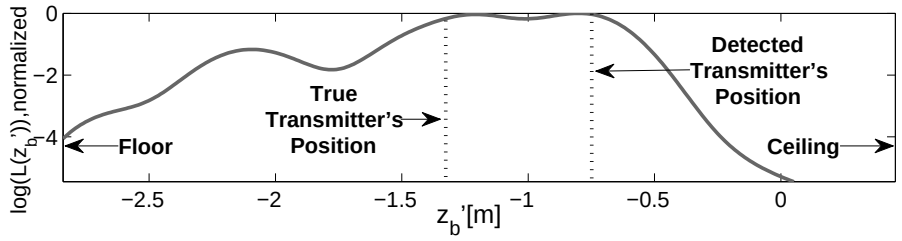

Figure 4.16: Logarithm of $L(z_b')$, total likelihood function, plotted vs. z_b', the position on the RC. Maximum is normalized to 0. The measurement data for the lecture room environment and $\mathrm{R_3}$ are used (see Fig. 5.5).

total likelihood for $\hat{\mathbf{b}}(z_b')$ will also be high. The total likelihood function can be calculated as:

$$L(z_b') = \prod_{n\in[1,N],m\in[1,M]} L_n^m(\mathbf{l}_{n,1}; z_b') \tag{4.30}$$

For this formula to be correct, $L_n^m(\mathbf{l}_{n,1}; z_b')$ should be mutually independent. This is not strictly true, but the error introduced by this assumption is small. Example of the total likelihood function $L(z_b')$, for the same transmitter as before, is presented in Fig. 4.6.2.

Finally, z_b' estimate can be found by maximizing likelihood:

$$\hat{z}_b' = \arg\max_{z_b'} \big(L(z_b')\big) \tag{4.31}$$

The result transmitter position estimate is $\hat{\mathbf{b}}(z_b')$.

4.7 Summary

The main aim of this chapter was to introduce the two proposed methods, RAML and DRAML. In order to do that, first, the reasons for using reflection-based positioning were investigated and it was shown that reflections can improve positioning. Next, the system model was detailed. then, in the third section, the conventional Direct Solution and Assumed Height methods, in the TOA and TDOA variations, were introduced in order to serve as benchmarks for the proposed methods. The most important benchmark is the Assumed height method, since it requires the same number of receivers as the proposed methods. Finally, in two sections, the TOA Reflection-Aided Maximum Likelihood(RAML) and TDOA Reflection-Aided Maximum Likelihood (DRAML) methods were presented.

Both RAML and DRAML methods use a similar approach: both methods are divided into two steps. In the first step, a circle or a curve containing the transmitter estimate is calculated using the most reliable direct-path ranges. Then, in the second step, using the maximum likelihood approach, the less reliable multipath ranges are used, together with reflector positions, to find the transmitter position on the circle/curve.

Chapter 5

Measurements Description

This chapter describes the measurements performed in order to obtain the data for verification of the proposed positioning methods. The chapter consists of two sections. The first section describes the measurement equipment and the organization of the measurement. The second section describes the three environments in which the measurements were conducted, together with the placement of receivers and transmitters in each environment.

The aim of the performed measurements is to provide data for verification of the proposed positioning methods. The initial verification of the methods was done using data obtained from a simulation (briefly discussed in Section 6.3). However, deterministic UWB propagation simulations usually grossly underestimate the number of detected MPCs in the received waveform[70]. In addition, the simulation did not take into account antenna radiation patterns, diffraction, as well as many other propagation effects. To verify the usefulness of the methods with a realistic number of MPCs, with the presence of propagation effects not included in the simulation, data obtained from real-world measurements was necessary.

Unfortunately, UWB transmitters, antennas, high frequency filters and multi-GHz sampling oscilloscope were not available in Katayama Laboratory, and assembling such setup would be very expensive and time-consuming. For this reason, the measurements were instead performed at Warsaw University of Technology (PW), Department of Electronics and Information Technology (EiTI) in September 2009, with the help and cooperation from Dr. Jerzy Kolakowski.

5.1 Measurement Setup

This section describes the measurement setup and equipment. Figures 5.1 and 5.2 present the schematic and the picture of the measurement setup, respectively.

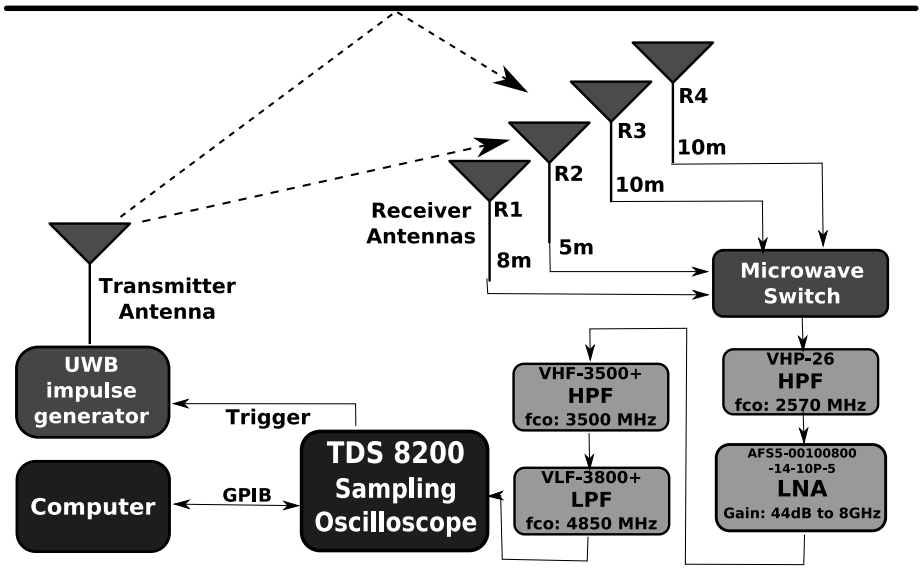

Figure 5.1: Measurement Setup, schematic

Operation of the measurement setup can be summarized as follows. An impulse generator generates a pulse signal when it receives a trigger from an oscilloscope. A single pulse signal is then transmitted using a transmitter antenna. Four signals are received by four receiver antennas. One of the four received signals is chosen in a microwave switch. The chosen signal is filtered and amplified before being transmitted to the oscilloscope. The sampling oscilloscope registers the filtered received signal waveform and passes the result to the computer. After the measurements, during post-processing, the MPCs in the received signal waveform are detected using CLEAN algorithm.

Each part of the setup will be discussed in the following subsections.

5.1.1 Impulse generator

The impulse generator was developed by Dr. Kolakowski and his team. It is based on an avalanche diode and a passive, transmission line filter. The transmitted waveform was designed for the 3.4-4.8 GHz band available for use in the USA, the EU and Japan. Fig. 5.3 presents the transmitted waveform and its spectrum. The generator is triggered by the oscilloscope, in order to achieve synchronization.

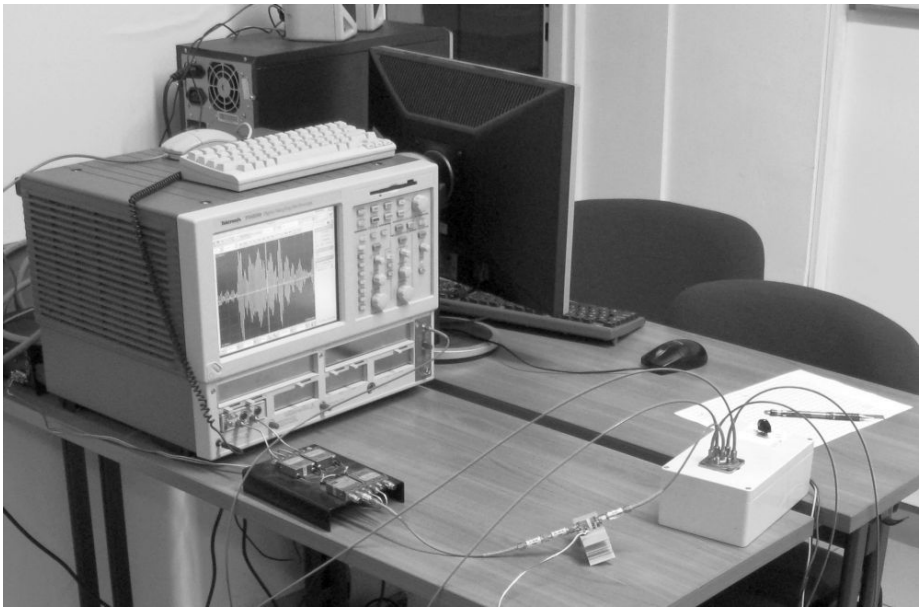

Figure 5.2: Measurement Setup, picture

5.1.2 Antennas

The antennas are elliptical planar monopoles. Fig. 5.4 presents the measured radiation pattern of the antenna, calculated using waveform amplitude. Like the impulse generator, the antennas were made by Dr. Kolakowski's team. The transmitter antenna was used facing upward. The receiver antennas were used facing away from the closest wall.

5.1.3 Microwave switch, filters and LNA

The microwave switch used for choosing between receiver antennas is a mechanical switch, fitted for manual operation. The initial signal filtering is done using a coaxial Mini-Circuits VHP-26 high-pass filter with a passband of 3GHz to 7GHz [71]. The signal is then amplified in an amplifier based on a surface-mounted Miteq AFS5-00100800-14-10P-5 low-noise amplifier[72]. Finally, the amplified signal is filtered using a coaxial Mini-Circuits VHF-3500+ high-pass filter[73] and VLF-3800+ low-pass filter[74], creating a 3500MHz-4850MHz pass-band filter (based on 3dB loss frequencies of filters).

5.1.4 Oscilloscope

The sampling oscilloscope used in the measurements is a Tektronix TDS8200[75]. In sampling oscilloscopes, synchronization is very important. This is achieved by

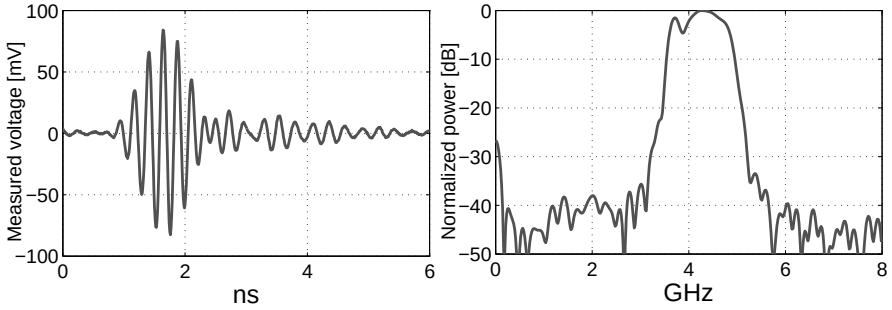

Figure 5.3: Transmitted waveform, measured at antenna's input.

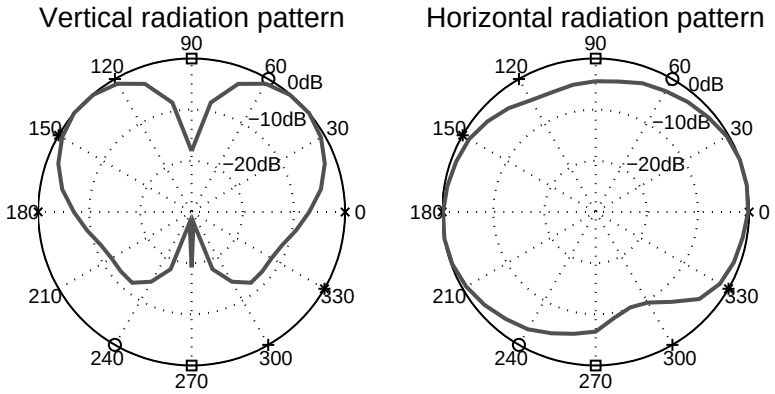

Figure 5.4: Measured radiation pattern of the elliptical planar monopole antenna used in the measurements.

using the oscilloscope to trigger the impulse generator. A 110ns-long waveform is recorded with 10ps resolution during each measurement. The start of the waveform is set to 150ns after the trigger. This value was chosen experimentally, after noting that the total delay of the system is greater than 150ns. The waveform is averaged over 16 measurements to limit the noise. The oscilloscope is controlled from the computer using the GPIB interface. Each measured waveform is transferred to computer using GPIB and then saved for post-processing.

5.1.5 Post-Processing

The aim of post-processing is to retrieve MPC delays and amplitudes from the received waveform. The MPC parameters are then used for positioning. The post-processing consists of three steps. In the first step, MPCs are detected in the received waveform using the CLEAN algorithm. In the second step, the results of the CLEAN algorithm are refined in order to solve common cases of

MPC mis-detection. In the third step, MPC delays are normalized.

CLEAN algorithm is used for detecting the MPCs in the received waveform. CLEAN is a resolution-enhancement algorithm first proposed in [76] for use in radio-astronomy, and in [46] for use in UWB radio. The simplified, 1D version of the algorithm used in the measurements is presented below (after [52]):

1. Calculate the autocorrelation of the template waveform $c_{ss}(t)$, and the initial cross-correlation of the template with the received waveform $c_{sr}^1(t)$.

$$c_{ss}(t) = \int_{-\infty}^{\infty} s(\tau)s(\tau - t)d\tau \tag{5.1}$$

$$c_{sr}^1(t) = \int_{-\infty}^{\infty} s(\tau)r(\tau - t)d\tau \tag{5.2}$$

   The transmitted waveform from Fig. 5.3 was used as the template waveform.

2. Find the largest correlation in $c_{sr}^k(t)$, record the normalized amplitudes α_k and the time delay τ^k of the correlation peak.

$$\alpha_k = \max(c_{sr}^k(t)), \qquad \tau^k = \arg\max(c_{sr}^k(t)) \tag{5.3}$$

   where $c_{sr}^k(t)$ is the updated cross-correlation function used at the k_{th} iteration of the algorithm.

3. Subtract $c_{ss}(t)$ scaled by α_k from $c_{sr}^k(t)$ at the time delay τ_k.

$$c_{sr}^{k+1}(t) = c_{sr}^k(t) - \alpha_k c_{ss}(t - \tau_k) \tag{5.4}$$

4. If a stopping criterion ($\max(c_{sr}^{k+1}(t)) <$ threshold) is not met, go to step 2. Otherwise, sort the delays in an ascending order and stop. The algorithm stop threshold was set to $\frac{1}{10}$ of the maximum MPC amplitude or $6\hat{\sigma}_e$, whichever was higher. $\hat{\sigma}_e$ is the calculated noise standard deviation after convolution with the template, calculated using a MPC-free part of the received waveform.

A vector of measured delays for each receiver n is the result of the algorithm.

The second post-processing step was introduced to solve common cases of MPC mis-detection. CLEAN algorithm results are refined in the following two ways:

1. If after the initial 1,2 or 3 MPCs there is a long pause ($>$ 5ns), these MPCs are deleted. This is to remove spurious early MPCs, caused most probably by LNA power cable acting as an antenna.

2. The threshold for the first MPC is raised to $\frac{1}{5}$ of maximum MPC amplitude. This is to combat spurious MPCs detected just before the first MPC. Those can be caused by a mismatch between the template and the real received waveforms.

Both measures were introduced to correct the mentioned problems, after examining the measured received waveform. The final result, for one $\mathrm{R}_n \in \mathcal{R}$, is a vector of measured delays $\boldsymbol{\tau}_n = [\hat{\tau}_n^1, \cdots, \hat{\tau}_n^{J_n}]^T$.

The third post-processing step is the MPC delay normalization. The normalization is necessary because the measured MPC delays contain a large delay introduced by the measurement setup, which is different for each receiver antenna. This delay has to be subtracted from each MPC delay in order for the MPC delays to contain only the propagation delay. In each environment, one transmitter position in the middle of the room is chosen for normalization, $\mathbf{b}_{\mathrm{REF}}$. The normalization delay for each receiver R_n, τ_{norm}^n, is calculated as follows:

$$\tau_{\mathrm{norm}}^n = \hat{\tau_n^1}' - ||\mathbf{r}_n - \mathbf{b}_{\mathrm{REF}}||/\mathrm{C} \tag{5.5}$$

Where $\hat{\tau_n^1}'$ is the delay of the first detected MPC, $||\mathbf{r}_n - \mathbf{b}_{\mathrm{REF}}||$ is the distance between the transmitter, and the receiver and C is the speed of light. Next, for all transmitter positions, τ_{norm}^n is subtracted from delays of all MPCs detected in R_n's waveform:

$$\hat{\tau}_n^j = \hat{\tau_n^j}' - \tau_{\mathrm{norm}}^n, \quad n = (1, ..., \mathrm{N}), \quad j = (1, ..., \mathrm{J}_n) \tag{5.6}$$

The resulting $\hat{\tau}_n^j$ should contain only the delay caused by the propagation.

5.2 Measurement Environments

This section describes the three environments in which the measurements were performed, a lecture room, a laboratory and a corridor. Each environment is a part of the Department of Electronics and Information Technology(EiTI) main building. In each measurement, the service area SA was the room the measurements took place in. Four receivers were used in each measurement, although subsets of them were used in the proposed methods.

The receiver heights were chosen so that receivers are at some distance from the ceiling and that different receivers have different heights. By removing the receivers from the ceiling, the ceiling reflection becomes more useful for positioning. By differing receiver heights, a symmetry between ceiling and floor reflections is broken. This counteracts a possible problem of mistaking the ceiling and floor reflections.

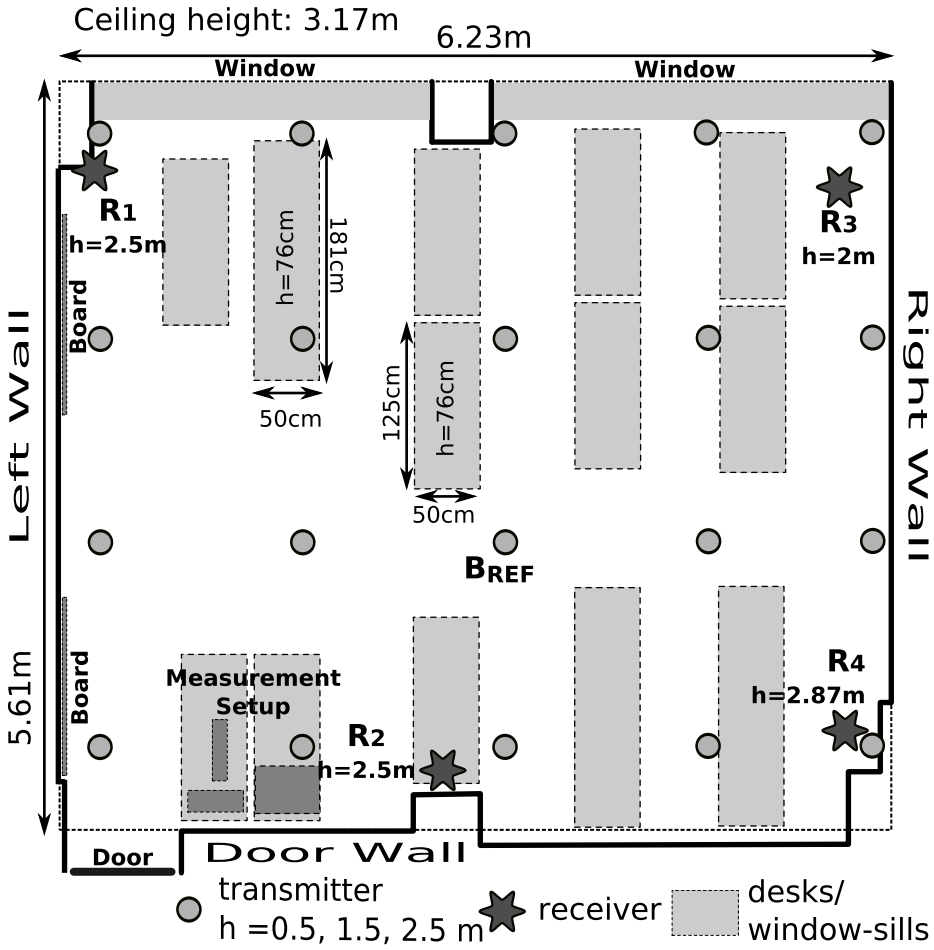

Figure 5.5: Layout of the environment No.1: Lecture room

5.2.1 Lecture Room

The first environment is a lecture room in the EiTI department. Fig. 5.5 presents the environment layout. The size of the room is 6.23[m] by 5.61[m], with ceiling at 3.17[m]. The room can be described as sparsely furnished. Apart from desks, chairs, a projector and an air conditioner, it does not contain any large objects.

Measurements were performed for each of the 20 positions marked in Fig. 5.5, placing the transmitter at heights of 0.5[m], 1.5[m] and 2.5[m], for a total of 60 transmitter positions. The transmitter positions were chosen so that to achieve uniform distribution. Transmitter B_{REF} at height 1.5[m] was used as reference.

In the proposed methods, ceiling, floor, left wall, right wall and door wall (see Fig. 5.5) were used, in that order, as reflectors.

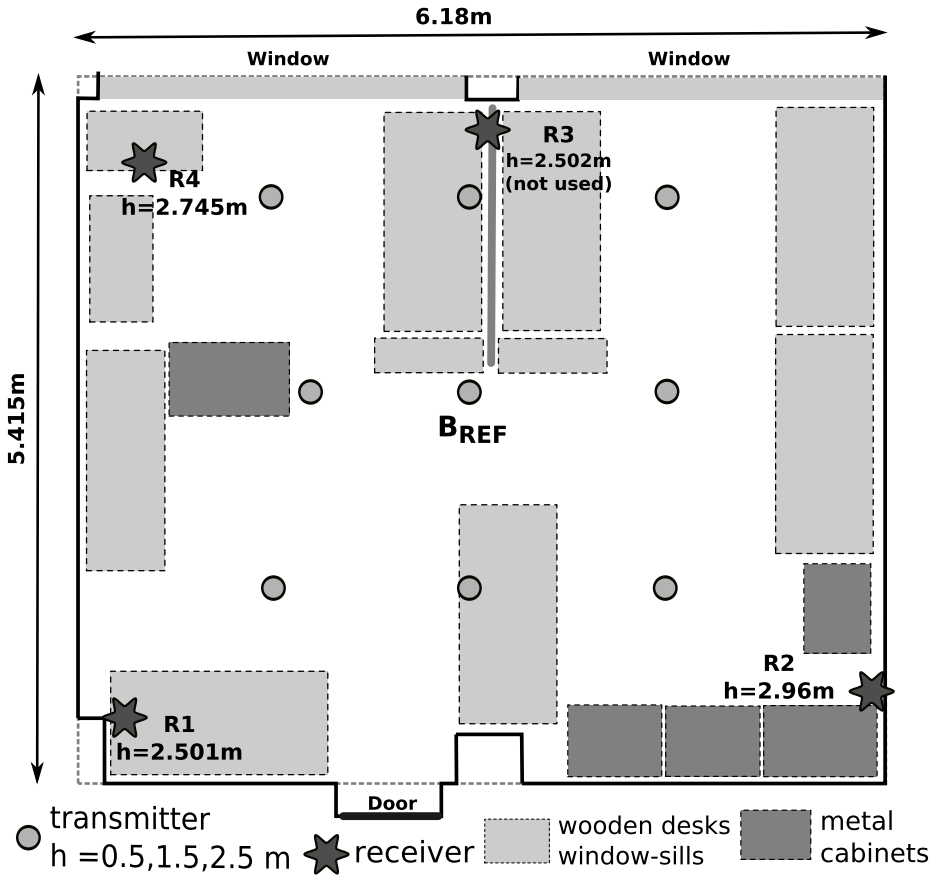

Figure 5.6: Layout of the environment No.2: Laboratory

5.2.2 Laboratory

The second environment is the laboratory room of the Radio-measurement Laboratory. Fig. 5.6 presents the environment layout. The size of the room is 5.42[m] by 6.18[m], with ceiling at 3.17[m]. The laboratory can be described as very cluttered. Most of the space is occupied by obstacles such as shelves, metal cases, measurement equipment, desks and tables, which cause reflections.

Measurements were performed for each of the 9 positions marked in Fig. 5.6, again placing the transmitter at heights of 0.5[m], 1.5[m] and 2.5[m], for a total of 27 transmitter positions. Transmitter positions near the center of the room were chosen for practical reasons: walls and corners of the room were hard to access. Transmitter B_{REF} at height 1.5[m] was used as reference. Ceiling, floor, left wall, right wall, door wall and window wall were used, in that order, as reflectors.

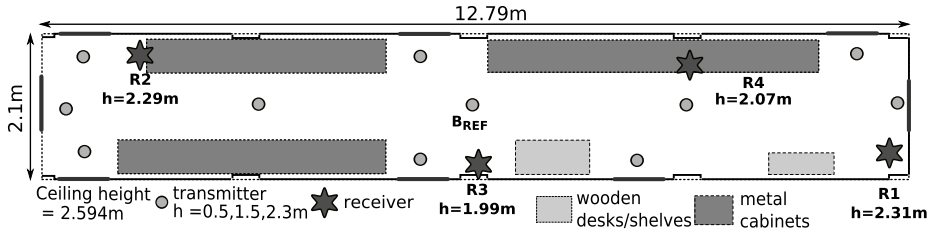

Figure 5.7: Layout of the environment No.3: Corridor

5.2.3 Corridor

The third environment is a corridor in one wing of the EiTI department building. Fig. 5.7 presents the environment layout. The size of the corridor is 12.8[m] by 2.1[m], with a low ceiling at 2.6[m]. The distinguishing feature of the corridor is its long shape. The corridor also contains metal cases that cause strong reflections.

Measurements were performed for each of the 11 positions marked in Fig. 5.7, placing the transmitter at heights of 0.5[m], 1.5[m] and 2.3[m], for a total of 33 transmitter positions. Positions corresponding to the most probable positions of people were chosen, ie. along the corridor and in front of each door. Transmitter B_{REF} at height 1.5[m] was used as reference. Ceiling, floor, left wall and right wall were used, in that order, as reflectors.

5.3 Summary

In this chapter, the measurements performed in order to obtain data for verification of the proposed positioning methods were presented.

In the first section, the measurement setup was presented. Each part of the measurement setup was described and references to the equipment datasheets were given when possible. Also, a detailed description of the measurement post-processing stage was given. In post-processing, propagation delays of MPCs are extracted from the received waveform using the CLEAN algorithm, then the results are refined and the delays normalized.

In the second section, three environments used for measurements were presented. The three environments were: an “orderly” lecture room, a “messy” laboratory and a long corridor. Used transmitter positions were explained in each case.

Chapter 6

Positioning Results

This chapter compares the results of the RAML, DRAML and RALS methods against the conventional methods. Measurement data gained in the campaign described in chapter 5, as well as simulation data, are used for the comparison.

The chapter begins with a discussion about the choice of the method parameters, especially the wall positions. A brief explanation of the used error metric follows. The next section presents the results for one, optimal TOA positioning case. Based on these results, the general properties of the proposed TOA methods are discussed. In the following section, the problem of the receiver placement in TOA case is investigated, using results for different receiver placement scenarios. Then, the accuracy of the methods in different environments is investigated. Finally, the accuracy of the TDOA positioning methods is investigated.

6.1 Determination of Parameters

Looking at the method descriptions presented in chapter 4, each method uses a set of parameters. The parameters common for RAML, RALS and DRAML are the MPC range error standard deviation, σ_n^j and the position and the roughness $\sigma^2_{\mathrm{FR}_m}$ of each used reflector. Additionally, RAML method requires the likelihood of non-detection (P_{ndet}) and the contribution of the first MPC (P_{fst}) parameters. On the other hand, DRAML requires the likelihood of non-detection P_{ndet}, the first MPC penalty (P_{fst}) and penalty length ($d_{\max}$) parameters. P_{fst} parameter, although it bears the same name for RAML and DRAML, is used differently and has different values.

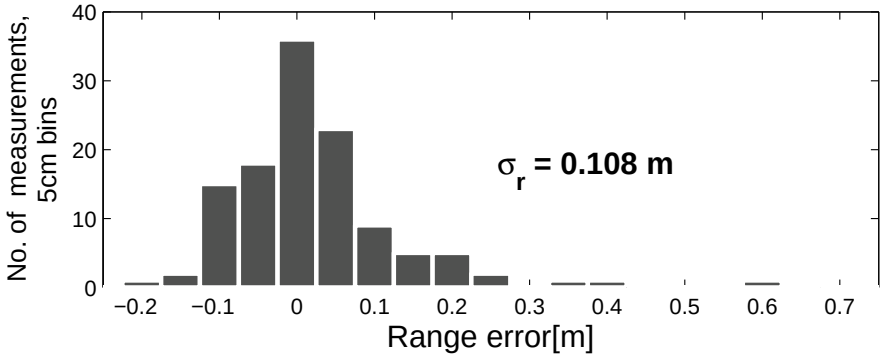

Figure 6.1: Direct-path (d_n^1) ranging error histogram for the Lecture Room, R_3 and R_4 (combined). Calculated error standard deviance is $\sigma_r = 0.108$m.

6.1.1 Range Error Standard Deviation

The basic parameter used by both the RAML and RALS methods is σ_n^j, the MPC range error standard deviation. This parameter should be, in an ideal case, calculated for each received MPC separately. However, in practice, one value was used for all σ_n^j. The assumed σ_n^j could be made a function of MPC's amplitude, but I noticed no improvement using that approach.

The value of σ_n^j was chosen based on the direct-path error standard deviation for receivers R_3 and R_4, in the Lecture Room. This corresponds to the positioning case that will be discussed in Section 6.3. A cumulative direct-path error histogram for both receivers is shown in Fig. 6.1. The value of σ_n^j was chosen to be 0.1m, a rounded calculated standard deviation of 0.108m.

6.1.2 Wall Positions

The proposed methods require the position and the roughness of each wall that will be used as a reflector. Two problems exist. The first is, which reflectors should be used in the method? The second is, how to determine the position and the roughness of a reflector that should be used?

It is hard to formulate strict rules on reflectors choice, but three criteria are important when choosing FR_m:

1. For most $\mathbf{b} \in$ SA and $R_n \in \mathcal{R}$, there is a FR_m-reflected path from transmitter to R_n. For example, small reflectors should not be used.

2. In most cases, the attenuation of that path, caused by reflection, distance, obstacles and other factors, is low enough to allow MPC detection. In

other words, the reflector should reflect well, [1] it cannot be too far, and large parts of it should not be covered with strongly-attenuating furniture.

3. Flat reflector model is a good approximation of the FR_m. In most cases the real reflected path length is close to the modeled path length. Problems might occur if the reflector has niches, alcoves, sticking-out pillars etc.

The problem of determining the positions and the roughnesses of the reflectors can be solved in two ways. The simpler solution, used in this dissertation, is to survey the SA during the system setup. This would be done only once, since the positions of walls will not, usually, change. The advantages of this approach is its simplicity and the good accuracy of the results, assuming accurate surveying equipment. However, surveying the environment might be cumbersome, and, in some cases, the strongest reflection might not be from the surface of the wall, but from its internal structure. The roughness σ_{FR_m} for each FR_m can then be calculated using measurement data, in a way similar to the σ_n^j calculation. Differences between the expected path length $|\mathbf{r}_n^m - \mathbf{b}|$ and the closest MPC range, using TOA ranging, can be used.

The other solution is to use a calibration step. During a calibration step, a known-position transmitter would be moved inside the SA, and the received waveforms would be used to estimate the $\mathrm{FR}_m \in \mathcal{FR}$ coefficients. An algorithm similar to SLAM algorithms, for example [77], should be used. This approach is less cumbersome, it will identify the perspective reflectors better, but the accuracy of surveying might be worse. Additional advantage of this approach is that the reflector roughness σ_{FR_m} would also be estimated at the same time.

The order of the reflectors considered in this thesis was determined experimentally. First, each reflector was used by itself, and RAML method's error noted. Then, the reflectors were ordered starting with the lowest error. The result, however, was predictable. Ceiling, floor and the opposite wall are in the majority of cases the first three reflectors.

6.1.3 Other Method Parameters

Apart from σ_n^j and σ_{FR_m}, The RAML method requires the likelihood of non-detection (P_{ndet}) and the contribution of the first MPC (P_{fst}) parameters. For the method used here, these have been chosen experimentally, by finding parameters delivering the best results. In practice, these parameters could be set during the calibration step, mentioned in the previous subsection. Comparing P_{ndet} and P_{fst} calculated for different environments, it was found that the

[1] In additional measurements, we found out that metal, glass, drywall and concrete produced strong reflections, while wood, plywood and Styrofoam didn't.

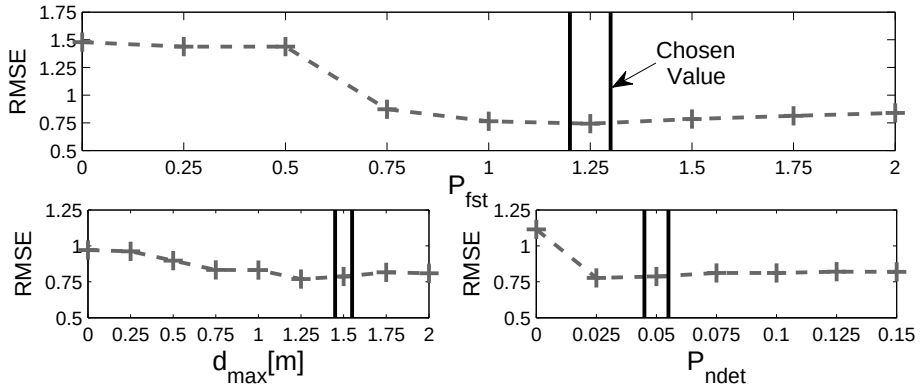

Figure 6.2: RMSE error of the DRAML method with four reflectors for different values of P_{fst}, $d_{\max}$ and P_{ndet} parameters.

values were similar. For that reason, the same values were used for all three environments.

The DRAML method requires the likelihood of non-detection (P_{ndet}), the first MPC penalty (P_{fst}) and penalty length ($d_{\max}$) parameters. These were also chosen experimentally, by finding parameters delivering best results. Fig. 6.2 presents graphs of the error versus the value of each of the parameters. P_{ndet} for DRAML has the same value as for RAML.

6.1.4 Parameter Changes

Over the lifetime of a positioning system, the environment the system operates in will change. This can have two consequences: change in the general number of reflections in the environment; and change in optimal method parameter values (σ_{FR_n}, P_{ndet}, P_{fst} ...). The number of reflections in the environment corresponds to the number of detected MPCs. Greater number of MPCs adversely affects the accuracy of the RAML and RALS methods. For this reason, if the environment becomes more cluttered, and thereby contain more objects for the signal to reflect from, the accuracy of the methods will be reduced. The other factor, the change of the optimal parameter values, should not strongly affect the accuracy. The change would normally be small, and a small difference from the optimal parameter value causes a very small decrease in accuracy, as can be seen from graphs in Fig. 6.2.

6.1.5 Overview of Chosen Parameters

Table 6.1 contains the values of σ_{FR_m} for each reflector in each environment. Table 6.2 contains the values of the parameters used by both the RAML and

Table 6.1: Roughness σ_{FR_m} set for reflectors in different environments

m	Lecture Room		Laboratory		Corridor	
	Description	σ_{FR_m}	Description	σ_{FR_m}	Description	σ_{FR_m}
1	Ceiling	0.1[m]	Ceiling	0.1[m]	Ceiling	0.1[m]
2	Floor	0.141[m]	Floor	0.141[m]	Floor	0.141[m]
3	Left Wall	0.141[m]	Right Wall	0.141[m]	Left Wall	0.245[m]
4	Right Wall	0.141[m]	Left Wall	0.141[m]	Right Wall	0.245[m]
5	Door Wall	0.245[m]	Window Wall	0.245[m]		
6			Door Wall	0.245[m]		

Table 6.2: Parameters used in the RAML and DRAML methods

σ_n	0.1[m]
P_{ndet}	0.05
P_{fst}	0.3

DRAML methods. Table 6.3 contains the values of the parameters used by the DRAML method.

6.2 Error Metric

In my research, I used two error metrics: Mean Absolute Error(MAE) and Root Mean Square Error(RMSE). In this dissertation, I use MAE for TOA cases results, and RMSE for TDOA case results, in keeping with the metric used in my published papers. 3D and 2D versions of the error metric are used. Two versions are used because some applications require a 3D position, while other applications will only use a 2D position. 3D position accuracy is used to evaluate the method usability in 3D position applications, and 2D position accuracy is used correspondingly for 2D position applications.

3D MAE error can be calculated as follows:

$$E_{\mathrm{3D}}^{\mathrm{MAE}} = \frac{1}{S}\sum_{s=1}^{S}\sqrt{(\hat{x}_b^s - x_b^s)^2 + (\hat{y}_b^s - y_b^s)^2 + (\hat{z}_b^s - z_b^s)^2} \tag{6.1}$$

where S is the number of transmitters, $\hat{\mathbf{b}_s} = [\hat{x}_b^s,\ \hat{y}_b^s,\ \hat{z}_b^s]^T$ is the transmitter's estimated position and $\mathbf{b}_s = [x_b^s,\ y_b^s,\ z_b^s]^T$ is the transmitter's real position. 2D MAE is calculated using only the flat 2D position, omitting the height coordinate

Table 6.3: Parameters used in the DRAML method

σ_n	$0.1m$
P_{ndet}	0.05
P_{fst}	1.25
$d_{\max}$	1.5[m]

(z):

$$E_{\text{2D}}^{\text{MAE}} = \frac{1}{S}\sum_{s=1}^{S}\sqrt{(\hat{x}_b^s - x_b^s)^2 + (\hat{y}_b^s - y_b^s)^2} \tag{6.2}$$

3D RMSE error can be calculated as follows:

$$E_{\text{3D}}^{\text{RMSE}} = \sqrt{\frac{1}{S}\sum_{s=1}^{S}(\hat{x}_b^s - x_b^s)^2 + (\hat{y}_b^s - y_b^s)^2 + (\hat{z}_b^s - z_b^s)^2} \tag{6.3}$$

2D RMSE is calculated using only the flat 2D position, omitting the height coordinate (z):

$$E_{\text{2D}}^{\text{RMSE}} = \sqrt{\frac{1}{S}\sum_{s=1}^{S}(\hat{x}_b^s - x_b^s)^2 + (\hat{y}_b^s - y_b^s)^2} \tag{6.4}$$

6.3 General TOA Results (RAML,RALS)

This section presents and discusses the TOA methods results for one case - sparsely furnished, rectangular room, with two receivers on one wall. This case is used to discuss the general properties of RAML and RALS, before the more in-depth discussion in the later sections. This case corresponds to the Lecture Room (see Fig. 5.5), receiver R_3 and R_4 measurements. The above mentioned Lecture Room measurements data and simulation data are used for comparisons. This section corresponds to the results section of our paper [67].

6.3.1 Results

The results of the RAML method, older RALS method, and the conventional methods, Assumed Height(TOA-AH) and Direct Solution(TOA-DS) are compared. Three cases are investigated: 3D positioning error using simulation data; 3D positioning error using measurement data and 2D positioning error using the same measurement data.

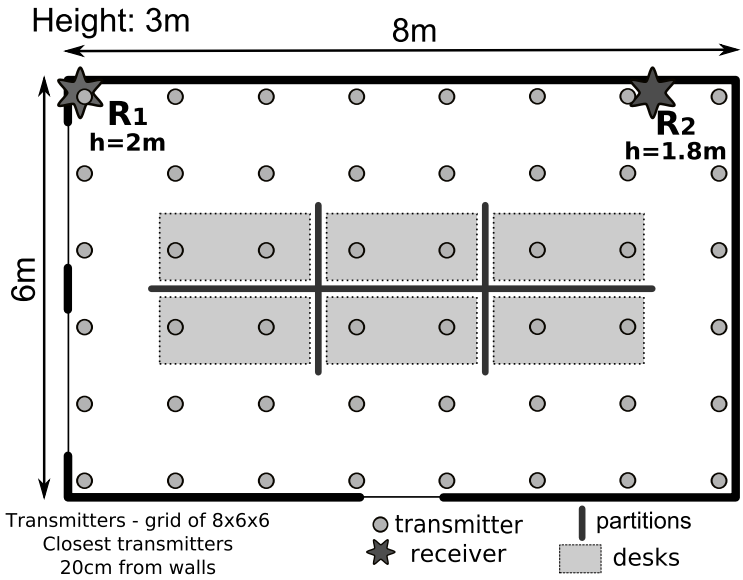

Figure 6.3: Simulation layout, with simulated transmitter positions marked.

In the first case, the methods were tested using data obtained from a simulation. The simulations were performed using our self-developed UWB propagation simulator. The simulated SA was a sparsely furnished room, as presented on Fig. 6.3. See [66] for simulation details.

Fig. 6.4 presents the methods' 3D MAE errors versus the number of reflectors considered. The TOA-AH method is the reference two receiver conventional method. Since AH method does not use reflectors, results for this method are independent of the number of reflectors. The earlier RALS method, originally presented in [66], outperforms AH when two or more reflectors are used. While the RALS method performs better than the TOA-AH method, the RAML method is even more accurate. The performance of both RALS and RAML methods improves with the number of reflectors, but only up to three. Adding fourth and fifth reflectors do not improve the results.

In the second case, the positioning methods were compared using the measurement data. 3D MAE results are presented in Fig. 6.5. 3D MAE results are useful in evaluating the methods for use in applications that require a full 3D transmitter's position. In Fig. 6.5, apart from the methods already mentioned, results for TOA-DS three receiver positioning method are shown. The TOA-DS method, like TOA-AH, is independent of the number of reflectors considered. The three receiver TOA-DS method, unsurprisingly, achieves the best accuracy. However, while being the method with the best accuracy, the TOA-DS method uses three receivers while the other three methods use only two. Of the three, the RALS method produces the worst results. This is because the method was

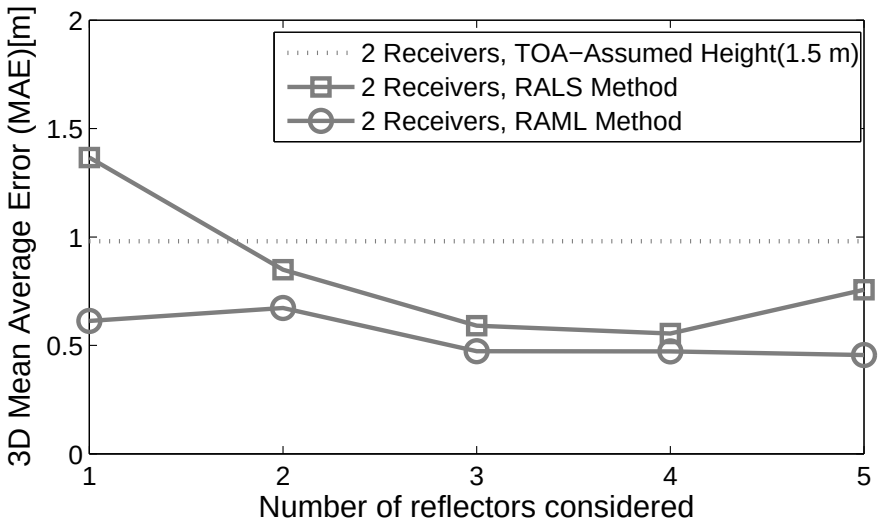

Figure 6.4: Results using simulation data – 3D MAE error versus the number of reflectors considered in the method. Simulation layout shown Fig. 6.3 in used .

originally verified only through the simulation. It proved to be inaccurate when used with measurement data. Measurement data contained a much higher number of detected MPCs than the simulated data, due to propagation effects that were not taken into consideration during the simulation. The TOA-AH method has an average error of 91 cm. This result is comparable to results when simulation data is used, because the main source of error is not the ranging error, but rather the assumption of height. The best of the two-receiver methods is the RAML method. For three or more reflectors, the average error of the RAML method is around 25% smaller than that of the TOA-AH method.

In the third case, the 2D MAE of the different positioning methods was compared, also using the measurement data. The results are presented in Fig. 6.6. 2D MAE results are useful in evaluating the methods for use in applications that require only a 2D transmitter's position. Even if 2D positioning case is considered, the RAML method retains its advantage over the TOA-AH method. Furthermore, somewhat surprisingly, the RAML method has an even larger lead over the TOA-AH method. This is because of the contributions of the left wall to the likelihood function. The left wall partial likelihood function has a symmetry that can, in some cases, lead to a big height error but small 2D error.

6.3.2 Results Discussion

The first conclusion that can be drawn from the results is that the RAML method is consistently better than RALS. RALS was the first method I pro-

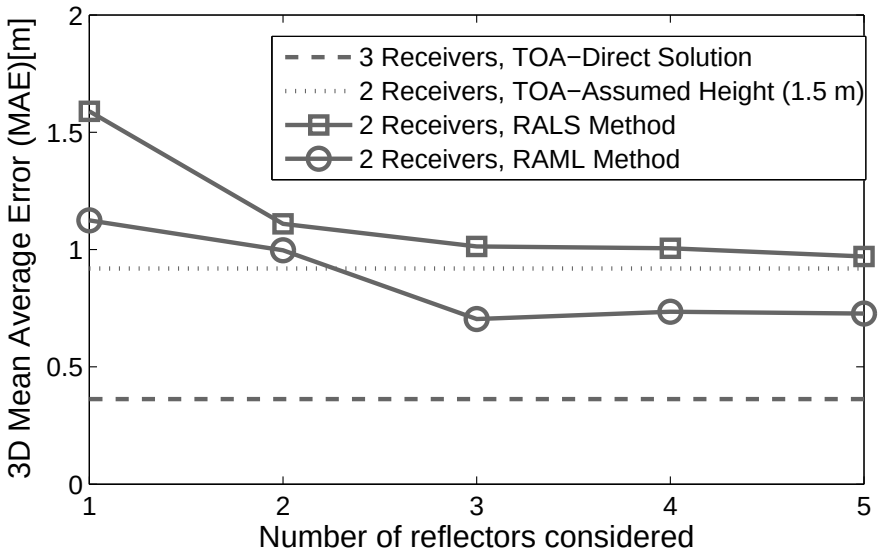

Figure 6.5: Measurement results – 3D MAE error versus the number of reflectors considered in the method. Lecture Room (see Fig. 5.5) and the (R_3,R_4) receiver pair used.

posed, and it was originally verified using only the simulation data. When used with measurement data, or more advanced simulation data, it clearly showed its weakness.

Another conclusion is that adding the fourth or the fifth reflectors did not improve the results in any of the cases. This has more than one cause. The first reason is the geometry of the problem. Both in the simulation and in the measurements, the fourth reflector is the wall near which the receivers are situated, while the fifth reflector is perpendicular to the receivers axis. MPCs reflected from the wall directly behind the receivers come soon after the the direct MPC, making them hard to detect. Additionally, because of a very short "baseline" between the receiver and the receiver's reflection, small range errors would translate into big position error, if only that reflector were to be used. In other words, little information is added by this reflection. Additionally, during the measurements, the receiver antennas' back was towards the wall, strongly attenuating the reflection from that wall.

As to the fifth reflector, walls nearly perpendicular to the receivers axis (line connecting both receivers) contribute only slightly to the positioning accuracy. This is because, in the exactly perpendicular reflector case, a receiver's reflection is collinear with the two receivers. Because of that, the reflected MPC range would be the same regardless of where on the RC the transmitter is. In other words, the reflection contains no information.

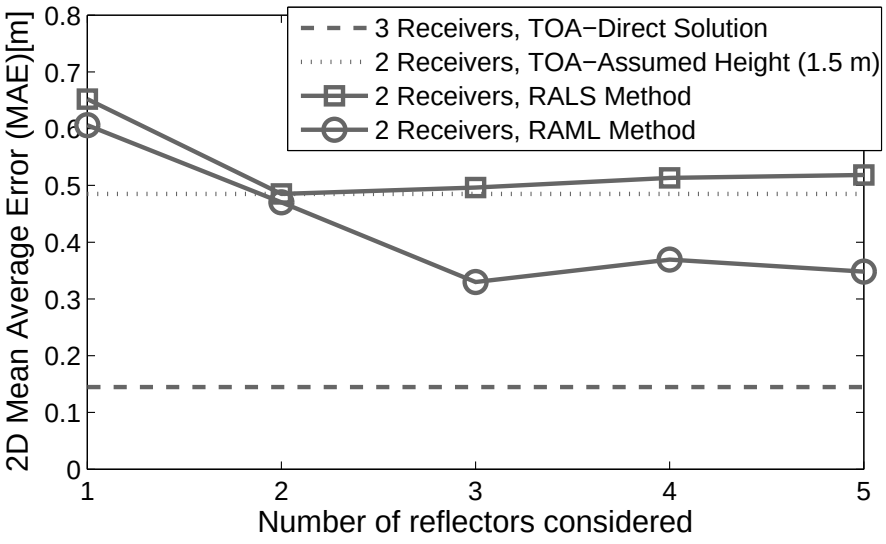

Figure 6.6: Measurement results – 2D, no height, MAE error versus the number of reflectors considered in the method. Lecture Room (see Fig. 5.5) and the (R_3,R_4) receiver pair used.

These two geometrical concerns limit the practical usable number of reflectors to three, in the case of rectangular rooms with both receivers on one wall. It should be noted, that including the reflections from the geometrically ill-conditioned reflectors should not adversely affect the result. Both the RAML and the RALS methods compensate for this problem.

The second reason is the error floor of the RAML and RALS methods. Depending on σ_n^j and σ_{FR_m} values, likelihood peaks, caused by two close MPC ranges, can overlap. Such overlapping causes the total peak to be in-between MPCs, corresponding to neither. This causes an error floor for the positioning methods. For that reason, values of σ_n^j and σ_{FR_m} should be set close to their measured values, and not higher.

The final reason, applicable to the Lecture Room environment's fifth reflector, is the quality of the reflector. As can be seen in Fig. 5.5, the fifth reflector, the door wall, is uneven, with a protruding pillar and sections on either side of the pillar of different depths. This makes a flat reflector a poor approximation of its shape.

Antenna's radiation pattern did not seem to influence the results significantly. However, apart from attenuating the reflection from the right wall, after examining the received waveforms, there were a few cases when the central null of the antenna's radiation pattern attenuated some reflected MPCs so much as to make them undetectable. A better radiation pattern would improve the

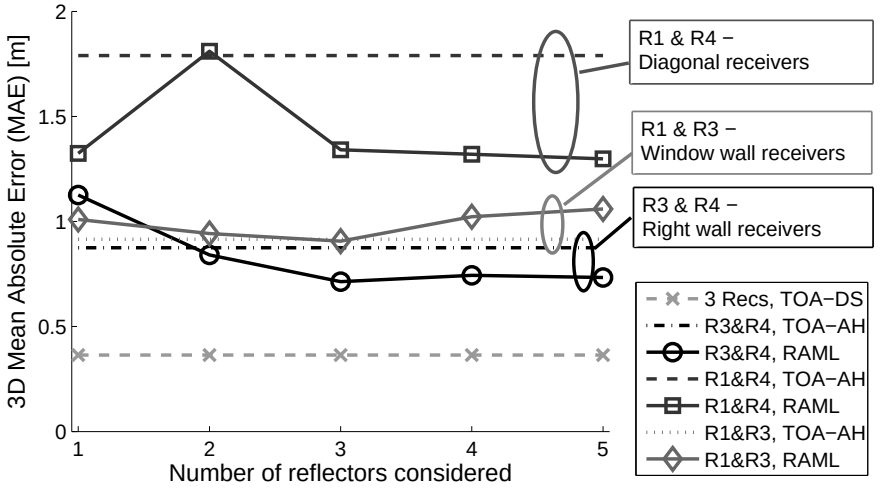

Figure 6.7: 3D MAE results of the methods for the three receiver pair choices. Lecture Room measurements (see Fig. 5.5) were used.

results.

6.4 Different Receiver Positions (RAML)

In this section, the influence of the receiver placement on the methods' results is investigated. Accuracy of a positioning system is heavily dependent on anchor placement [78]. Receiver placement in the RAML method is of special interest, because the position of receivers in relation to reflectors is an additional factor influencing the accuracy. The Lecture Room(Fig. 5.5) measurement data were used.

The comparison of the results for the different receiver placements is presented in Fig. 6.7. Three receiver pairs were used: (R_1,R_3), window wall receivers, (R_1,R_4), diagonal receivers, and right wall receivers(R_3,R_4), as investigated in the previous section. The considered methods are: TOA-DS, RAML, and TOA-AH. Results for the TOA-AH and RAML methods are presented for three receiver pair choices. Mean Average Error(MAE) results as a function of the number of considered reflectors are shown. In TOA-AH, the transmitter's assumed height is 1.5[m], which is the average transmitter height. Since TOA-AH and TOA-DS do not use reflectors, their results are independent of the number of reflectors.

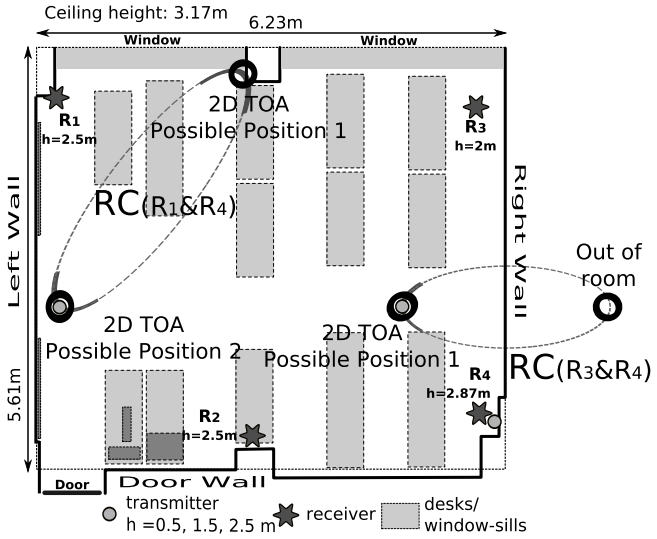

Figure 6.8: Comparison of the RC for (R_1,R_4) and (R_3,R_4) receiver pairs. Both position candidates are inside the SA for (R_1,R_4) pair, but only one is inside for the (R_3,R_4) pair.

6.4.1 Conventional Methods

First, the results for the TOA-AH and TOA-DS methods are compared. As mentioned before, from the considered methods, TOA-DS has the best accuracy, but it requires three receivers, unlike TOA-AH and RAML.

If the TOA-AH method is considered, results for (R_1,R_3) and (R_3,R_4) receiver pairs are very similar. This is because in both cases the receivers are close to one wall: the window wall in the first case, the right wall in the second. Since TOA-AH corresponds to 2D two receiver TOA positioning, the initial result contains two transmitter position candidates. However, if both receivers are on the same wall, which is the case here, one of the candidates can be discarded because it falls outside of the SA bounds.

If the third receiver pair, (R_1,R_4) is used, the error of the TOS-AH method is significantly larger. In this case, the receivers are placed diagonally. Because of that, both transmitter position candidates generally fall inside the SA bounds. One of the candidates has to be chosen randomly, generating a large error if the wrong one is chosen. Fig. 6.8 compares the placement of position candidates in the case (R_1,R_4) and (R_3,R_4) receiver pairs.

6.4.2 R_3 and R_4 - Right Wall Receivers

The (R_3,R_4) receiver pair case was discussed in the previous Section 6.3.

6.4.3 R_1 and R_3 - Window Wall Receivers

Looking at the RAML method results for (the R_1,R_3) receiver pair, the results for one and two reflectors are similar to the results for the (R_3,R_4) receiver pair. However, the accuracy does not increase with adding the third (left wall) or later reflectors, and consequently the conventional TOA-AH method is more accurate for any number of reflectors.

The reason for this is the geometry of the left and right walls and the unevenness of the door wall. Left and right walls do not improve the accuracy because they are perpendicular to the receiver axis, as already discussed in Sec. 6.3.2. The fifth reflector, the door wall, is not affected by this problem, but, as mentioned in Sec. 6.3.2, it is very uneven. Using it does not improve the accuracy either.

6.4.4 R_1 and R_4 - Diagonal Receivers

When diagonal receivers (R_1,R_4) are considered, results for both the TOA-AH and RAML methods are clearly worse than the results for the other receiver pairs. However, the RAML method is consistently better than TOA-AH. As mentioned in subsection 6.4.1, in the diagonal receiver case two transmitter position candidates, or, in the case of RAML, two transmitter position candidate regions, exist. RAML method is better at choosing the right transmitter position candidate region then TOA-AH, which uses random selection. However, this effect is observed for as few as one reflector; adding more does not increase accuracy. We could not find an adequate explanation for the bad result in the case of two reflectors. It might be that, in reality, the good result for a single reflector is a coincidence, therefore, using three or four reflectors, all well-approximated reflectors, is recommended.

6.4.5 Discussion of Results

For both the TOA-AH and RAML methods, higher accuracy can be achieved if receivers are placed along a wall, SA bound. This placement avoids the problem of two separate transmitter position candidates/candidate regions.

Additionally, in along-wall receiver placement case, the RAML method, as used with current measurement data, requires three good reflectors to achieve accuracy better than the TOA-AH method. Two of the reflectors are readily available: ceiling and floor. The third reflector should be a wall opposite the receivers. In the case of the (R_3,R_4) pair, this is the left wall, well approximated by the flat reflector model. The RAML method's accuracy is consequently better than the AH method's for this pair, for three or more reflectors. However, in the

case of the (R_1,R_3) reflector pair, the opposite wall is the door wall, not well approximated by a flat reflector model. Consequently, accuracy of the RAML method is never better than accuracy of the TOA-AH method in this case.

In other words, to achieve the best results with two receiver TOA positioning, receivers which were positioned near one wall, opposite a flat wall, should be chosen. An example of this placement is the (R_3,R_4) receiver pair.

It is possible that in some cases only a diagonal receiver placement will be available. The most probable cause of such a placement is a failure of some of the receivers in a larger positioning system. In that case, the RAML method has better accuracy than the TOA-AH method, and should be used with all well approximated reflectors (4 in the measured case).

6.4.6 Summary

Three receiver placements were compared using measurement data. Unlike in conventional methods, if RAML is used, the availability of good reflectors has to be taken into consideration during receiver placement choice. The best result using RAML method is achieved with two receivers lined along a wall and a flat opposite wall (R_3,R_4), the case that was investigated in the previous section. This is the optimal case for reflection-based two receiver positioning. Although the sub-optimal case of diagonally placed receivers (R_1,R_4) should not be used, if this case does occur, the RAML method achieves significantly better accuracy than conventional method.

6.5 Different Environments (RAML)

In this section, the influence of different environments on the methods' accuracy is compared. All three measured environments are used, the Lecture Room, the Laboratory and the Corridor. This section corresponds to our paper [79].

6.5.1 Results

The cases investigated are:

- Lecture Room with receivers on one wall (R_3,R_4)
- Lecture Room with diagonal receivers (R_1,R_4)
- Laboratory with receivers on one wall (R_2,R_3)
- Laboratory with diagonal receivers (R_2,R_3)
- Corridor with receivers in opposite ends

In the first case, the RAML method was tested using the Lecture Room measurements and receivers on one wall, R_3 and R_4. This case was discussed in

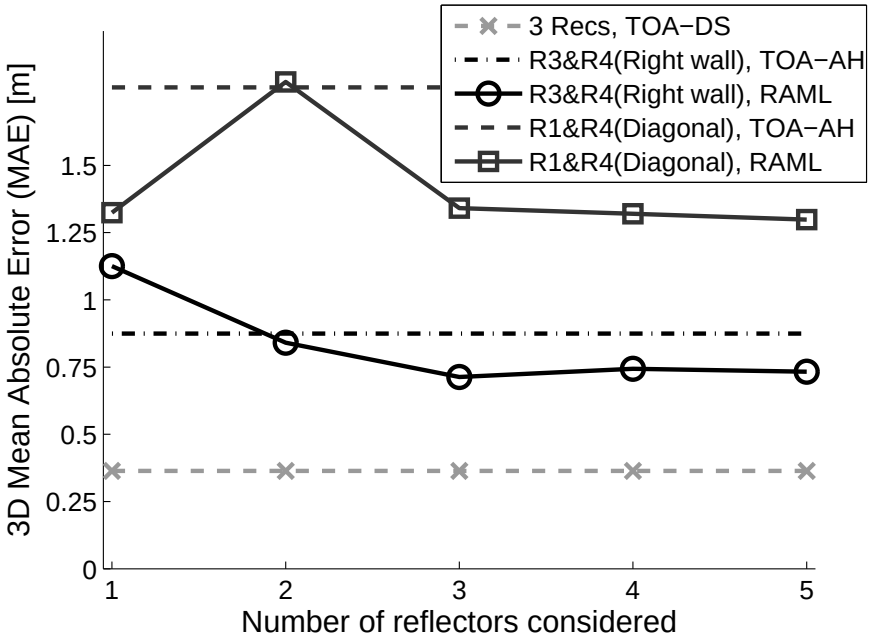

Figure 6.9: Lecture Room, same wall receivers(R_3,R_4) and diagonal receivers (R_1,R_4) – 3D MAE error versus the number of reflectors considered in the method. (Results same with Fig. 6.5)

Section 6.3.2, but the results for this and the next, diagonal, case are repeated in Fig. 6.9.

In the second case, the RAML method was tested using Lecture Room measurements and receivers in diagonal corners, R_1 and R_4. This case, and its difference with the first case, were already discussed in Section 6.4.4 The results are nevertheless repeated in Fig. 6.9.

In the third case, the RAML method was tested using the Laboratory measurements and receivers on one wall, R_1 and R_4. The results for this and the next, diagonal, case are presented in Fig. 6.10. In this case, the RAML method is less accurate than the AH method, for any number of reflectors. This is caused by the very cluttered nature of the environment. The equipment, shelves, metal cases etc. cause many reflections, and consequently many MPCs, which lowers the accuracy of the RAML method. It can also be noted that the TOA-DS method also does not perform as well in the Laboratory Room as in the Lecture Room. This is caused by the direct path being blocked to some of the transmitter positions.

In the fourth case, the RAML method was tested using the Laboratory measurements and receivers in diagonal corners, R_2 and R_4. The results are presented in Fig. 6.10.

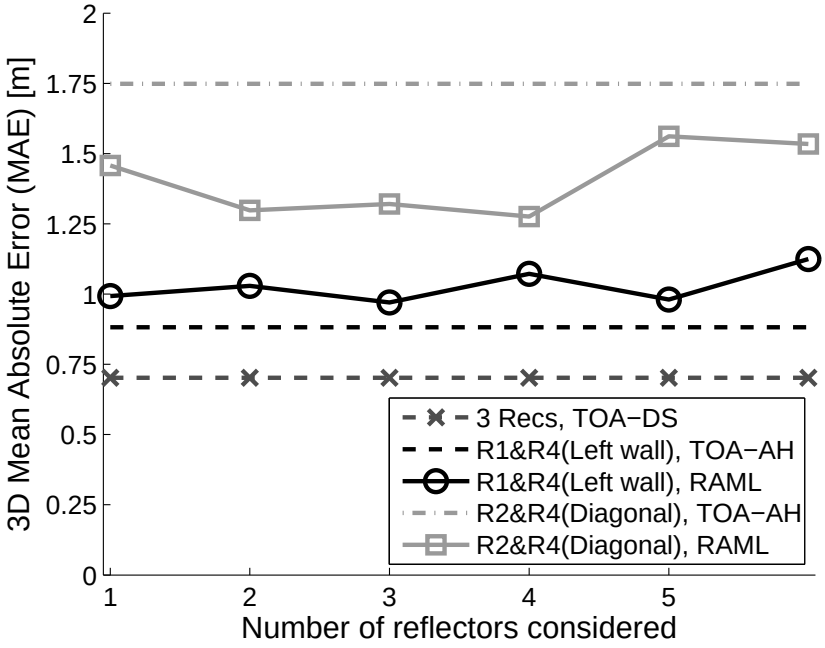

Figure 6.10: Laboratory, same wall receivers(R_1,R_4) and diagonal receivers (R_2,R_4)– 3D MAE error versus the number of reflectors considered in the method.

The RAML method is more accurate than the AH method in this case. The cause is the same as in the second case, diagonal receivers in the Lecture Room, as already explained in Section 6.4. In the presence of two transmitter position candidates/RC regions in SA, the RAML method is better at choosing the right one. It can also be noted that the fifth and sixth reflectors worsen the accuracy of the RAML method. These reflectors are the door wall and the window wall. The door wall is highly uneven, while the windows have anti-burglary grilles, causing additional strong reflections not directly from the window.

In the fifth, final, case, the RAML method was tested using the measurement performed in the Corridor, with receivers at the opposite ends of the Corridor. Results are presented in Fig. 6.11. First of all, the TOA-DS method's accuracy is very bad in this case. This is caused by the three receivers being nearly collinear, a geometry strongly damaging to the precision of positioning. Secondly, the RAML method's accuracy is better than TOA-AH method's. This is again caused by the presence of two transmitter position candidates/ RC regions in the SA, although these are much closer together, given the shape of the SA.

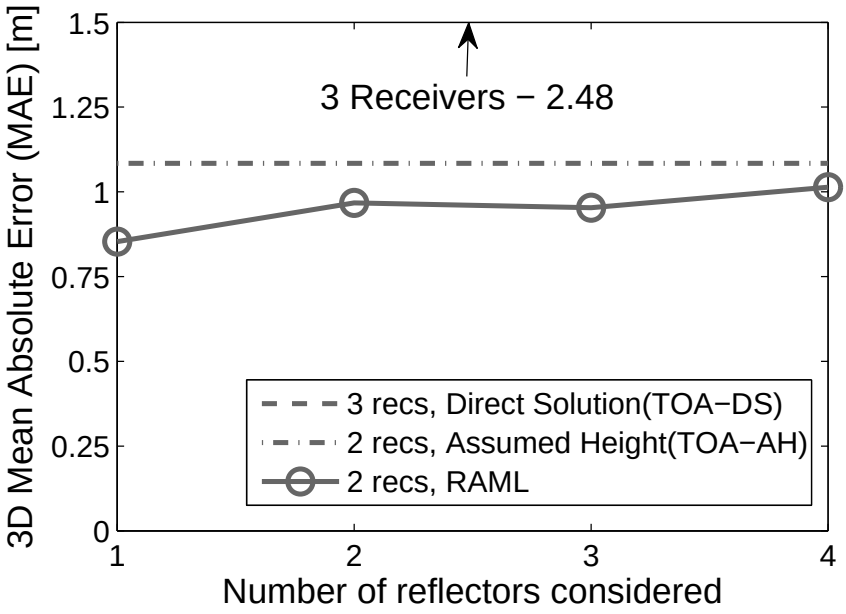

Figure 6.11: Corridor, receivers at both ends – 3D MAE error versus the number of reflectors considered in the method.

6.5.2 Results Discussion

The first thing to notice from the environment comparison is that the result of the RAML method strongly depends on the environment. The RAML method functions badly in cluttered environments, with a large number of reflections. However, if the number of reflections is within a limit, positioning accuracy is improved.

However, in all environments, the RAML method is good at choosing the right transmitter position/position region, making it better than the TOA-AH method if two transmitter position candidates/ RC regions are in the SA.

6.6 TOA Positioning Summary

The results of TOA positioning using the RAML and RALS methods were compared with the conventional methods. Three aspects of positioning using the RAML method were examined: the general properties of RAML, the dependence on the receiver placement, and the dependence on the environment.

It was found that the RAML method outperforms the conventional TOA-AH method with three or more reflectors, for receivers placed along a wall. It was also found that the practical limit on the number of useful reflectors in the case of a rectangular room and along-wall receiver placement is three.

While examining the dependence of the method's accuracy on receiver placement it was found that the optimal receiver placement is along a wall, with a flat opposite wall. Also, if the receivers are placed diagonally, the RAML method outperforms the TOA-AH method, although the results are generally much worse than in the along-wall placement case.

Finally, while examining the RAML positioning method results in three different environments, it was found that the method performs best in the case of not too cluttered rooms, and may be worse than TOA-AH in the case of cluttered rooms. However, even in the case of very cluttered rooms, it can be successfully used to distinguish between two transmitter position candidates, achieving higher accuracy than the TOA-AH method in the case where that is required.

6.7 TDOA Results (DRAML)

This section compares the results of the DRAML method with two conventional, three receiver methods: TDOA Assumed Height(TDOA-AH) and TOA Direct Solution(TOA-DS). All the methods are defined in chapter 4. 3D and 2D positioning errors are investigated.

Fig. 6.12 presents the 3D RMSE results of the three methods for different number of reflectors used. Since neither TOA-DS nor TDOA-AH methods use reflectors, their performance is independent of the number of reflectors. As expected, the lowest error is achieved by TOA-DS method. However, TOA-based methods may be impossible to use, especially if cheap disposable tags are employed and two-way ranging or synchronization cannot be used. The reference conventional TDOA method, TDOA-AH achieves RMSE of 89cm. In comparison, the proposed DRAML method achieves better results for three or more reflectors.

Fig. 6.13 presents the 2D RMSE results. Similarly to the 3D case, the DRAML method outperforms TDOA-AH for three or more reflectors. A better 3D position estimate translates into a better 2D estimate. However, the advantage of the DRAML method is smaller than in the 3D case. This result is opposite the result achieved for the RAML method in the previous chapter(See section 6.3).

6.7.1 Results Discussion

Analyzing Figs 6.12 and 6.13, it can be seen that the DRAML method's positioning accuracy improves with the number of reflectors. However, a fifth reflector did not improve the results. This is because the fifth reflector is the Door Wall,

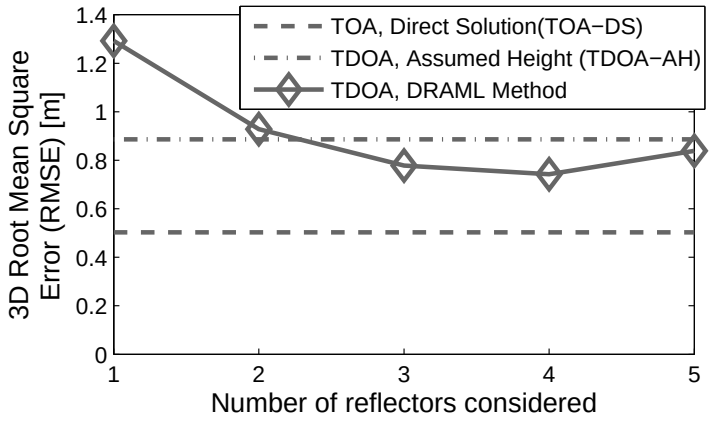

Figure 6.12: Measurement results – 3D RMSE error versus the number of reflectors considered. All methods use three receivers. Only the DRAM method depends on the number of receivers. Lecture Room measurements (see Fig. 5.5) and (R_1, R_3,R_4) receivers were used.

which, as discussed in Section 6.3.2, is highly uneven and therefore very poorly approximated by a flat reflector.

It is interesting to note that in the case of the RAML method, already the fourth reflector did not improve the results. The difference between the RAML and DRAML methods is that DRAML uses three receivers. Both receivers used by the RAML method are placed near the fourth reflector, the Right Wall, which, as already discussed, makes the reflections from this wall carry little positioning information. This is not the case for the third receiver, R_1, used only by the DRAML method, which makes the fourth reflector useful. This result suggests, that for DRAML method, the degree to which the reflector can be approximated by a flat reflector model should be the main criterion for the reflector choice, while the placement of the reflector can be generally disregarded.

6.8 Summary

This chapter presented the results of RALS, RAML and DRAML methods in comparison with conventional positioning methods in three environments, with different receiver positions. The results have shown that RAML method can outperform the conventional TOA-AH method in a an uncluttered room, with both receivers on one wall and a flat opposite wall. RAML can also outperform TOA-AH in the sub-optimal case of diagonal receivers. DRAML, can also outperform the conventional method, TDOA-AH in this case, in a an uncluttered

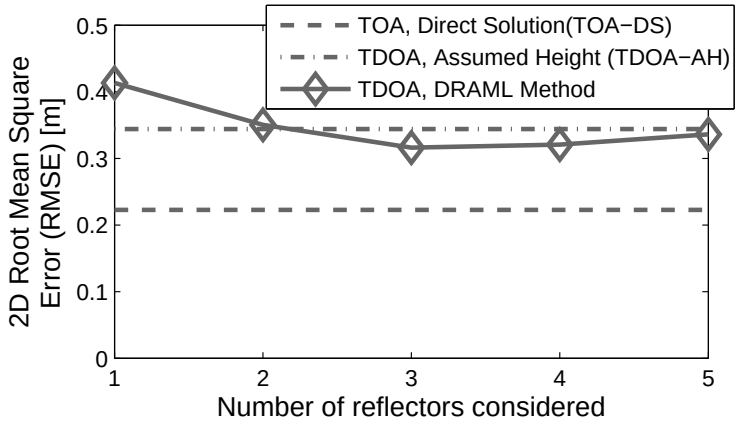

Figure 6.13: Measurement results – 2D RMSE error(discounting height) versus the number of reflectors used. Lecture Room measurements (see Fig. 5.5) and (R_1, R_3,R_4) receivers were used.

room. RALS method was shown to be always worse than RAML.

Chapter 7

Conclusions

This final chapter presents the summary of the disseration, discusses the contribution of the thesis, as well as proposes possible ways of improvement for the methods presented in the thesis.

7.1 Summary of the Dissertation

This dissertation was divided into five parts, an introductory chapter 1 was followed by the description of the indoor positioning field in Chapter 2, the description of the UWB positioning field in chapter 3, the description of the proposed methods in Chapter 4, measurements description in Chapter 5 and method results in Chapter 6.

The first part, Chapter 2, showed that the time-based UWB is a very good candidate for positioning. The chapter presented an introduction of the field, as well as an overview of the technologies and techniques that can be used for indoor positioning. Among the presented technologies, UWB was shown to be the best candidate, because of its ranging accuracy, ability to penetrate obstacles, and resistance to multipath fading. Among the presented positioning techniques, it was shown that only TOA, TDOA and AOA are suitable for high precision ranging in indoor environments, although RSS and Fingerprinting are also suitable for medium-precision ranging.

The second part, Chapter 3, showed the place of my research subject, reflection-aided positioning, in the broader indoor UWB positioning field, as well as its usefulness. The chapter presented an introduction to UWB technology, UWB regulations and characteristics, and an overview of research subjects in the UWB field. The regulations limit the power levels of UWB, making only short-range positioning possible, and forcing the use of many reference nodes in order to cover building-sized service areas. The overview of the research subjects shows

the problems in the UWB field, and how my research might help solve some of them.

The third part, Chapter 4, introduced the two proposed methods, RAML and DRAML. Apart from the proposed methods, also the conventional methods used for comparison were introduced.

The fourth part, Chapter 5, introduced measurements used for method verification. The chapter presented the measurement setup and the three environments in which the measurements were conducted. Measurements for a total of 120 transmitter positions were performed.

The fifth part, Chapter 6, compared the results of the proposed and conventional methods in the three measured environments. A total of four studies were presented: general TOA results, results for different receiver positions, results for different environments, and general TDOA results. Both TOA RAML and TDOA DRAML can achieve better accuracy than the conventional methods. The two main requirements are the availability of at least three reasonably flat reflectors/walls and a relatively uncluttered environment. In the case of RAML, the position of the reflectors in respect to the receivers also strongly influences the results.

The results show that, in the right conditions, both the RAML and DRAML methods outperform the conventional methods, when using the same number of receivers. The two most important requirements were found to be the availability of at least three reasonably flat reflectors/walls and a relatively uncluttered environment. Also, especially in the case of the RAML method, the position of the reflectors in respect to the receivers strongly influences the results.

7.2 Contribution of the Thesis

As mentioned in the introduction, this dissertation makes three main contributions. The first contribution are the two, new positioning methods. The second contribution is the verification of those methods, and the analysis of methods' results. Finally, the most important contribution is proving the validity of the Reflection-Aided approach in general.

7.2.1 Positioning Methods

The first contribution are the two novel positioning methods: RAML and DRAML. These are the first reported methods that use reflections to improve accuracy of an indoor positioning system. The main proposed application of those methods is as a part of a larger positioning system, for the cases when, due to sparse receiver placement or attenuation caused by obstacles, only two (TOA)

or three(TDOA) LOS paths from the transmitter to the receivers are available. The methods require receivers capable of MPC ranging and many calculations, but no additional or special antennas.

7.2.2 Validation of the Proposed Methods

The second contribution is the validation of the methods using real world measurements. Both TOA RAML and TDOA DRAML can achieve better accuracy than the conventional methods. The two main requirements are the availability of at least three reasonably flat reflectors/walls and a relatively uncluttered environment. The two identified problems, flat reflectors availability and cluttered environments/high number of MPCs, will be a challenge for all reflection-based systems.

7.2.3 Reflection-Aided Positioning Approach

The final, most important contribution, is proving the validity of the Reflection-Aided approach in general. Validation clearly showed that using reflections can improve results, even if single antenna receivers without tracking are used.

However, the proposed methods will most probably not be used in their current form. First of all, commercial systems, such as Ubisense platform, have currently a higher claimed accuracy. This is because those systems use AOA ranging and tracking in addition to TDOA ranging, which were not considered in the proposed method. Secondly, the cost of receivers capable of detecting MPCs is currently very high. This, however, should change in time, with constantly increasing capabilities and falling prices of integrated circuits.

Although the proposed methods will not be used directly, they provide a good base for more advanced, reflection-based methods. In particular, AOA and tracking are the two technologies that can be added to reflection-based positioning, improving the overall results significantly.

All things considered, I believe that in the future, when UWB receivers capable of detecting MPCs become affordable, the reflection-using UWB positioning systems will become mainstream. I hope my work will contribute to those future systems.

The proposed approach and methods are not limited to the UWB positioning. In the measurements, UWB was used, but the real condition for using the presented methods is a good time resolution of the received signal. In other words, the same methods could be used with, for example, ultrasound signals, or with not as wideband systems in bigger spaces.

7.3 Future Avenues of Improvement and Research

No research is ever complete. This is also true for my research. Here I will present different ideas for future research based on my thesis.

The first interesting research problem is using angle-of-arrival(AOA) information together with reflection-aided positioning system. Using AOA should greatly improve the results, because AOA information can be used to reject MPCs coming from the wrong directions when looking for a MPC caused by a given reflector. This would dramatically limit the problem of multiple MPCs. I did not explore the use of AOA because of lack of measurements for AOA positioning.

The second future research problem is using tracking together with reflection-aided positioning. Tracking should also significantly improve the results, because of the increased diversity. The proposed methods can sometimes result in a few near-equally probable position candidates. Tracking can be used to filter out the position candidates that do not match a trajectory, greatly improving the results. Because there can be more than one position candidate, particle filters rather than simple Kalman filters should be used. As for AOA, I did not explore tracking because of lack of suitable measurements.

The third interesting research problem is developing reflection-based methods for different numbers of receivers. In my research, I developed methods for two receiver TDOA positioning and a general algorithm for positioning accuracy improvement through reflections. However, the achieved results were not exceptional, and therefore they were not presented. A different perspective, or using the reflections approach together with some other techniques, could however provide better results.

The fourth research problem would be verifying the proposed methods in more usage scenarios. In particular the influence of the following factors could be checked:

- Simpler receiver architectures (Energy Receiver)
- Signal's shape and bandwidth
- Antenna radiation pattern
- Different noise levels
- More different environments

Finally, the fifth research problem would be incorporating the knowledge of the transmitter position probability distribution into the positioning system. That should be reasonably straightforward, since the methods are ML-based.

Bibliography

[1] S. J. Ingram, D. Harmer, and M. Quinlan, "Ultra-Wideband indoor positioninng systems and their use in emergencies," in *Proc. IEEE Position Location and Navigation Symp. (PLANS)*, April 2004, pp. 706–715.

[2] K. Siwiak and J. Gabig, "IEEE 802.15.4IGa informal call for application response, contribution#11," Doc.: IEEE 802.15-04/266r0, July 2003. [Online]. Available: http://www.ieee802.org/15/pub/TG4a.html

[3] "First Report and Order 02-48," Federal Communications Comission, Tech. Rep., February 2002. [Online]. Available: http://hraunfoss.fcc.gov/edocs_public/attachmatch/FCC-02-48A1.pdf

[4] "Commision Decision of February 2007 on allowing the use of radio spectrum for equipment using ultra-wideband technology in a harmonised manner in the Comunity. Official Journal of the European Union, 2007/131/EC," The Commission of the European Communities, Tech. Rep., February 23 2007. [Online]. Available: http://eur-lex.europa.eu/LexUriServ/site/en/oj/2007/l_055/l_05520070223en00330036.pdf

[5] R.Kohno, "Interpretation and future modification of Japanese regulation for UWB." IEEE P802.15-06/261r0, Tech. Rep., May 16 2006.

[6] "Wimedia Alliance." [Online]. Available: http://www.wimedia.org

[7] "IEEE standard for information technology - telecommunications and information exchange between systems - local and metropolitan area networks - specific requirement part 15.4: Wireless medium access control (MAC) and physical layer (PHY) specifications for low-rate wireless personal area networks (WPANs)," pp. 1–203, iEEE Std 802.15.4a-2007 (Amendment to IEEE Std 802.15.4-2006).

[8] "IEEE 802.15 standard 4f Task Group webpage. One of the alternative PHYs is OOK-UWB." [Online]. Available: http://www.ieee802.org/15/pub/TG4f.html

[9] M. Z. Win and R. A. Scholtz, "Impulse radio: how it works," *IEEE Commun. Lett.*, vol. 2, no. 2, pp. 36–38, 1998.

[10] "Ubisense systems." [Online]. Available: http://www.ubisense.net

[11] "Time domain plus rtls webpage," retrieved on 2011.01.16. [Online]. Available: http://www.timedomain.com/plus.php

[12] "Dart UWB System." [Online]. Available: http://zes.zebra.com/technologies/location/dart-ultra-wideband.jsp

[13] R. J. Dippy, "GEE: a radio navigational aid," *Journal of the Institution of Electrical Engineers -Part IIIA: Radiolocation*, vol. 93, no. 2, pp. 468–480, 1946.

[14] J. A. Pierce, "An Introduction to LORAN," *Proceedings of the IRE*, vol. 34, no. 5, pp. 216–234, 1946.

[15] B. Hoffmann-Wellenhof, H. Lichtenegger, and J. Collins, *Global Positioning System: theory and practice*, 4th ed. New York: Springer-Verlag, 1997.

[16] T. R. RM-8143, "FCC Docket No. 94-102. Revision of the commissions rules to insure compatibility with enhanced 911 emergency calling systems," Federal Communicarions Commission, Tech. Rep., July 1996.

[17] A. Michalski and J. Czajewski, "The accuracy of the global positioning systems," *IEEE Instrumentation & Measurement Magazine*, vol. 7, no. 1, pp. 56–60, 2004.

[18] X. Wang, F. Silva, and J. Heidemann, "Demo Abstract: Follow-Me Application—Active Visitor Guidance System," in *Proceedings of the 2nd ACM SenSys Conference*. Baltimore, Maryland, USA: ACM, November 2004. [Online]. Available: http://www.isi.edu/~johnh/PAPERS/Wang04d.html

[19] N. Patwari, J. N. Ash, S. Kyperountas, I. Hero, A. O., R. L. Moses, and N. S. Correal, "Locating the nodes: cooperative localization in wireless sensor networks," *IEEE Signal Process. Mag.*, vol. 22, no. 4, pp. 54–69, 2005.

[20] S. Krishnan, P. Sharma, Z. Guoping, and O. H. Woon, "A UWB based Localization System for Indoor Robot Navigation," in *Proc. IEEE Int. Conf. Ultra-Wideband ICUWB 2007*, 2007, pp. 77–82.

[21] J. R. Gonzalez and C. J. Bleakley, "Robust Ultrasonic Spread-Spectrum Positioning System using a AoA/ToA Method," in *Proc. IEEE Int. Symp. Intelligent Signal Processing WISP 2007*, 2007, pp. 1–6.

[22] G. Retscher and Q. Fu, "Continuous indoor navigation with RFID and INS," in *Proc. IEEE/ION Position Location and Navigation Symp. (PLANS)*, 2010, pp. 102–112.

[23] M. De Agostino, A. M. Manzino, and M. Piras, "Performances comparison of different MEMS-based IMUs," in *Proc. IEEE/ION Position Location and Navigation Symp. (PLANS)*, 2010, pp. 187–201.

[24] J. A. Pierce, "Omega," *IEEE Aerospace and Electronic Systems Magazine*, vol. 4, no. 7, pp. 4–13, 1989.

[25] "Skyhook wireless." [Online]. Available: http://www.skyhookwireless.com/

[26] A. J. Weiss, "Direct position determination of narrowband radio transmitters," in *Proc. IEEE Int. Conf. Acoustics, Speech, and Signal Processing (ICASSP '04)*, vol. 2, 2004.

[27] Y. Qi, H. Kobayashi, and H. Suda, "Analysis of wireless geolocation in a non-line-of-sight environment," *IEEE Trans. Wireless Commun.*, vol. 5, no. 3, pp. 672–681, 2006.

[28] D. Chazan, M. Zakai, and J. Ziv, "Improved Lower Bounds on Signal Parameter Estimation," *IEEE Trans. Inf. Theory*, vol. 21, no. 1, pp. 90–93, 1975.

[29] S. Gezici, Z. Tian, G. B. Giannakis, H. Kobayashi, A. F. Molisch, H. V. Poor, and Z. Sahinoglu, "Localization via ultra-wideband radios: a look at positioning aspects for future sensor networks," *IEEE Signal Process. Mag.*, vol. 22, no. 4, pp. 70–84, July 2005.

[30] Y. Qi, "Wireless geolocation in a non-line-of-sight environment," Ph.D. dissertation, Princeton University, 2003.

[31] D. Dardari, C.-C. Chong, and M. Z. Win, "Improved Lower Bounds on Time-of-Arrival Estimation Error in Realistic UWB Channels," in *Proc. IEEE 2006 Int Ultra-Wideband Conf*, 2006, pp. 531–537.

[32] I. Guvenc, S. Gezici, and Z. Sahinoglu, "Ultra-wideband range estimation: Theoretical limits and practical algorithms," in *Proc. IEEE Int. Conf. Ultra-Wideband ICUWB 2008*, vol. 3, 2008, pp. 93–96.

[33] D. Dardari, C.-C. Chong, and M. Z. Win, "Threshold-Based Time-of-Arrival Estimators in UWB Dense Multipath Channels," *IEEE Trans. Commun.*, vol. 56, no. 8, pp. 1366–1378, 2008.

[34] Y. Qi and H. Kobayashi, "A Unified Analysis for Cramer-Rao Lower Bound For Non-line-of-sight Geolocation," in *Proc. 36th Annu. CISS, Mar. 2002, pp. 598-602.*, 2002.

[35] Y. Qi and H. Kobayashi, "On relation among time delay and signal strength based geolocation methods," in *Proc. IEEE Global Telecommunications Conf. GLOBECOM '03*, vol. 7, 2003, pp. 4079–4083.

[36] Y. Qi, H. Kobayashi, and H. Suda, "On Time-of-arrival Positioning in a Multipath Environment," *IEEE Trans. Veh. Technol.*, vol. 55, no. 5, pp. 1516–1526, 2006.

[37] Z. Sahinoglu, S. Gezici, and I. Guvenc, *Ultra-wideband positioning systems: theoretical limits, ranging algorithms, and protocols.* Cambridge Univ Press, 2008.

[38] P. Bahl and V. N. Padmanabhan, "RADAR: an in-building RF-based user location and tracking system," in *Proc. IEEE Nineteenth Annual Joint Conf. of the IEEE Computer and Communications Societies INFOCOM 2000*, vol. 2, 2000, pp. 775–784.

[39] A. Chehri, P. Fortier, and P.-M. Tardif, "Geolocation for UWB Networks in underground mines," in *Proc. IEEE Annual Wireless and Microwave Technology Conf. WAMICON '06*, 2006, pp. 1–4.

[40] C. Steiner and A. Wittneben, "Low Complexity Location Fingerprinting With Generalized UWB Energy Detection Receivers," *IEEE Trans. Signal Process.*, vol. 58, no. 3, pp. 1756–1767, 2010.

[41] J. Schroeder, S. Galler, K. Kyamakya, and K. Jobmann, "NLOS detection algorithms for Ultra-Wideband localization," in *Proc. 4th Workshop on Positioning, Navigation and Communication WPNC '07*, 22–22 March 2007, pp. 159–166.

[42] "IMEC - first 802.15.4a transceiver." [Online]. Available: http://www.imec.be/ScientificReport/SR2007/html/1384152.html

[43] "Decawave webpage." [Online]. Available: http://www.decawave.com/

[44] A. F. Molisch, "Ultrawideband propagation channels-theory, measurement, and modeling," *IEEE Trans. Veh. Technol.*, vol. 54, no. 5, pp. 1528–1545, 2005.

[45] A. Molish, K. Balakrishnan, and C. Chong, "IEEE 802.15.4a channel model - final report," Sep. 2004. [Online]. Available: http://www.ieee802.org/15/pub/TG4a.html

[46] R.-M. Cramer, R. Scholtz, and M. Win, "Evaluation of an ultra-wide-band propagation channel," *Antennas and Propagation, IEEE Transactions on*, vol. 50, no. 5, pp. 561 –570, may 2002.

[47] A. F. Molisch, D. Cassioli, C.-C. Chong, S. Emami, A. Fort, B. Kannan, J. Karedal, J. Kunisch, H. G. Schantz, K. Siwiak, and M. Z. Win, "A Comprehensive Standardized Model for Ultrawideband Propagation Channels," *IEEE Trans. Antennas Propag.*, vol. 54, no. 11, pp. 3151–3166, 2006.

[48] A. Saleh and R. Valenzuela, "A Statistical Model for Indoor Multipath Propagation," *IEEE J. Sel. Areas Commun.*, vol. 5, no. 2, pp. 128–137, 1987.

[49] D. Dardari and M. Z. Win, "Ziv-Zakai bound on time-of-arrival estimation with statistical channel knowledge at the receiver," in *Proc. IEEE Int. Conf. Ultra-Wideband ICUWB 2009*, 2009, pp. 624–629.

[50] D. Dardari, A. Conti, U. Ferner, A. Giorgetti, and M. Z. Win, "Ranging With Ultrawide Bandwidth Signals in Multipath Environments," *Proc. IEEE*, vol. 97, no. 2, pp. 404–426, 2009.

[51] H. Zhan, J.-Y. Le Boudec, J. Ayadi, and J. Farserotu, "Theoretical Limit of Impulse Radio Ultra-WideBand TOA Positioning and TDOA Positioning," in *Proc. IEEE Int Communications (ICC) Conf*, 2010, pp. 1–6.

[52] J. Reed, *Introduction to ultra wideband communication systems, an.* Prentice Hall Press Upper Saddle River, NJ, USA, 2005.

[53] Q. Li and L. A. Rusch, "Hybrid RAKE/multiuser receivers for UWB," in *Proc. Radio and Wireless Conf. RAWCON '03*, 2003, pp. 203–206.

[54] T. Q. S. Quek, M. Z. Win, and D. Dardari, "Unified Analysis of UWB Transmitted-Reference Schemes in the Presence of Narrowband Interference," *IEEE Trans. Wireless Commun.*, vol. 6, no. 6, pp. 2126–2139, 2007.

[55] A. Rabbachin and I. Oppermann, "Comparison of UWB auto-correlation and transmitted reference schemes," in *Proc. IEEE Int. Conf. Ultra-Wideband ICU 2005*, 2005, pp. 497–501.

[56] L. Stoica, A. Rabbachin, H. O. Repo, T. S. Tiuraniemi, and I. Oppermann, "An ultrawideband system architecture for tag based wireless sensor networks," *IEEE Trans. Veh. Technol.*, vol. 54, no. 5, pp. 1632–1645, 2005.

[57] M. Tuchler and A. Huber, "An improved algorithm for UWB-bases positioning in a multi-path environment," in *Proc. Int Communications Zurich Seminar*, 2006, pp. 206–209.

[58] P.-C. Chen, "A non-line-of-sight error mitigation algorithm in location estimation," in *Proc. WCNC Wireless Communications and Networking Conf. 1999 IEEE*, 1999, pp. 316–320.

[59] J.-Y. Lee, Y.-H. Jo, S.-H. Kang, A. Y. Kang, D.-H. Ha, and S.-J. Yoon, "Determination of the Existence of LoS Blockage and Its Application to UWB Localization," in *Proc. Military Communications Conference MILCOM 2006*, 23–25 Oct. 2006, pp. 1–4.

[60] J. Schroeder, S. Galler, K. Kyamakya, and T. Kaiser, "Three-dimensional indoor localization in Non Line of Sight UWB channels," in *Proc. IEEE International Conference on Ultra-Wideband ICUWB 2007*, 2007, pp. 89–93.

[61] S. Al-Jazzar and J. Caffery, J., "ML and Bayesian TOA location estimators for NLOS environments," in *Proc. VTC 2002-Fall Vehicular Technology Conf. 2002 IEEE 56th*, vol. 2, 2002, pp. 1178–1181.

[62] R. E. Kalman, "A New Approach to Linear Filtering and Prediction Problems," *Transactions of the ASME–Journal of Basic Engineering*, vol. 82, no. Series D, pp. 35–45, 1960.

[63] D. B. Jourdan, J. Deyst, J. J., M. Z. Win, and N. Roy, "Monte Carlo localization in dense multipath environments using UWB ranging," in *Proc. IEEE Int. Conf. Ultra-Wideband ICU 2005*, 2005, pp. 314–319.

[64] D. E. Gustafson, J. M. Elwell, and J. A. Soltz, "Innovative Indoor Geolocation Using RF Multipath Diversity," in *Proc. IEEE/ION Position, Location, And Navigation Symposium*, April 25–27, 2006, pp. 904–912.

[65] P. Meissner, C. Steiner, and K. Witrisal, "UWB Positioning with Virtual Anchors and Floor Plan Information," in *Workshop on Positioning, Navigation and Communication*, 2010.

[66] J. Kietlinski-Zaleski, T. Yamazato, and M. Katayama, "TOA UWB position estimation with two receivers and a set of known reflectors," in *Proc. IEEE International Conference on Ultra-Wideband ICUWB 2009*, 2009, pp. 376–380.

[67] J. Kietlinski-Zaleski, T. Yamazato, and M. Katayama, "TOA UWB Positioning with Two Receivers Using Known Indoor Features," *IEICE Trans. on Communications*, vol. E93-B, no. 12, pp. 3624–3631, December 2010.

[68] J. Kietlinski-Zaleski and T. Yamazato, "TDOA UWB Positioning with Three Receivers Using Known Indoor Features," *IEICE Trans. on Fundamentals of Electronics, Communications and Computer Sciences*, vol. E94-A, no. 3, March 2011.

[69] B. Fang *et al.*, "Simple solutions for hyperbolic and related position fixes," *IEEE Transactions on Aerospace and Electronic Systems*, vol. 26, no. 5, pp. 748–753, 1990.

[70] J. Jemai, P. Eggers, G. Pedersen, and T. K
"urner, "On the applicability of deterministic modelling to indoor UWB channels," in *The 3rd Workshop on Positioning, Navigation and Communication (WPNC)*, 2006.

[71] "Mini-Circuits VHP-26 High-Pass Filter Datasheet." [Online]. Available: http://www.minicircuits.com/pdfs/VHP-26.pdf

[72] "Miteq AFS amplifiers line catalogue." [Online]. Available: http://www.ukrf.com/controlpanel/shoppics/pdfs/AFSCatalogue.pdf

[73] "Mini-Circuits VHF-3500+ High-Pass Filter Datasheet." [Online]. Available: http://www.minicircuits.com/pdfs/VHF-3500+.pdf

[74] "Mini-Circuits VLF-3800+ Low-Pass Filter Datasheet." [Online]. Available: http://www.minicircuits.com/pdfs/VLF-3800+.pdf

[75] "Tektronix TDS8200 datasheet." [Online]. Available: http://www.teknetelectronics.com/DataSheet/TEKTRONIX/WEBTEKTRTDS8200.pdf

[76] J. Hogbom, "Aperture synthesis with a non-regular distribution of interferometer baselines," *Astronomy and Astrophysics Supplement Series*, vol. 15, p. 417, 1974.

[77] T. Deissler and J. Thielecke, "Feature based indoor mapping using a bat-type UWB radar," in *Proc. IEEE International Conference on Ultra-Wideband ICUWB 2009*, 2009, pp. 475–479.

[78] I. Sharp, K. Yu, and Y. J. Guo, "GDOP Analysis for Positioning System Design," *IEEE Trans. Veh. Technol.*, vol. 58, no. 7, pp. 3371–3382, 2009.

[79] J. Kietlinski-Zaleski and T. Yamazato, "UWB Positioning Using Known Indoor Features - Environment Comparison," in *Proc. International Conference on Indoor Positioning and Indoor Navigation(IPIN 2010)*, 2010.

[80] J. Kietlinski-Zaleski, T. Yamazato, and M. Katayama, "Experimental Validation of TOA UWB Positioning with Two Receivers Using Known Indoor Features," in *Proc. IEEE/ION Position, Location and Navigation Symposium PLANS 2010*, 2010.

[81] J. Kietlinski-Zaleski, T. Yamazato, and M. Katayama, "TDoA UWB positioning with three receivers using known indoor features," in *Proc. IEEE Int Ultra-Wideband (ICUWB) Conf*, vol. 2, 2010, pp. 1–4.

[82] J. Kietlinski-Zaleski, T. Yamazato, and M. Katayama, "TOA UWB Position Estimation with 2 receivers and one known reflector," in *IEICE Technical Report*, ser. WBS2008-90, vol. 108, no. 474, Hokkaido, March 2009, pp. 211–216, mon, Mar 9, 2009 - Tue, Mar 10 : Hakodate Mirai Univ. (WBS, IT, ISEC).

Acknowledgment

The author would like to express his great appreciation to his thesis director, Dr. Takaya Yamazato, Professor of Liberal Arts and Sciences, Nagoya University, Japan, for his continuous encouragement and sincere advice during the research work of the PhD course.

I would also like to express the great appreciation to my academic advisor, Dr. Masaaki Katayama, Professor of EcoTopia Science Institute, Nagoya University, Japan, for his continuous support and his sincere constructive critique during the research work.

I also express my sincere appreciation to Dr. Jerzy Kolakowski, Professor of Department of Electronics and Information Technology, Warsaw University of Technology, Poland. Without his help and cooperation the measurements presented in this dissertation would be impossible. I am also thankful for his insightful comments about my research work.

I would also like to express my gratitude and thanks to Dr. Kawaguchi Nobuo, Professor of Graduate School of Engineering, Nagoya University, Japan, for his review of this dissertation.

I also express my gratitude to Dr. Hara Shinsuke, Professor of Graduate School of Engineering, Osaka City University, Japan, for his review of this dissertation.

I would also express my sincere thanks to Dr. Melissa Kennedy, Assistant Professor at Nagoya University of Commerce and Business, Japan, for her careful language checking of this dissertation and many insightful comments.

I would also extend my great thanks to all colleagues in Katayama Laboratory, Graduate School of Engineering, Japan, who have helped me a lot by creating an enjoyable, but dynamic, atmosphere.

List of Acronyms

AOA Angle of Arrival
CIR Channel Impulse Response
CRLB Cramer-Rao Lower Bound
DRAML TDOA Reflection-Aided Maximum Likelihood - proposed method
DS-UWB Direct Spread UWB, other term for IR-UWB
FCC Federal Communications Commission - regulatory body in USA
GPS Global Positioning System
IR-UWB Impulse Radio UWB
LORAN LOng RAnge Navigation
LOS Line of Sight
MAE Mean Average Error
MEMS Micro-Electro-Mechanical System
MPC Multi Path Component
MSE Mean Square Error
NLOS Non-Line of Sight
PAN Personal Area Network
RAML TOA Reflection-Aided Maximum Likelihood - proposed method
RC Result Circle or Result Curve
RF Radio Frequency
RFID Radio Frequency Identification
RMSE Root Mean Square Error
RSS Received Signal Strength
RTLS Real Time Location System
OFDM Orthogonal Frequency Division Multiplexing
SA Service Area
SNR Signal to Noise Ratio
TDOA Time Difference of Arrival
TDOA-AH TDOA - Assumed Height - Reference 3 receiver positioning method

TDOA-DS TDOA - Direct Solution - Reference 4 receiver positioning method

TOA Time of Arrival

TOA-AH TOA - Assumed Height - Reference 2 receiver positioning method

TOA-DS TOA - Direct Solution - Reference 3 receiver positioning method

TOD Time of Departure

UWB Ultra-Wideband

WPAN Wireless Personal Area Network

WSN Wireless Sensor Network

ZZLB Ziv-Zakai Lower Bound

List of Related Papers by the Author

I. Transaction Papers

1. [67] J. Kietlinski-Zaleski, T. Yamazato, and M. Katayama, "TOA UWB Positioning with Two Receivers using Known Indoor Features," *IEICE Trans. on Communications*, vol. E93-B, no. 12, pp. 3624-3631, December 2010.
2. [68]' J. Kietlinski-Zaleski and T. Yamazato, "TDOA UWB Positioning with Three Receivers using Known Indoor Features," *IEICE Trans. on Fundamentals of Electronics, Communications and Computer Sciences*, vol. E94-A, no. 3, March 2011.

II. International Conference Papers

1. [66] J. Kietlinski-Zaleski, T. Yamazato, and M. Katayama, "TOA UWB Position Estimation with Two Receivers and a Set of Known Reflectors," in *Proc. IEEE International Conference on Ultra-Wideband ICUWB 2009*, 2009, pp. 376–380.
2. [80] J. Kietlinski-Zaleski, T. Yamazato, and M. Katayama, "Experimental Validation of TOA UWB Positioning with Two Receivers Using Known Indoor Features," in *Proc. IEEE/ION Position, Location and Navigation Symposium PLANS 2010*, 2010.
3. [79] J. Kietlinski-Zaleski, T. Yamazato, and M. Katayama, "UWB Positioning using Known Indoor Features - Environment Comparison," in *Proc. International Conference on Indoor Positioning and Indoor Navigation(IPIN 2010)*, 2010.
4. [81] J. Kietlinski-Zaleski, T. Yamazato, and M. Katayama, "TDOA UWB Positioning with Three Receivers using Known Indoor Features," in *Proc. IEEE Int Ultra-Wideband (ICUWB) Conf*, vol. 2, 2010, pp. 1–4.

III. Domestic Conference Papers

1. [82] J. Kietlinski-Zaleski, T. Yamazato, and M. Katayama, "TOA UWB Position Estimation with 2 Receivers and One Known Reflector," in *IEICE Technical Report*, ser. WBS2008-90, vol. 108, no. 474, Hokkaido, March 2009, pp. 211–216, mon, Mar 9, 2009 - Tue, Mar 10 : Hakodate Mirai Univ. (WBS, IT, ISEC).